

Synthesis and Reactivity of Gold(III) Complexes

Dissertation for the degree of *Philosophiae Doctor*

Eirin Langseth



Faculty of Mathematics and Natural Sciences

University of Oslo

2014

© Eirin Langseth, 2014

*Series of dissertations submitted to the
Faculty of Mathematics and Natural Sciences, University of Oslo
No. 1531*

ISSN 1501-7710

All rights reserved. No part of this publication may be reproduced or transmitted, in any form or by any means, without permission.

Cover: Inger Sandved Anfinsen.
Printed in Norway: AIT Oslo AS.

Produced in co-operation with Akademia Publishing.
The thesis is produced by Akademia Publishing merely in connection with the thesis defence. Kindly direct all inquiries regarding the thesis to the copyright holder or the unit which grants the doctorate.

Acknowledgements

The work presented in this thesis was carried out at the Department of Chemistry, University of Oslo, in the time period from the autumn of 2010 until the spring of 2014 under the supervision of Professor Mats Tilset and Dr. Richard H. Heyn (SINTEF). June 2012 through November 2012 was spent at The University of Washington, USA, under the supervision of Professor Karen I. Goldberg.

First, I would like to thank the Department of Chemistry for financing my Ph.D. Of course, gold is expensive so I luckily got financial support from other sources as well. Kristine Bonnevie's stipend, together with the tax-agreement between Norway and the US, allowed me to visit The University of Washington in Seattle. COST (COST Action CM1205) allowed Marte Sofie Holmsen and I to visit École Polytechnique Fédérale de Lausanne (EPFL) for a two week research stay (February 2014), which is greatly appreciated.

I would like to thank my two supervisors, Mats and Rick. The two of you have been a great combination, I could choose between all your great ideas what I wanted to follow. You are both very enthusiastic when I show you some new chemistry, always just in time for a group meeting, weekend or Christmas, right. Thank you Mats, for the enormous enthusiasm when I show you a beautiful NMR spectrum. And maybe most, for letting me go in the directions I wanted to. I would also like to thank SINTEF for allowing me to use their facilities to get the ethylene insertion chemistry started.

I want to thank all past and present group members. Dr. Anthony Shaw, thank you for introducing me to the world of gold(III) at all our group meetings. Eline and Ainara, it has been a pleasure working together with the two of you. Ainara, your helpfulness and suggestions are greatly appreciated. Thanks to you Katinka, the gold NHC project was in good hands. A large thanks goes to Marte for sharing an office with me for the last three years, finally you can turn the heat down! It has always (Coca Cola) been a lot of fun! And thank you for continuing all the projects that I did not have time to finish, no pressure. It will be sad to leave all of you at the Organic Section, you made the years at the Department consist of more than just chemistry. I will miss all the lunches, floorball, BBQ and Christmas parties, it was all good fun.

I would like to thank Karen for welcoming me in her group at UW. To work in your lab with all the friendly group members and to see the US were both great experiences! All the evenings in front of the NMR with you, Margaret were both educational and fun. I would also like to thank the group at EPFL, especially Professor Gábor Laurenczy, for being so friendly and helpful when Marte and I were visiting.

Thanks to the two of you Professor Frode Rise and Senior Engineer Dirk Pedersen, the NMR facility at Department of Chemistry is excellent, you do a great job and are always helpful. I appreciate the help you gave me Professor Carl Henrik Gørbitz with X-ray structures and when the instrument decided to become difficult. And Sigurd Øien, thank you for all the X-ray structures you have provided! And especially, that you never threw away those crystals so that you could magically come up structures of the four complexes I really wanted, and that less than two weeks before my thesis was to be handed in. Engineer Osamu Sekiguchi is acknowledged for the help with MS.

I appreciate all of the comments from the kind people who have proofread my thesis: Peter Molesworth, Marte Sofie Holmsen, Mats Tilset, Richard Heyn and my husband Martin Gjerde Jakobsen (who had to suffer through it more than once).

Thank you to all my family and friends. Thanks to you non-chemistry friends, I realise there is a world outside Blindern as well. Dad, you seem to actually understand quite a bit of what I do, I am impressed. And Sally, I barely blew up anything at all. Ragnar, thank you for always being there when we grew up, you will always be 'Lillebror' to me. I have been walking in my mum's footsteps, but sadly you can only be with me in thought (and through my genes).

And last, but not least, I want to express my gratitude to my husband, Martin, for being there for me through these four years, you mean the world to me. Without you, there would be no Ph.D. and now we are actually both finished!

Eirin Langseth
Oslo, May 2014

Abstract

The interest in organogold compounds continues to grow. Gold(III) complexes are being investigated as catalysts for organic transformations as well as tested as potential anti-cancer drugs. Despite this wide-ranging interest in the properties of such complexes, the synthetic methods for preparing them are underdeveloped. Thus, Chapter 2 discusses the synthesis of cyclometalated gold(III) complexes bearing the C–N chelating ligand 2-(*p*-tolyl)pyridine (tpy). Monoalkylation and -arylation were possible by use of Grignard reagents, whereas alkyl and aryl lithium reagents gave the dialkylated and diarylated gold(III) complexes. By a combination of the two alkylation procedures, mixed alkyl/aryl complexes of the type AuMePh(tpy) were obtained and both isomers were available.

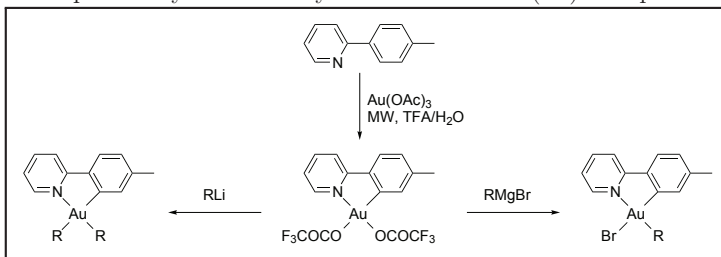
Chapter 3 discusses the reactivity of the cyclometalated gold(III) complexes towards different gases such as carbon monoxide and oxygen. Most of the cyclometalated gold(III) complexes prepared react with acids. The monoalkylated and -arylated complexes of the type AuBrR(tpy) (R = Me, Et, CHCH₂, CCH, Ph) react with silver(I) salts to give a potential open coordination site at gold(III).

Ethylene formally inserts into the Au–O bond *trans* to nitrogen in the chelating C–N ligand of the complex Au(OCOCF₃)₂(tpy) (**62**) in trifluoroacetic acid or dichloromethane, to yield Au(CH₂CH₂OCOCF₃)(OCOCF₃)(tpy) (**94**). In trifluoroethanol, a slightly different complex resulted due to nucleophilic attack by trifluoroethanol rather than trifluoroacetate, Au(CH₂CH₂OCH₂CF₃)(OCOCF₃)(tpy) (**95**). The mechanism of the insertion was investigated experimentally as well as computationally and the results are discussed in Chapter 4. The formal insertion takes place with alkenes other than ethylene, and alkynes react too.

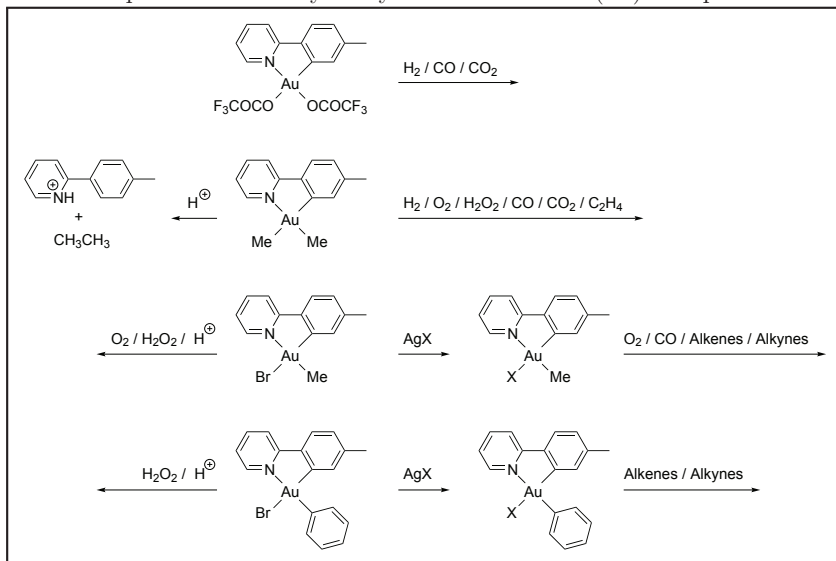
A key step in the catalytic reactions involving gold(III) is assumed to be the coordination of a C–C multiple bond to the gold centre. Various catalytic cycles involving a gold(III) π-complex have been proposed. However, gold(III) alkene, alkyne, allene, or arene complexes have until recently not been conclusively detected and characterised. Chapter 5 discusses the first, and thus far only, crystallographically characterised gold(III) alkene complex, Au(cod)Me₂BArF (**133**–**BArF**, BArF = tetrakis[3,5-bis(trifluoromethyl)phenyl]borate, cod = 1,5-cyclooctadiene).

Graphical Abstract

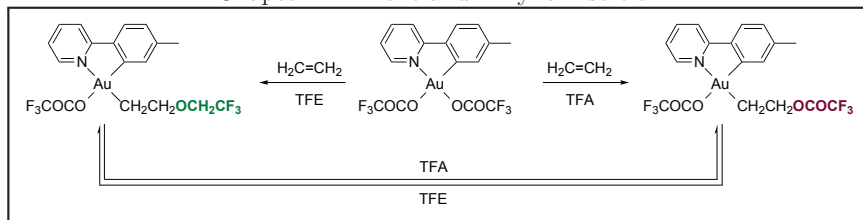
Chapter 2: Synthesis of Cyclometalated Gold(III) Complexes



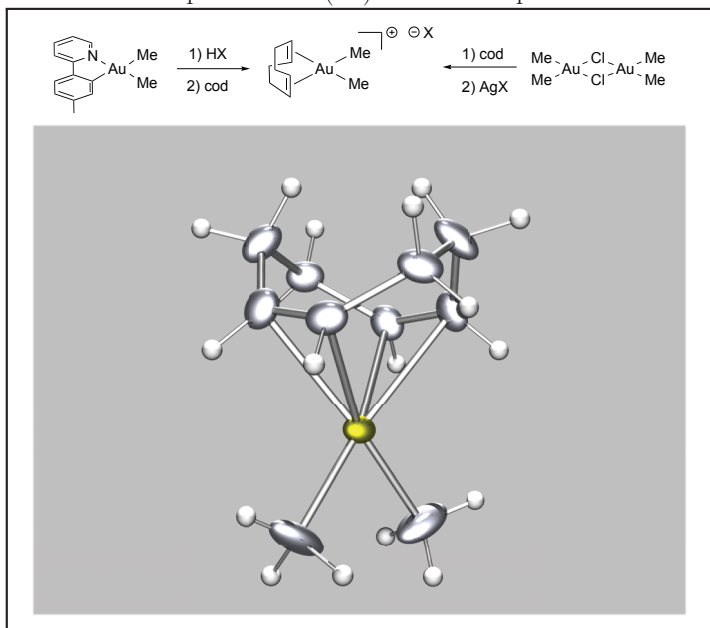
Chapter 3: Reactivity of Cyclometalated Gold(III) Complexes



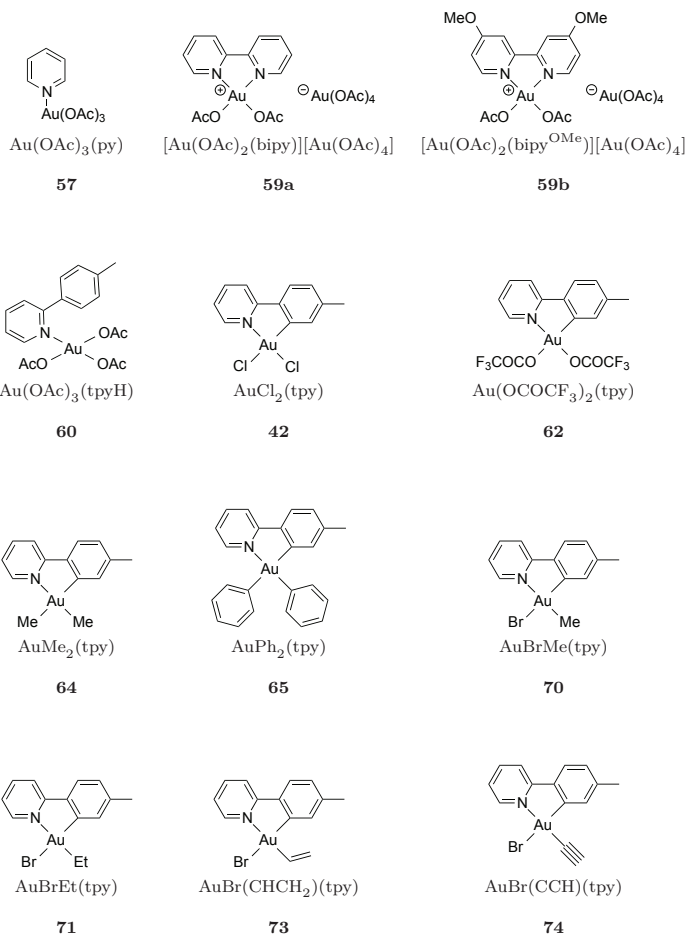
Chapter 4: Alkene and Alkyne Insertion

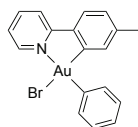


Chapter 5: Gold(III) Alkene Complexes



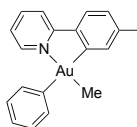
List of Compounds



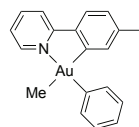


AuBrPh(tpy)

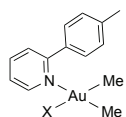
72

*cis*-AuMePh(tpy)

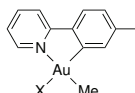
76

*trans*-AuMePh(tpy)

75

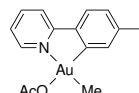
AuMe₂(tpyH)X

77-X

X=OTf, NTf₂, BF₄
(OMe₂ coordinates to Au,
BF₄ as counteranion)

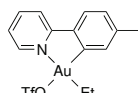
AuMe(tpy)X

55-X

X=OTf, NTf₂, BF₄, PF₆

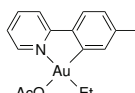
AuMeOAc(tpy)

69



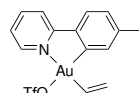
AuEt(tpy)OTf

83

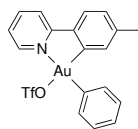


AuEtOAc(tpy)

84

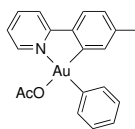
Au(CHCH₂)(tpy)OTf

81



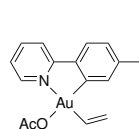
AuPh(tpy)OTf

85

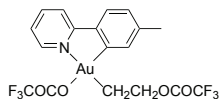


AuPhOAc(tpy)

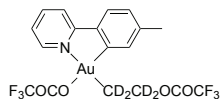
86

Au(CHCH₂)OAc(tpy)

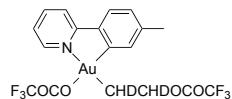
82



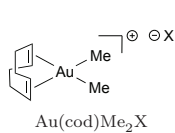
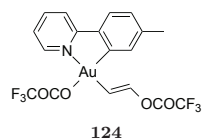
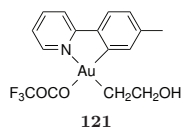
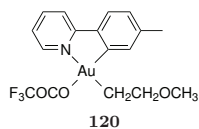
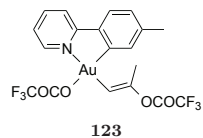
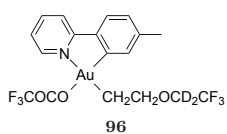
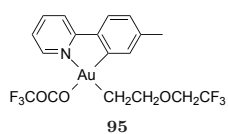
94



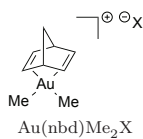
97



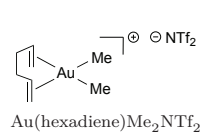
98



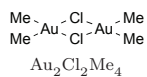
133-X
X=OTf, NTf₂, BArF, BF₄



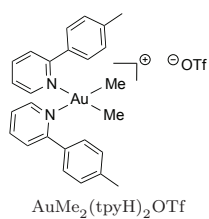
145-X
X=OTf, NTf₂



146



135



144

The list of compounds is not intended as a full list of all complexes discussed herein, it is simply included to aid the reader.

List of Appendices

- I** *Versatile Methods for Preparation of New Cyclometalated Gold(III) Complexes*
Eirin Langseth, Carl Henrik Görbitz, Richard H. Heyn and Mats Tilset
Organometallics **2012**, *31*, 6567–6571
- II** *A Gold Exchange: A Mechanistic Study of a Reversible, Formal Ethylene Insertion Into a Gold(III)–Oxygen Bond*
Eirin Langseth, Ainara Nova, Eline Aa. Tråseth, Frode Rise, Sigurd Øien, Richard H. Heyn and Mats Tilset
J. Am. Chem. Soc. **2014**, *136*, 10104–10115
- III** *Generation and Structural Characterization of a Gold(III) Alkene Complex*
Eirin Langseth, Margaret L. Scheuermann, David Balcells, Werner Kaminsky, Karen I. Goldberg, Odile Eisenstein, Richard H. Heyn and Mats Tilset
Angew. Chem., Int. Ed. **2013**, *52*, 1660–1663

List of Contributors

- I** Eirin Langseth (experimental work and writing of publication)
Carl Henrik Görbitz (help with X-ray crystallographic work)

- II** Eirin Langseth (experimental work and writing of publication)
Ainara Nova (computational work and writing of publication)
Eline Tråseth (experimental work)
Frode Rise (NMR guidance)
Sigurd Øien (X-ray crystallographic work)

- III** Eirin Langseth (experimental work, writing of publication)
Margaret L. Scheuermann (experimental work, writing of publication)
David Balcells (computational work, writing of publication)
Werner Kaminsky (X-ray crystallographic work)
Odile Eisenstein (computational work)

Abbreviations

Ac	acetyl (COCH ₃)
AIBN	azobisisobutyronitrile/2,2'-azobis(2-methylpropionitrile)
aq	<i>aqueous</i> /acquisition time (NMR)
Ar	aryl
AuNP	gold nano particles
BArF	tetrakis[3,5-bis(trifluoromethyl)phenyl]borate
bipy	2,2'-bipyridine
bnpy	2-benzylpyridine
br	broad (NMR)
Bu	butyl
cod	1,5-cyclooctadiene
COSY	correlation spectroscopy (NMR)
δ	chemical shift (NMR)
d	days/doublet (NMR)
d1	relaxation delay (NMR)
d8	mixing time (NMR)
DFT	density functional theory
DMSO	dimethyl sulfoxide
ε	dielectric constant
ECP	effective core potential
EDA	ethyl diazoacetate
EI	electron ionisation (MS)
EPFL	École Polytechnique Fédérale de Lausanne
equiv	equivalent(s)
ESI	electrospray ionisation (MS)
Et	ethyl
G	Gibbs free energy
η	descriptor of hapticity
h	hour(s)
HP NMR	high pressure NMR
HR (MS)	high resolution (mass spectrometry)

Hz	Hertz
<i>i</i>	<i>iso</i>
IR	infrared
ISTD	internal standard
<i>J</i>	coupling constant (NMR)
L	ligand (2 electron donor)
LA	Lewis acid
<i>m</i>	<i>meta</i>
m	multiplet (NMR)
Me	methyl
MS	mass spectrometry
MW	microwave
<i>n</i>	normal
nbd	norbornadiene
NBO	natural bonding orbital
n.d.	not determined
NHC	<i>N</i> -heterocyclic carbene
NLMO	natural localised molecular orbital
NMR	nuclear magnetic resonance
NOE(SY)	Nuclear Overhauser effect (spectroscopy) (NMR)
n.r.	no reaction
ns	number of scans (NMR)
NTf ₂	bis(trifluoromethanesulfonyl)imide (N(SO ₂ CF ₃) ₂)
<i>o</i>	<i>ortho</i>
ORTEP	Oak Ridge thermal ellipsoid plot
OTf	triflate (OSO ₂ CF ₃)
<i>p</i>	<i>para</i>
P	pressure
PBE	Perdew-Burke-Ernzerhof
Ph	phenyl
ppm	parts per million
ppy	2-phenylpyridine
Pr	propyl
q	quartet (NMR)
QNP	quattro nucleus probe (NMR)
rt	room temperature
s	singlet (NMR)
sw	sweep width (NMR)
<i>t</i>	tertiary
t	time/triplet (NMR)
T	temperature

TFA	trifluoroacetic acid (CF_3COOH)
TFE	trifluoroethanol ($\text{CF}_3\text{CH}_2\text{OH}$)
TGA	thermogravimetric analysis
THF	tetrahydrofuran
tpy	2-(<i>p</i> -tolyl)pyridine
TS	transition state
X	generalised one electron anionic donor
Å	Ångström (10^{-10} m)

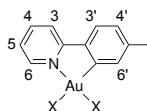


Figure 1: Atomic numbering system for NMR assignments.

Contents

1	Introduction to Gold Chemistry	1
1.1	General Introduction	1
1.1.1	Metallic Gold	4
1.1.2	Redox-Chemistry of Gold	5
1.1.3	Gold(I) and Gold(III)	6
1.1.4	Spectroscopic Limitations and Benefits for Organogold Complexes	7
1.1.5	Aurophilic Interactions	7
1.2	Homogenous Gold Catalysis	7
1.2.1	Gold(I)	10
1.2.2	Gold(III)	11
1.3	Synthesis of Cyclometalated Gold(III) Complexes	15
2	Synthesis of Cyclometalated Gold(III) Complexes	21
2.1	General Introduction	21
2.2	Initial Observations Regarding Au(OAc) ₃	22
2.3	Synthesis and Characterisation of Au(OCOCF ₃) ₂ (tpy)	25
2.3.1	Characterisation	26
2.4	Alkylation and Arylation of Cyclometalated Gold(III) Complexes	31
2.4.1	Dialkylation And Diarylation	31
2.4.2	Monoalkylation And Monoarylation	35
2.4.3	Mixed Aryl And Alkyl Complexes	42
2.5	Conclusions	44
2.6	Experimental	44
3	Reactivity of Cyclometalated Gold(III) Complexes	55
3.1	General Introduction	55
3.2	Reactivity of Au(OCOCF ₃) ₂ (tpy)	55
3.3	Reactivity of AuMe ₂ (tpy)	58
3.3.1	Reactivity Towards Gases	58
3.3.2	Reactivity Towards Oxygen Sources	58

3.3.3	Reactivity Towards Acids	59
3.4	Reactivity of Monoalkylated and -Arylated Gold(III) Complexes . .	64
3.4.1	Reactivity Towards Silver Salts	64
3.4.2	Reactivity Towards Gases	65
3.4.3	Reactivity Towards Oxygen Sources	65
3.4.4	Reactivity Towards Acids	67
3.4.5	Reactivity Towards Alkenes and Alkynes	69
3.5	Conclusions	72
3.6	Experimental	74
4	Alkene and Alkyne Insertion	83
4.1	General Introduction	83
4.2	Initial Trials	85
4.3	Formal Ethylene Insertion	87
4.3.1	Characterisation	90
4.4	Mechanistic Investigations	93
4.4.1	Reversibility of Nucleophilic Attack	93
4.4.2	Reversibility of Ethylene Insertion	97
4.4.3	External Versus Internal Nucleophilic Addition of Trifluoroacetate	99
4.4.4	DFT Calculations on the Reaction Mechanism	100
4.4.5	Attempts at Achieving a Catalytic Process	108
4.4.6	Different Solvents	110
4.5	Other Alkenes and Alkynes	114
4.5.1	Au(OCOCF ₃) ₂ (tpy) with Propyne	115
4.5.2	Au(OCOCF ₃) ₂ (tpy) with Acetylene	116
4.6	Conclusions	118
4.7	Experimental	119
5	Gold(III) Alkene Complexes	125
5.1	General Introduction	125
5.2	Generation of a Gold(III) Alkene Complex	126
5.2.1	Another Approach Towards Au(cod)Me ₂ ⁺	127
5.2.2	Characterisation of Au(cod)Me ₂ ⁺	128
5.2.3	Attempts of Crystal Growth	131
5.2.4	X-Ray Structure of Au(cod)Me ₂ BARf	133
5.2.5	DFT Calculations	135
5.2.6	Attempts at Isolation of Au(cod)Me ₂ ⁺	138
5.3	Other Gold(III) Alkene Complexes	139
5.4	Conclusions	142
5.5	Experimental	143

6	Conclusions and Future Prospects	147
6.1	Synthetic Work	147
6.2	Reactivity of Cyclometalated Gold(III) Complexes	148
6.3	Alkene and Alkyne Insertion	149
6.4	Gold(III) Alkene and Alkyne Complexes	151
6.5	Coordinatively Unsaturated Gold(III) Complexes	151
	Appendices I–III	169

Chapter 1

Introduction to Gold Chemistry

1.1 General Introduction

Gold is amongst the best known of all metals. Due to gold's highly positive normal potential ($E^\circ = +1.692 \text{ V}^1$) gold occurs in nature in its metallic form, e.g. as ores or nuggets. Gold does not form oxides as easily as silver. Gold's tendency not to form oxides is what keeps the metal shiny over time, although the brown gold(III) oxide Au_2O_3 can form in basic solutions. The possession of gold has through centuries been a measure of wealth. The early history of chemistry was to some extent dominated by the alchemists in their desire to make gold. The shiny gold colour of the metal is attributed to relativistic effects, resulting from the transition from the $5d$ to the Fermi level (separation of 2.3 eV) causing gold to absorb in the region of blue-violet and thus reflecting red and yellow; without relativistic effects gold would be grey like silver.²

Gold is one of the noble metals that are quite abundant in nature and thousands of tons of gold are mined each year.³ Due to gold's high electrical conductivity and resistance to corrosion, metallic gold is heavily used in technical applications such as mobile phones and computers. From technical devices, thousands of tons of gold are being recycled each year.^{3,4} The cost of gold is comparable to other noble metals like platinum, rhodium and palladium,¹ all frequently used as catalysts

¹Noble metal prices pr gram in US \$ mid May 2014: Au, 42; Pt, 48; Pd, 27; Rh, 33. BASF (May 14th): <http://apps.catalysts.basf.com/apps/eibprices/mp/defaultmain.aspx>.

for various chemical transformations. The abundance of the metal influences the stability of its price. Gold is quite abundant, however one drawback regarding the gold prices from a chemical point of view, is people's desire to possess gold in an economic crisis, as was seen by a large increase in the gold prices in years 2011–2012. When it comes to homogenous catalysis, it is not just the price of the metal which is of importance; the price of the catalyst complex is often dominated by the price of the ligand rather than by the metal itself.³

Gold is used within dental care and medicine.⁵ Metallic gold is biocompatible;⁴ it even has an E-number,ⁱⁱ E175, which allows metallic gold to be used as a food additive. Although metallic gold is biocompatible, it is toxic in its ionic form. Use of gold in medicine is in this respect a better drug candidate than for example platinum or nickel, as the decomposition product of gold complexes is non-toxic metallic gold. Another consequence is that the metal content in drugs produced using gold catalysts might be less troublesome than for reactions catalysed by more toxic metals. Cisplatin (*cis*-PtCl₂(NH₃)₂) is a widely used chemotherapy drug.⁶ Cisplatin has a high general toxicity and is becoming ineffective due to drug resistance, hence alternatives are desirable. As gold(III) complexes are isoelectronicⁱⁱⁱ with platinum(II) it makes the gold complexes interesting in that respect. Gold complexes are thus investigated for cytotoxic properties and several candidates have been tested.⁶ The gold(I) complex auranofin (**1**, Figure 1.1) is used in the treatment of arthritis and has been shown to inhibit tumour growth in cells *in vitro*.^{3,5,6} Several gold(III) compounds have been reported to be stable under physiological-like conditions.⁴ The gold(III) complexes **2** and **3** (Figure 1.1) show antitumor activity.⁶ Besides the potential applications within medicine, several organogold(III) complexes have been shown to possess luminescent properties, for use in e.g. organic light-emitting devices (OLEDs).⁸ The gold(III) complexes **4** and **5** (Figure 1.1) are two examples,^{9–14} and their structures are strongly related

ⁱⁱE-numbers are codes for substances approved for use as food additives within the European Union and Switzerland ('E' stands for Europe).

ⁱⁱⁱIsoelectronic: Complexes with the same structure and number of electrons, usually extended to include complexes of metals in different rows in the periodic table. Isolobal: Similar orbital properties; same number of electrons in the frontier orbitals and the number, symmetry properties, approximate energies and shapes of the frontier orbitals are similar. Au⁺ and AuL⁺ are considered isolobal with H⁺ and R⁺ (where R⁺ is a carbocation).⁷ Two isoelectronic or isolobal structures are said to be more similar than those that are not.

to the complexes which will be discussed in Chapter 2.

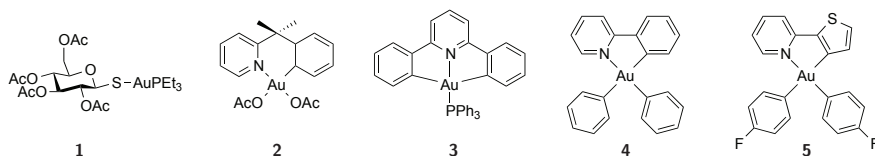


Figure 1.1: Auranofin used as anti-arthritis drug,^{5,6} two Au(III) complexes with cytotoxic properties⁶ and two Au(III) complexes with luminescent¹⁴ properties.

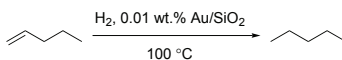
Gold in its metallic form has been used widely for centuries. However in oxidised form gold has not been as extensively used as other noble metals like platinum and palladium. Gold was long thought to be catalytically ‘dead’.^{15,16} This preconception persisted for a long time even though there were indeed significant reports of reactions catalysed by gold.^{15–17} One early example of gold(III) catalysis was reported by Thomas *et al.*, who found that gold(III) catalysed the oxidation of phenyl acetylene to acetophenone.¹⁸ In 1973, Bond *et al.* reported the use of supported gold as a catalyst for hydrogenation of olefins.¹⁹ In the mid 1980s, Haruta²⁰ and Hutchings²¹ independently reported the use of heterogeneous gold to oxidise CO and hydrochlorinate acetylene, and laid the ground for heterogeneous gold catalysis. The breakthrough for the use of gold within homogeneous catalysis came at approximately the same time, when Ito *et al.* reported a catalytic asymmetric aldol reaction.²² A chiral ferrocenylphosphine gold(I) complex was used to catalyse the aldol reaction between aldehydes and isocyanates. It was seen that gold is indeed useful for catalysing several transformations, and not as inert as often believed.⁴ There has been a paradigm shift for gold; it is now frequently investigated for its use within catalysis and the number of publications regarding gold catalysis is increasing.¹⁶

Since 2000, homogeneous gold catalysis has become an important topic in the field of catalysis,^{23–25} and gold(I) catalysts clearly dominate over gold(III) catalysts. Gold can catalyse a range of organic transformations such as nucleophilic addition to C–C multiple bonds, activation of alcohols, carbonyl or imine groups, hydrogenation, C–H bond functionalisation, selective oxidations and reductions.^{3,4,17,26} The key feature of gold catalysis is that it often promotes reactions

under milder conditions than other transition metal catalysts; lower temperatures, shorter reaction times and more tolerant to air and moisture.⁴ The benchmark reaction of gold catalysis is the addition of water and alcohols to alkynes.²³ In the case of terminal alkynes the Markovnikov product is produced cleanly.²³ The typical textbook example of how to achieve the Markovnikov product is by use of HgSO_4 under acidic conditions,²⁷ gold catalysis is obviously preferable over toxic mercury.

1.1.1 Metallic Gold

Metallic gold is included in this introduction to give a brief overview of what this brilliant metal can do, as well as to make the reader aware that a catalytic reaction believed to be homogenous in nature might indeed be heterogeneous. Metallic gold has a melting point of 1065 °C (boiling point of 2807 °C)² and is commonly dissolved in *aqua regia* ($\text{HCl}:\text{HNO}_3$, 1:3). Gold in bulk form has the characteristic gold colour, but when finely divided it can be purple, ruby red or blue.² ‘Purple of Cassius’, a ceramic colorant, is a gold colloid made by reduction of gold compounds by tin(II) chloride.² ‘Purple of Cassius’ was used in the manufacturing of ruby glass in Potsdam around 1679 and the colorant was in fact already used in the middle of the 17th century, some 25 years before the ‘discovery’ by Andreas Cassius.²⁸ Gold in the form of metallic nano particles (AuNP) are able to catalyse several types of reactions.¹⁶ One selected example of a heterogeneous gold catalysed reaction is shown in Scheme 1.1. Au/SiO₂ effectively catalyses the hydrogenation of 1-pentene with low catalyst loadings.²⁹



Scheme 1.1: Hydrogenation of 1-pentene to pentane over Au/SiO₂.²⁹

Due to the reduction potential of gold, reduction to metallic gold occurs easily. The reduction of organometallic complexes to gold(0) is often apparent with a colour change to purple or black due to formation of AuNP. Within the world of homogeneous organogold chemistry formation of AuNP is not desirable but it turns out that only very little decomposition can give a quite strong colour; what

appears to be a solution is in fact a suspension of a small amount of AuNP.

1.1.2 Redox-Chemistry of Gold

Gold is in group 11 in the periodic table and appears in the oxidation states 0, +1 and +3, as well as +2 in bimetallic systems. In the cases of gold paired with very electropositive metals, for example in Cs^+Au^- , gold can appear in oxidation state -1.² The oxidation states IV and V are also known for gold, gold(V) being stabilised by fluorines in a 6-coordinate complex.²

Gold(I) in the absence of stabilising ligands will spontaneously disproportionate into gold(0) and gold(III) in *aqueous* solution.^{2,3} Oxidative addition of gold(I) produces gold(III), for example by Br_2 or other halogens. Oxidative addition of gold(III) would lead to gold(V), hence does not commonly happen. For gold(III), reductive elimination of two ligands in a *cis* relationship happens quite readily to give gold(I) species.³⁰ There is no evidence in the elimination reactions that organic radicals are involved.³⁰ The oxidation state of gold is usually unchanged during the catalytic cycle as it has proven difficult to re-oxidise gold.²⁵ There are a few examples of catalytic reactions where gold(I)/gold(III) redox cycles are suggested,³¹⁻³⁴ but the reports are still rather few and whether or not trace amounts of palladium were present in some cases has been debated.^{25,35}

In the heavier elements, the *s* electrons that approach the nucleus are so strongly attracted by the high nuclear charge that the velocities of the electrons approach the speed of light. This causes a contraction of the *s* shells.^{2,36} The relativistic effects reach a maximum in gold and come in addition to the lanthanide contraction allowing the outermost orbital to be 6*s* rather than 5*s* without a size increase.² The effect of relativity destabilises the 5*d* orbitals, stabilises the 6*p* orbitals and stabilises the 6*s* orbital to a greater extent, leading to a small 5*d*-6*s* separation and a large 6*s*-6*p* separation.² As a consequence, gold forms shorter and stronger covalent bonds than what would have been the case without the relativistic effect, and is likely the reason for the 'aurophilic' interactions discussed later.^{37,38} Au-Au distances in metallic gold are shorter than Ag-Ag distances in silver, and gold has a smaller atomic radius than silver.^{2,36} The stability of gold in the oxidation state +3 has been attributed to relativistic effects causing destabili-

sation of the $5d$ shell.² The relativistic effects for gold are especially important to consider in computational chemistry.³⁶

1.1.3 Gold(I) and Gold(III)

Oxidation states +1 and +3 are by far the most common for organogold complexes. Gold(I) strongly prefers a linear geometry, thus gives d^{10} 14 electron complexes. Gold(III) on the other hand, usually gives square planar d^8 16 electron complexes. Gold(III) is isoelectronic with Pt(II) meaning similar reactivity is expected for the two. Gold(I) is isoelectronic with Hg(0) and the fragment LAu^+ is isolobal to Hg^{2+} .⁷

Both gold(I) and gold(III) are relatively soft Lewis acids^{iv} and prefer soft ligands. Hence, they will undergo substitution reactions where a ligand is replaced with a softer one.³⁰ Ligand exchange is usually rapid, although slower for gold(III) than for gold(I), with exchange occurring *via* an associative mechanism.^{3,30} If a soft ligand is to be exchanged with a harder one, more forcing conditions are needed. For example, reaction of a gold complex with a silver(I) salt to generate an insoluble silver(I) salt that precipitate out from solution, will shift the equilibrium towards the desired product.³⁰ In the square planar geometry preferred by gold(III), the general rules of *trans* effect^v apply for ligand substitution. However, the thermodynamically preferred product is usually where two soft ligands have a *cis* relationship. This is of course due to the *trans* influence rather than the *trans* effect.

^{iv}How ‘hard’ or ‘soft’ a ligand or metal ion is, roughly corresponds to their polarisability; small and highly charged metal ions are ‘hard’ and small and electronegative ligands are ‘hard’. Larger metal ions and ligands are hence ‘soft’. Decreasing softness of ligands (where R = alkyl): $\text{R}^- > \text{Ar}^- > \text{PR}_3 > \text{RS}^- > \text{I}^- > \text{Br}^- > \text{Cl}^- > \text{RCO}_2^- > \text{F}^-$.

^v*trans* influence: Thermodynamic, the ligand with the highest *trans* influence weakens the bond to the ligand *trans* to itself (observed by longer bond lengths, lower IR stretching frequencies, smaller NMR coupling constants *etc.*³⁹).

trans effect: Kinetic, the ligand with the highest *trans* effect directs an incoming ligand *trans* to itself (due to the labilisation of the bond from the *trans* influence). The same trend is followed as for the ‘hard-soft’ principle. Ligands with decreasing *trans* influence (approximate series⁴⁰): $\text{R}_3\text{Si}^- > \text{H}^-$, $\text{H}_2\text{C}=\text{CH}_2$, R^- , $\text{CO} > \text{PR}_3$, $\text{I}^- > \text{Br}^- > \text{Cl}^- > \text{RNH}_2$, $\text{NH}_3 > \text{OH}^- > \text{H}_2\text{O}$. For a deeper understanding of the *trans* effect/influence, the reader is referred to a review by Appleton, Clark and Manzer.³⁹

1.1.4 Spectroscopic Limitations and Benefits for Organogold Complexes

^{197}Au is the only isotope of gold so no distinct isotope distribution is observed in mass spectrometry. ^{197}Au has nuclear spin $\frac{3}{2}$.⁴¹ Because of low sensitivity and a quadrupolar moment, there are few ^{197}Au NMR spectra reported.^{42–45} Both gold(I) and gold(III) are diamagnetic which allows for easy analysis of organogold complexes and catalytic reactions by ^1H and ^{13}C NMR spectroscopy through observation of the ligand. Information on the oxidation state can be retrieved using Mössbauer spectroscopy.³

1.1.5 Auophilic Interactions

The Au–Au distances are in many complexes unusually short in the solid-state. These so-called auophilic interactions can occur between gold atoms within the same molecule or between molecules. The auophilic interactions are in the range of 2.50–3.50 Å.³⁷ The sum of the van der Waals radii for gold is 3.32 Å (van der Waals radius for Au 1.66 Å),^{46,47} hence auophilic interactions are shorter or in the same region as the sum of the van der Waals radii. Auophilic interactions are believed to be related to relativistic effects, hence being the strongest for gold and most common for gold(I) due to the overlap of the filled $5d$ orbitals and the empty $6p$ orbitals.^{37,47} Several other metals are also known to have metallophilic interactions,^{38,47,48} a common one is between gold and silver. Auophilic interactions are common for gold(I), less so for gold(III) although they have been reported.^{47,48} Although less likely for gold(III) compared to gold(I), this interaction is important to be aware of when gold complexes are investigated. In addition to the electronic effects, there are significant steric restrictions for the formation of auophilic interactions.

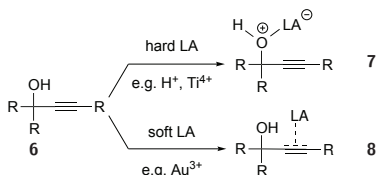
1.2 Homogenous Gold Catalysis

The aim of this study was to prepare organometallic complexes of gold(III) and study them. The discussion of homogenous gold catalysis will therefore be focused

upon gold in oxidation state +3.

Gold catalysts are often significantly more active than other transition metals if they catalyse the same reaction.³ Perhaps the best sign of new a catalyst system becoming important is when another research group decides to use it to synthesise new organic molecules.⁴ Homogenous gold catalysis is now at the point where its use is indeed frequently reported within total synthesis.⁴⁹ The total synthesis of α -inone, bryostatin 16 and prostaglandins are worth noting in this regard.⁴⁹ α -Inone is an important target for the perfume industry, bryostatins are investigated with respect to antitumor properties as well as against Alzheimer's disease, while the prostaglandin lipids are found in most tissues and organs.⁴⁹

Addition reactions to alkenes or alkynes can be achieved with the soft electrophile mercury(II), as often mentioned in introductory organic textbooks, rather than by a Brønsted acid which requires harsher conditions.²⁷ Softer Lewis acids can be more tolerant to amongst others, oxygen functionalities as depicted in Scheme 1.2 and hence give complementary selectivities.⁴ Addition reactions of mercury(II) to alkynes can in several cases be performed catalytically, whereas the



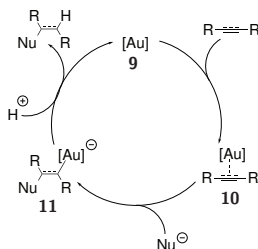
Scheme 1.2: Reaction of a functionalised alkyne with hard or soft Lewis acids (LA).⁴

analogous reactions of alkenes, an additional step is required to release the organic ligand due to kinetic stability.⁴ This means that the transformation of alkenes is usually stoichiometric in mercury salts.⁴ Mercury is known to be highly toxic,^{50,51} hence the use of stoichiometric amounts of mercury salts on larger scale is unacceptable today. The relatively high vapour pressure of mercury in its metallic form leads to mercury being absorbed in the lungs and then carried by the blood into the brain where it can damage the central nervous system irreversibly.⁵² Surely all are familiar with the Mad Hatter in *Alice in Wonderland*.⁵³ The inspiration comes from the time when solutions of mercury ions were used in the treatment of animal fur for hat manufacture, hence the expression 'Mad as a Hatter' stems from the

symptoms that the hatters could get from mercury poisoning.⁵² Metallic mercury is also slightly water soluble, making any leakage of mercury an environmental problem. In contrast to the inorganic mercury salts (due to their low solubility in water), the organomercury compounds are highly toxic.^{51,54} Organomercury compounds such as HgMe^+ are readily absorbed by the body and the body retains organomercury more strongly than inorganic mercury salts.⁵² Due to the high toxicity of mercury, its use is heavily restricted.⁵¹

Gold can replace toxic mercury in many instances. Vinyl chloride, the monomer for polyvinyl chloride (PVC), is produced on a large industrial scale. Mercuric chloride catalyses the hydrochlorination of acetylene, and was the preferred catalyst in commercial production of vinyl chloride.^{4,17} Supported gold(III), also a soft metal, was suggested as a viable catalyst for the hydrochlorination process instead of mercuric salts.⁴ Gold(III) was found to be the most active catalyst for the transformation of acetylene to vinyl chloride.^{21,55} Before the application of gold catalysis on an industrial scale could take place, the economically preferred method of oxidative hydrochlorination of ethylene was developed (rather than from acetylene).³

The most important mode of reactivity of homogeneous gold catalysis is the activation of C–C multiple bonds.^{3,4,16,56} Scheme 1.3 shows the general catalytic cycle for C–C multiple bond activation by gold(I) or gold(III) followed by nucleophilic addition. First, an alkene or alkyne is believed to coordinate to the gold catalyst **9** yielding the gold alkene or alkyne complex **10**, followed by nucleophilic attack to give the gold alkyl or vinyl complex **11**. The last step involves protodeauration to release the product and regenerate the gold catalyst **9**.

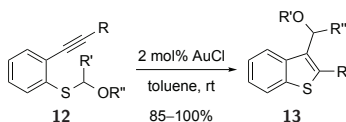


Scheme 1.3: Activation of C–C multiple bonds using Au catalysts.

1.2.1 Gold(I)

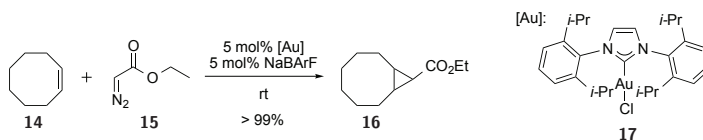
Within organic synthesis, organometallic gold(I) complexes have become widely used but will only be briefly discussed here. Perhaps the most used ligand systems for gold(I) are the *N*-heterocyclic carbene (NHC) ligands.⁵⁷ This ligand type is a good electron donating ligand with tuneable steric and electronic properties.⁵⁸ Examples of dual gold catalysis, where two gold nuclei are involved in the catalytic cycle, are appearing in the literature.²⁴

One additional feature of gold catalysis is the ability of gold in some cases to catalyse reactions involving sulfur. Transition metals are usually incompatible with sulfur as sulfur poisons the catalyst; sulfur binds too strongly to the catalyst complex thus terminating the catalytic cycle.⁴ One example is synthesis of benzothiophenes using AuCl depicted in Scheme 1.4.⁵⁹ Benzothiophenes are of interest as the framework is found in biologically active compounds.⁴



Scheme 1.4: Synthesis of benzothiophenes catalysed by AuCl.⁵⁹

Gold(I) catalysts have also been shown to catalyse cyclopropanation reactions.^{60,61} One example of a gold(I) catalysed cyclopropanation reaction between cyclooctene (**14**) and ethyl diazoacetate (EDA, **15**) is shown in Scheme 1.5.



Scheme 1.5: Cyclopropanation reaction between cyclooctene and EDA catalysed by a NHC Au(I) complex.⁶¹

1.2.2 Gold(III)

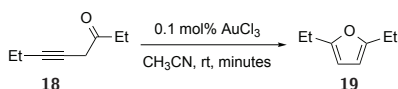
The utilisation of organometallic complexes of gold(III) is gaining more and more interest. Especially for intramolecular cyclisations, gold(III) has found its use.⁶² Still, most of the catalytic processes reported for gold(III) use the simple and commercially available tetrachloroaurate either in the form of the acid (HAuCl_4) or in the form of the sodium or potassium salt (NaAuCl_4 or KAuCl_4).^{16,62} Another similar gold(III) complex used is AuBr_3 .¹⁶ There are however, many fewer reports using organometallic complexes of gold(III). The reason for this is perhaps that the synthetic methods for synthesising organometallic complexes have been underdeveloped. In the recent years many reports of gold bearing NHC ligands have appeared. Most of these are gold(I) complexes but many can be oxidised to gold(III) by addition of, amongst others chlorine or bromine in various forms. In our research group there has been interest in gold NHC complexes of both gold(I) and gold(III).^{63,64} Although the author of this thesis initiated the investigations of NHC gold(I) complexes in the research group and has been slightly involved in a later stage as well, this topic will not be covered here. The interested reader is referred to the Master thesis by Katinka Dankel.⁶³

1.2.2.1 Simple Gold(III) Complexes as Catalysts

As mentioned, most reports with gold(III) as the catalyst use the commercially available tetrachloroaurates. It is desirable to use auxiliary ligands, other than just simple halogens, to improve the stability and reduce the sensitivity of the pre-catalyst.⁶² Commercial tetrachloroauric acid is usually delivered as the trihydrate ($\text{HAuCl}_4 \cdot 3\text{H}_2\text{O}$) but will absorb moisture from the air during handling resulting in an orange liquid on a humid day. Tetrachloroauric acid can act as a protic acid and as a Lewis acid in catalysis since it can dissociate into H^+ and AuCl_4^- , or to HCl and AuCl_3 .⁶² AuCl_3 is a mild Lewis acid and has been used instead of the traditional and more aggressive Lewis acids in reactions where the need for milder conditions are required.^{4,62} Halogenation of arenes are superior using AuCl_3 compared to standard Lewis acids such as FeCl_3 , BF_3 or AlCl_3 .⁶² Insertion of nitrenes into aromatic and benzylic C–H bonds to produce substituted anilines or benzylamines is another reaction possible using AuCl_3 catalysis.⁶²

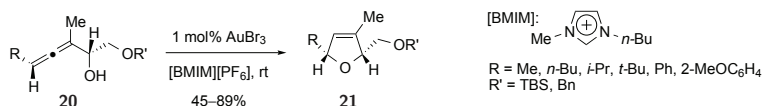
As early as 1931, a publication by Kharasch and Isbell described selective functionalisation of aryl C–H bonds by gold(III).⁶⁵ AuCl₃ was reacted with benzene to give AuCl₂Ph which reacted further with benzene to AuClPh₂, presumably, which was unstable and hence gave AuCl, benzene and chlorobenzene. AuCl₂Ph could be trapped by addition of diethyl ether, but Kharasch and Isbell were not able to isolate AuClPh₂.⁶⁵

AuCl₃ is used successfully in numerous cases to activate allenes, alkynes and alkenes.⁶² One example of catalysis by AuCl₃ is shown in Scheme 1.6 for the quantitative cycloisomerisation of propargyl ketone **18**.⁶⁶



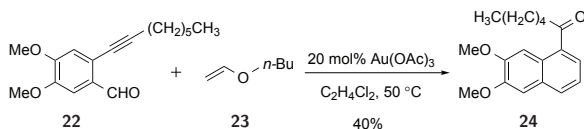
Scheme 1.6: Cycloisomerisation of propargyl ketone **18** using AuCl₃.⁶⁶

The assumed mechanism for activation and cyclisation of substituted allenes by AuCl₃ is through coordination of gold to one of the double bonds followed by nucleophilic attack usually *via* an internal nucleophile.⁶² AuBr₃ can be used as a catalyst for the cycloaddition shown in Scheme 1.7 giving isolated yields of 45–89%.⁶⁷ The reaction is performed in an ionic liquid as solvent.



Scheme 1.7: Cyclisation of allene **20** by AuBr₃ in an ionic liquid.⁶⁷

Au(OAc)₃ has been used successfully to catalyse the cycloisomerisation reaction leading to compound **24** (see Scheme 1.8).⁶⁸

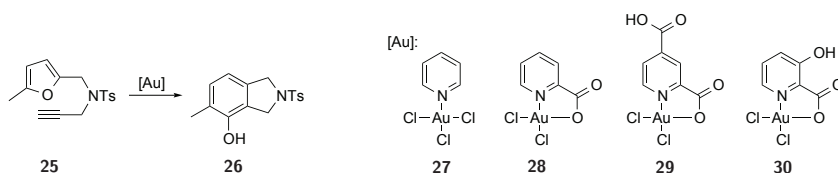


Scheme 1.8: Catalytic performance of Au(OAc)₃.⁶⁸

Simple adducts of the type LAuCl_3 where L is a phosphine are used as well.⁶² LAuBr_3 is in only few cases a better catalyst than the cheaper and more common LAuCl_3 .⁶² A full overview of all reactions possible with gold(III) complexes are indeed too lengthy for this thesis and there are some good reviews available for the interested reader.^{3,4,25,62} The focus will be directed towards gold(III) catalysis where the pre-catalyst is a chelated gold(III) complex.

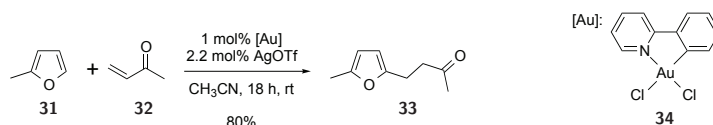
1.2.2.2 Chelated Gold(III) Complexes as Catalysts

The pyridine-2-carboxylates, also called picolinates, are perhaps the most frequently used chelated gold(III) complexes (**28–30**, Scheme 1.9).^{69–72} The reaction shown in Scheme 1.9 is an example of an enyne cyclisation catalysed by such complexes, a reaction type where gold catalysts are now frequently used.¹⁶ There is experimental evidence, such as long induction periods, indicating that these complexes are pre-catalysts and not the actual catalytic species.⁶²



Scheme 1.9: Enyne cyclisation of **25** catalysed by Au(III) complexes **27–30**.⁶⁹

Another highly relevant gold(III) catalyst (or pre-catalyst) with respect to the work described in this thesis, is $\text{AuCl}_2(\text{ppy})$ (**34**, ppy = phenyl pyridine). $\text{AuCl}_2(\text{ppy})$ (**34**) together with AgOTf catalyses the addition reaction of methyl vinyl ketone (**32**) to 2-methylfuran (**31**, Scheme 1.10).⁷³

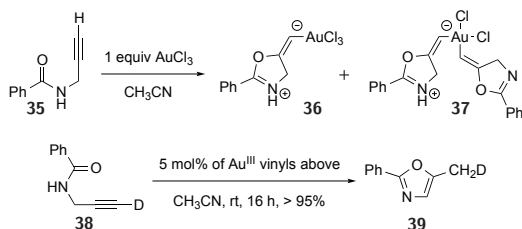


Scheme 1.10: Au catalysed addition of 2-methylfuran to methyl vinyl ketone.⁷³

1.2.2.3 Characterised Possible Intermediates in Gold Catalysis

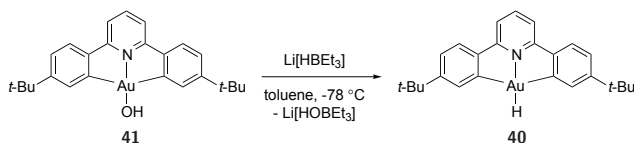
Several of the complexes described in this thesis are of relevance when discussing possible intermediates in catalysis. To gain insight into the mechanisms in operation for any reaction, it is necessary to look for possible intermediates. Of course one cannot prove a mechanism, only disprove, but it is still of importance to get beyond speculation and assumptions.⁷⁴ This section will deal with both gold(I) and gold(III) as the proposed intermediates are often of similar character for the two oxidation states. It is a tendency that the structures of the proposed intermediates are first observed for gold(I), and then later are proven to exist also for gold(III). Activation of C–C multiple bonds using gold catalysts was shown in Scheme 1.3. The activation of an alkene or alkyne is accepted to proceed *via* a gold alkene or gold alkyne complex, followed by nucleophilic attack to generate a gold alkyl or vinyl complex and last product release and catalyst regeneration. As a consequence, gold alkene, alkyne, alkyl and vinyl complexes should be intermediates in gold catalysis. However, the isolation of such species has been easier said than done in several cases. Another important potential intermediate in gold catalysed transformations is gold hydrides.

The first indication of a gold(I) vinyl intermediate in a catalytic cycle was presented by Hammond *et al.* as late as year 2008.⁷⁵ Several other gold(I) vinyl complexes appeared shortly after.^{76,77} The crystallographically characterised gold(III) vinyl complex **36** was reported in 2011.⁷⁸ The gold(III) vinyl compounds **36** and **37**, formed together with **36**, were catalytically active in the cyclisation of benzamide **39** shown in Scheme 1.11.⁷⁸



Scheme 1.11: Crystallographically characterised Au(III) vinyl complex **36**. The combination of the two Au(III) vinyl complexes shown were used to catalyse the cyclisation of benzamide **38**.⁷⁸

Transition metal alkyl complexes often undergo β -H elimination however this does not seem to be the case for gold. There is one example from Kochi from 1976 where isomerisation of $\text{AuMe}_2t\text{-BuL}$ to $\text{AuMe}_2i\text{-BuL}$ was observed ($\text{L} = \text{PPh}_3$), likely *via* a β -H elimination.⁷⁹ The low propensity for β -H elimination from gold alkyl complexes was long attributed to the low stability of gold hydrides, gold was even thought to be unable to form gold hydrides.³⁰ Bochmann *et al.* reported the isolation of the first gold(III) hydride in 2012 verifying their existence.⁸⁰ The gold(III) hydride complex **40** (Scheme 1.12) was crystallographically characterised.



Scheme 1.12: The first Au(III) hydride isolated.⁸⁰

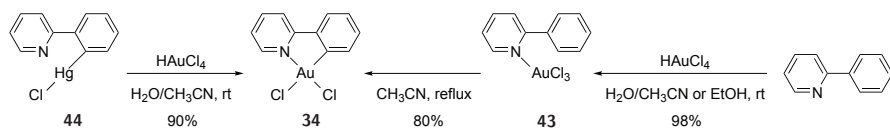
The next important group of gold intermediates are the gold alkenes and alkynes. Au(I) alkene complexes have been known for some time and several complexes are reported^{81–90} and in part reviewed.^{3,16,74,91–93} Alkene, allene and alkyne complexes of gold(I) have been structurally characterised both by NMR spectroscopy and single-crystal X-ray crystallography.^{93,94} In 1964, Chalk proposed the generation of $\text{C}_8\text{H}_{12}\cdot\text{AuCl}_3$,⁸¹ based solely on an IR spectrum and elemental analysis of mixtures containing two species.^{94,95} When the studies presented in this thesis were initiated, no clear identification of π -complexes of gold(III) had been achieved.^{17,94}

1.3 Synthesis of Cyclometalated Gold(III) Complexes

When attempts are made to synthesise cyclometalated complexes of gold(III) there is a large tendency towards reduction to metallic gold or to gold(I) species.^{96,97} Gold(III) complexes are more challenging to cyclometalate compared to palladium and platinum.⁹⁶ Traditionally, this has been overcome by transmetalation from organomercury compounds to gold.⁹⁶ The method of transmetalation of an

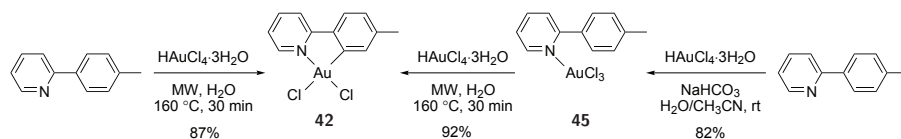
organic group from mercury to gold is versatile and useful for substrates that do not undergo direct cyclometalation themselves.⁹⁸ The organomercury complexes RHgCl are prepared by reacting *n*-butyl lithium with the organic compound (an organohalide) followed by reaction with HgCl_2 . In the transmetalation step from mercury to gold, $\text{Me}_4\text{N}^+\text{Cl}^-$ is often added to give an insoluble chloromercurate salt $[\text{Me}_4\text{N}]_2[\text{Hg}_2\text{Cl}_6]$ to ease the separation.⁹⁶ There are however several reasons why transmetalation from mercury is undesirable; one being an additional step in the synthesis, but the major concern is the use of highly toxic organomercury compounds. A large variety of cyclometalated gold(III) complexes exist⁹⁶ even though they are not frequently used within catalysis for the time being.

The procedure cited most frequently in the literature for the synthesis of $\text{AuCl}_2(\text{ppy})$ (**34**) and $\text{AuCl}_2(\text{tpy})$ (**42**, $\text{tpy} = 2\text{-}(p\text{-tolyl})\text{pyridine}$) was reported by Constable and Leese.⁹⁸ In this paper a procedure using transmetalation from mercury is reported to give 90% yield of $\text{AuCl}_2(\text{ppy})$ (**34**), whereas direct cyclometalation is said to happen in 80% yield from $\text{AuCl}_3(\text{ppyH})$ (**43**), however when referring to this paper some do not indicate which of the procedures are used (Scheme 1.13). There are reports of yields much lower than the 80% reported by Constable and Leese for the mercury-free cyclometalation, including results from our own laboratory.^{96,99,100} Eisenberg *et al.* report quantitative recovery of **43** when following the thermal procedure by Constable and Leese to prepare the cyclometalated product **34**.⁹⁹ Thermogravimetric analysis (TGA) of the noncyclometalated **43** under a nitrogen atmosphere showed clean thermal decomposition to the cyclometalated complex **34**, as indicated by a weight loss corresponding to 1 equivalent of HCl . The degradation to the cyclometalated product started at 150 °C and continued up to 220 °C.⁹⁹ This high thermal decomposition temperature compared to the reflux temperature of an acetonitrile/water mixture, made Eisenberg *et al.* question whether or not it is possible to form **34** at the temperature reported by Constable and Leese.⁹⁹ It was also showed that **34** was stable up to 360 °C.⁹⁹ A frequently used work-up procedure in the case of **34** is precipitation followed by filtration, as the product **34** is sparsely soluble in organic solvents. Small amounts of metallic gold can easily be present and might remain undetected if an elemental analysis is not performed. In the report by Constable and Leese, elemental analysis is only reported for $\text{AuCl}_2(\text{ppy})$ (**34**) obtained from transmetalation from mercury.⁹⁸



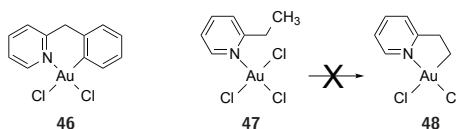
Scheme 1.13: Synthesis of $\text{AuCl}_2(\text{ppy})$ reported by Constable and Leese.⁹⁸

The desire to circumvent the use of toxic organomercury compounds led a former postdoctoral researcher in our group, Dr. Anthony P. Shaw, to develop a procedure using microwave technology as means of heating the reaction.⁹⁷ Microwave heating affords efficient heating and when using a suitable microwave oven equipped with a thermocouple, it also enables a high degree of temperature control.¹⁰¹ Another desirable feature is the ability to use temperatures above the boiling point of the solvent. In this case 160 °C was sufficient to obtain $\text{AuCl}_2(\text{ppy})$ (**34**) and $\text{AuCl}_2(\text{tpy})$ (**42**) in 83 and 87% yield, see Scheme 1.14 for the synthesis of **42**. The procedure also enabled the direct cyclometalation of the six-membered ring structure $\text{AuCl}_2(\text{bnpy})$ (**46**, Scheme 1.15). Several cyclometalated gold(III) complexes were thus available through a procedure that gives higher yields and cleaner product without the use of mercury.⁹⁷ Attempts to synthesise **48** (Scheme 1.15) following the same microwave procedures proved unsuccessful and TGA of **47** did not show decomposition to the six-membered cyclometalated complex **48**.⁹⁷ This is not too surprising as it is significantly more challenging to activate an sp^3 C–H rather than an sp^2 C–H bond.⁹⁶



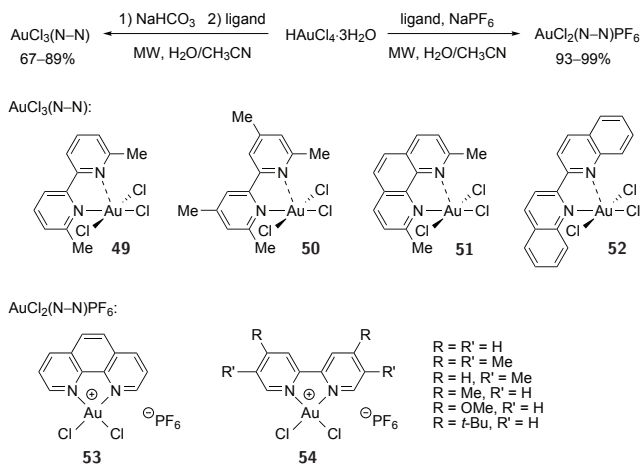
Scheme 1.14: Synthesis of cyclometalated Au(III) complex $\text{AuCl}_2(\text{tpy})$ using microwave heating.⁹⁷

In addition to the cyclometalated gold(III) complexes bearing chelated C–N ligands, some gold(III) complexes bearing bipyridine (bipy) ligands were also synthesised using microwave technology (Scheme 1.16).^{97,102} When the bipyridines were unsubstituted in the 6 and 6' positions (*ortho* to N), the expected four co-



Scheme 1.15: Cyclometalated Au(III) complexes bearing a six-membered ring chelate. **47** did not cyclometalate using microwave heating or under TGA.⁹⁷

ordinate gold(III) complexes resulted.⁹⁷ If however the 6 and 6' positions were substituted, pentacoordinated complexes resulted where one of the Au–N bonds were significantly longer in the solid-state whereas in solution at room temperature an average structure was observed.¹⁰² Neutralisation of the gold acid, HAuCl_4 , is frequently achieved with the strong base NaOH . The microwave procedure developed by Shaw uses the weaker base NaHCO_3 as it can be added until no further gas evolves to minimise the possibility of addition of too much base, as a basic solution can lead to decomposition to metallic gold.⁹⁷ The microwave procedure to synthesise $\text{AuCl}_2(\text{bipy})\text{PF}_6$ (**54**, $\text{R} = \text{R}' = \text{H}$) has since been used by Atwood *et al.*¹⁰³



Scheme 1.16: Au(III) complexes from microwave synthesis bearing bipy ligands.^{97,102}

Alkylation and arylation of cyclometalated gold(III) complexes is another matter that has proved difficult; reduction to gold(0) often being the outcome.¹⁰⁴ In

1907, Pope and Gibson alkylated AuBr_3 with ethyl magnesium bromide starting from 22 g of auric bromide which yielded 2–3 g of AuBrEt_2 (about 15%) and metallic gold.¹⁰⁵ As previously mentioned, reduction to gold(0) can often be apparent by change of colour to different shades of purple to black. During the work presented in this thesis the author has experienced that small amounts of metallic gold can alter the appearance of solids or solutions of organogold(III) compounds dramatically. The topic of alkylation and arylation will be discussed in Chapter 2 and reduction to gold(0) will be discussed briefly in Chapter 3.

Chapter 2

Synthesis of Cyclometalated Gold(III) Complexes

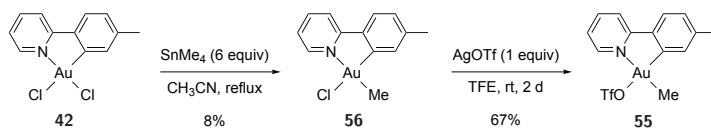
2.1 General Introduction

In this chapter, the results published in Paper I¹⁰⁶ (Appendix) will be discussed, some of the results from Paper II¹⁰⁷ are also included here, as well as some unpublished results.

Transmetalation from organomercury compounds has been the traditional route to access different cyclometalated gold(III) complexes,^{96,98} and is still frequently used.^{14,108,109} For cyclometalated gold(III) complexes to become more utilised as catalysts their availability must be improved. Developing mercury-free methods are therefore of the utmost importance.

Alkylation of cyclometalated gold(III) complexes is another issue that has proved challenging.¹⁰⁴ A monomethyl complex AuMe(tpy)OTf (**55-OTf**) with the labile triflate ligand (Scheme 2.1) was previously only accessible via methylation by tetramethyl tin. AuClMe(tpy) (**56**) was obtained in only 8% yield and the primary byproduct was metallic gold (62%).¹⁰⁴ Like organomercury compounds, organotin compounds are highly toxic,⁵⁰ and tetramethyl tin is particularly treacherous due to its high vapour pressure. Alternatives to the low yielding methylation procedure that use a toxic tin compound were highly desirable.

Having the new microwave method by Dr. Anthony P. Shaw⁹⁷ available, it



Scheme 2.1: Methylation of AuCl₂(tpy) with SnMe₄ to obtain monoalkylated AuClMe(tpy) that can be treated with a Ag(I) salt to give **55-OTf**.¹⁰⁴

provided a great entry point to prepare other cyclometalated gold(III) complexes. Working with tetrachloroauric acid (HAuCl₄·3H₂O), the gold(III) precursor used to synthesise AuCl₂(tpy) (**42**), can be a challenge on a humid day as it is highly hygroscopic, actually deliquescent so that the orange solid turns into a liquid. Hence when tetrachloroauric acid is weighed out, no dawdling is possible and when used as the limiting reagent, it can give slightly varying results. Another issue is that tetrachloroauric acid reacts with metal spatulas making it necessary to use plastic spatulas when working with this material. Handling Au(OAc)₃ is easier with respect to moisture sensitivity and regular metal spatulas can be used, but it is unfortunately rather sensitive to static electricity. In addition to the difficulties of weighing out the starting gold complex HAuCl₄·3H₂O, switching to Au(OAc)₃ will give a more soluble cyclometalated gold(III) complex than AuCl₂(tpy) (**42**), although Au(OAc)₃ itself is quite insoluble. AuCl₂(tpy) (**42**) is insoluble in water and nearly insoluble in organic solvents; dimethyl sulfoxide-*d*₆ (DMSO-*d*₆) was the only solvent that gave a decent ¹H NMR spectrum.

In Chapter 1, the use of both 2-phenylpyridine and 2-(*p*-tolyl)pyridine was mentioned as chelating C–N ligands for gold(III). There are at least two good reasons to choose tpy over ppy; the methyl group is a way of distinguishing between the two aromatic rings in X-ray crystallography thereby reducing crystallographic disorder⁹⁶ and it is a convenient handle especially in ¹H NMR spectroscopy.

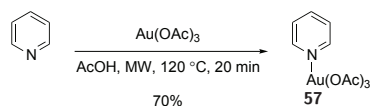
2.2 Initial Observations Regarding Au(OAc)₃

As will become evident later in the thesis, the decision to use Au(OAc)₃ as the gold(III) starting material rather than tetrachloroauric acid opened up to a variety of interesting chemistry. However, the research group had no prior knowledge of

this gold starting material which meant a great deal of trial and error for the author of this thesis. This section will therefore include material that is more initial studies rather than fully characterised systems.

Au(OAc)₃ is commercially available and a brownish, quite static sensitive powder. The solubility of the gold compound is rather limited, enough for ¹H NMR analysis and perhaps in catalytic systems but for synthesising new complexes the solubility is challenging at the least. It was thought that perhaps the limited solubility in water at room temperature would not be crucial for a microwave reaction that was performed at high temperature (160 °C) and hence slightly higher pressure than ambient. Attempts at reacting Au(OAc)₃ with tpy or different bipyridines in water however turned out unsuccessful.

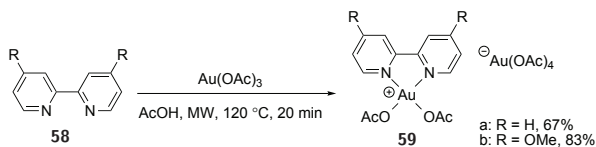
In the literature, Au(OAc)₃ has been used for catalysis in solvents such as acetic acid¹¹⁰ and 1,2-dichloroethane.⁶⁸ Acetonitrile and water were not good solvents for reactions starting from Au(OAc)₃. To utilise the protocol developed by Shaw,⁹⁷ the product should ideally precipitate out of solution after the microwave reaction. Acetic acid proved, as expected, to be a good solvent for synthesis of complexes based on Au(OAc)₃ although the solubility at room temperature is not exceptionally good. It was discovered that with microwave heating of Au(OAc)₃, temperatures above 120 °C were generally not the way to proceed, as this generated black precipitate whereas the desired compounds, usually light yellow, were not detected. Using acetic acid enabled synthesis of the complex Au(OAc)₃(py) (**57**) in 70% yield by microwave heating (Scheme 2.2).



Scheme 2.2: Synthesis of Au(OAc)₃(py) by microwave heating.

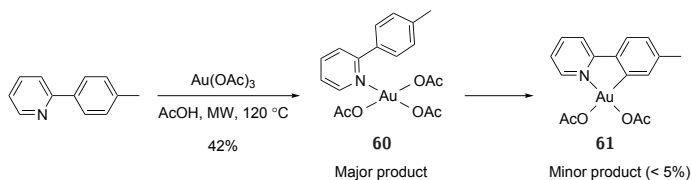
Acetic acid was a good solvent for synthesising the two bipyridine complexes **59a** and **59b** (Scheme 2.3). As no counter anion like PF₆⁻ (in the form of e.g. NaPF₆) was added, the anion was Au(OAc)₄⁻. **59b** was also synthesised using conventional heating, actually in better yields, probably due to a better work-up rather than the actual synthesis itself. Cinellu *et al.* showed that Au(OAc)₃ with

6,6'-dimethoxy-2,2'-bipyridine gave the 'rollover' product where gold is bonded through carbon in one ring and nitrogen in the other obtaining a C–N chelate¹¹⁰ rather than a N–N chelate, likely due to steric effects in the case of the 'rollover'.



Scheme 2.3: Synthesis of two $[\text{Au}(\text{OAc})_2(\text{bipy})][\text{Au}(\text{OAc})_4]$ complexes by microwave heating.

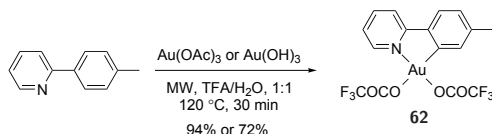
In an attempt to make the cyclometalated complex $\text{Au}(\text{OAc})_2(\text{tpy})$ (**61**), only the noncyclometalated complex $\text{Au}(\text{OAc})_3(2\text{-}(p\text{-tolyl})\text{pyridine})$ (**60**) resulted. Isolated **60** was dissolved in acetonitrile and heated at 120 °C yielding only a small amount of cyclometalated product **61**. Both traditional refluxing and microwave heating were attempted without much formation of the desired product. The reaction depicted in Scheme 2.4 was attempted using trifluoroethanol (TFE) as solvent apparently yielding neither **60** nor any cyclometalated product. In addition, water, water/acetonitrile mixtures and acetic acid were tried at different temperatures by microwave heating, as well as conventional heating rather than microwaves. The switch to the stronger acid trifluoroacetic acid (TFA) provided a breakthrough, described in the next section.



Scheme 2.4: Failure to cyclometalate $\text{Au}(\text{OAc})_3(\text{tpyH})$ in isolatable yields.

2.3 Synthesis and Characterisation of Au(OCOCF₃)₂(tpy)

Au(OAc)₃ turned out to be soluble in TFA and acetic acid; the only solvents found suitable by the author. Using acetic acid or acetic acid/water mixtures led only to small amounts of cyclometalated product, but high conversion to Au(OAc)₃(tpyH) (**60**). Use of TFA however, led to the cyclometalated complex Au(OCOCF₃)₂(tpy) (**62**), where the acetate ligands have been exchanged with trifluoroacetate. From Au(OAc)₃ and 2-(*p*-tolyl)pyridine in a mixture of water and TFA, it was possible to synthesise **62** in high yields by microwave heating. Crucial for the procedure to succeed, was the use of TFA as solvent, because Au(OAc)₃ is only sparingly soluble in organic solvents or water even at higher temperatures. After a quick work-up of precipitation, filtration and washing with water, the product was dried and was pure by elemental analysis.



Scheme 2.5: Synthesis of Au(OCOCF₃)₂(tpy) by microwave heating.

To prepare cyclometalated gold(III) complexes from Au(OH)₃ would be desirable as Au(OAc)₃ is quite expensive. The synthesis of **62** was later found to work from the less expensive Au(OH)₃. Synthesis of Au(OCOCF₃)₂(tpy) (**62**) from Au(OH)₃ instead of from Au(OAc)₃ does however have some issues associated with it. At some instances, Au(OH)₃ led to a muddy liquid with a slight green colour, whereas when the synthesis of **62** was performed from Au(OAc)₃ it always provided a light yellow powder of **62**. This might be due to the supplier, the procedure of making the Au(OH)₃ or some factor our research group is at the time being unaware of. Both of the commercially available gold(III) sources used, Au(OAc)₃ and Au(OH)₃, contained some metallic gold, as determined by powder X-ray diffraction.¹¹¹ Slightly different crystallinity for **62** was observed by powder X-ray diffraction depending on the purity of the complex.¹¹¹ Thermal heating of Au(OH)₃ and 2-(*p*-tolyl)pyridine in a 1:1 mixture of TFA and water (v/v) at reflux

for 3 hours afforded **62** in 70% yield, but here as well $\text{Au}(\text{OH})_3$ might have led to slightly impure material although pure by ^1H NMR. When the reproducibility issues connected with the synthesis of **62** from $\text{Au}(\text{OH})_3$ were evident, a return to $\text{Au}(\text{OAc})_3$ was made.

It was investigated if **62** could be synthesised from yet another gold(III) complex, HAuCl_4 (more precisely, $\text{HAuCl}_4 \cdot 3\text{H}_2\text{O}$), that would be less expensive than $\text{Au}(\text{OAc})_3$. If $\text{AuCl}_2(\text{tpy})$ (**42**) was heated in TFA it, unfortunately, did not produce **62**. In a hopeful attempt HAuCl_4 was dissolved in TFA (or AcOH) to see if any $\text{Au}(\text{OCOFCF}_3)_3$ (or $\text{Au}(\text{OAc})_3$) resulted, which it did not. Also, when the microwave reaction described in Scheme 2.5 was performed from HAuCl_4 in either TFA/water or only TFA solutions, it did not yield **62**.

The microwave procedure starting from $\text{Au}(\text{OAc})_3$ can also be used together with the *meta*-disubstituted ligand 2-(3,5-dimethylphenyl)pyridine.¹¹²

2.3.1 Characterisation

$\text{Au}(\text{OCOFCF}_3)_2(\text{tpy})$ (**62**) was characterised by ^1H , ^{19}F and ^{13}C NMR spectroscopy, mass spectrometry, elemental analysis and single-crystal X-ray diffraction. The ^{19}F NMR spectrum of **62** shows two singlets. In acetonitrile- d_3 , NOE interactions were observed between the CF_3 -groups and the protons *ortho* to N–Au and C–Au in the tpy ligand, enabling unambiguous assignment of the resonances in the ^{19}F NMR spectrum by a ^1H – ^{19}F HOESY experiment.

When **62** is dissolved in nonpolar solvents like dichloromethane- d_2 or benzene- d_6 , two sharp singlets are seen in the ^{19}F NMR for the two CF_3 -groups. However, in polar solvents like acetic acid- d_4 or acetonitrile- d_3 the singlet corresponding to the CF_3 -group *trans* to carbon in the chelating C–N ligand is now quite broad. A comparison of the ^{19}F NMR spectra recorded in different solvents is shown in Figure 2.1 and the measured widths at half-height are listed in Table 2.1. The broadness observed for the CF_3 -group *trans* to carbon in polar solvents could be that on the NMR timescale, the trifluoroacetate ligand *trans* to carbon is dissociating and reassociating in solution. What is apparent though, is that both ligands are in close proximity in space, meaning both are likely bonded to gold. This is seen by the correlations observed in the ^{19}F – ^{19}F NOESY spectrum ob-

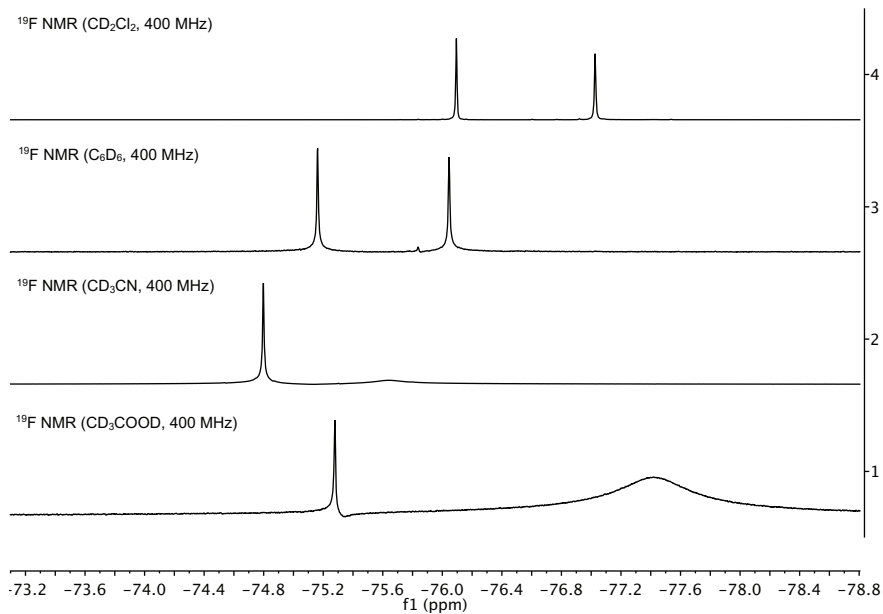


Figure 2.1: A comparison of the ^{19}F NMR spectra of $\text{Au}(\text{OCOCF}_3)_2(\text{tpy})$ (**62**) obtained in CD_3COOD (bottom), CD_3CN , C_6D_6 and CD_2Cl_2 (top).

Table 2.1: Measured half height peak width (ω) in ^{19}F NMR spectra.

Solvent	$\omega_{\text{downfield}}$	ω_{upfield}
CD_2Cl_2	3.5 Hz	4.0 Hz
C_6D_6	4.5 Hz	4.7 Hz
CD_3CN	4.3 Hz	124 Hz
CD_3COOD	4.3 Hz	281 Hz

tained for **62** in acetonitrile- d_3 shown in Figure 2.2. There are some examples of ^{19}F - ^{19}F NOESY spectra in the literature,¹¹³⁻¹¹⁸ although not many, and possible multidimensional fluorine NMR applications have been reviewed.¹¹⁹ Examples of ^{19}F - ^{19}F NOESY experiments for organometallic complexes are rare. One example is a ^{19}F - ^{19}F NOESY experiment that was conducted for a ruthenium complex.¹¹³

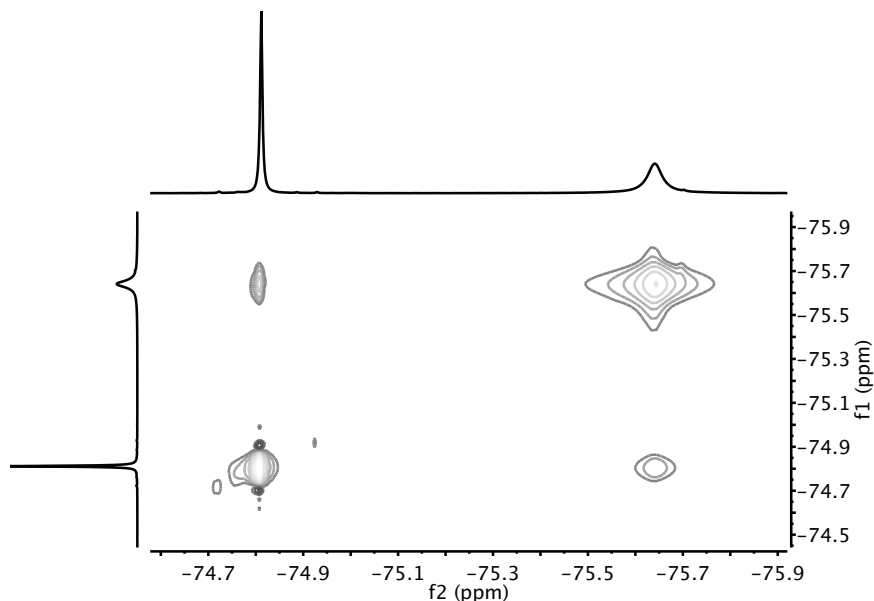


Figure 2.2: ^{19}F - ^{19}F NOESY spectrum (188 MHz, CD_3CN , QNP-probe) of $\text{Au}(\text{OCOCF}_3)_2(\text{tpy})$ (**62**). $d_8 = 0.30$ s, $n_s = 8$, $d_1 = 2.0$ s, $\text{aq}(\text{F2},\text{F1}) = 0.50$ s, 0.06 s, $\text{sw} = 10.85$ ppm. The broad singlet corresponds to the CF_3 -group *trans* to C.

As **62** turned out to be a valuable starting material as well as a complex interesting in itself, its solubility was investigated. $\text{Au}(\text{OCOCF}_3)_2(\text{tpy})$ (**62**) is soluble in a range of organic solvents, but insoluble in water. However, the ^1H NMR spectra in different solvents indicated (Figure 2.3) instability in chloroform- d (over time, so instability not apparent in Spectrum 6 in Figure 2.3), methanol- d_4 , DMSO- d_6 and acetone- d_6 as more species appear in solution.

X-Ray quality crystals of $\text{Au}(\text{OCOCF}_3)_2(\text{tpy})$ (**62**) were obtained by crystalli-

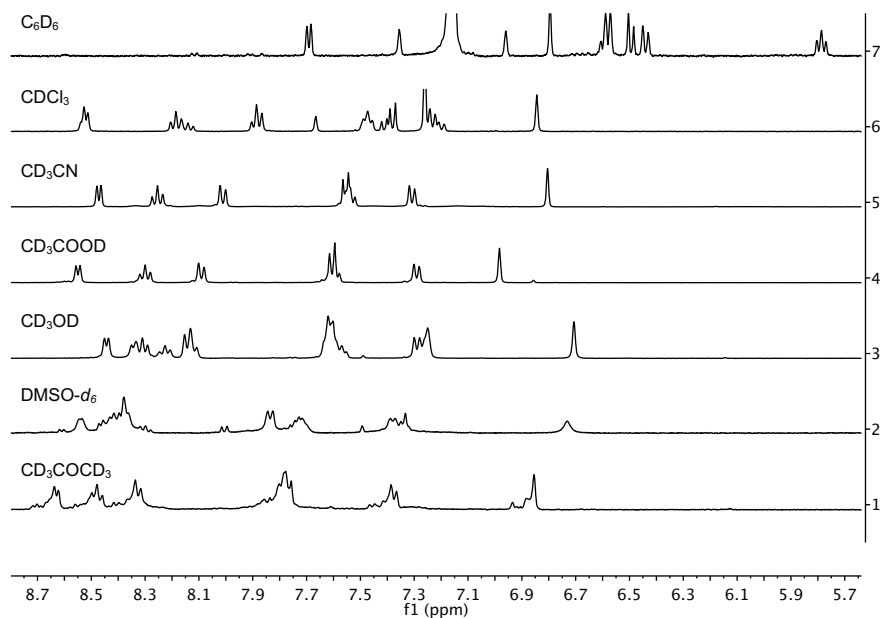


Figure 2.3: ^1H NMR spectra (400 MHz) of $\text{Au}(\text{OCOFC}_3)_2(\text{tpy})$ (**62**) comparing the aromatic region obtained in CD_3COCD_3 (bottom), $\text{DMSO-}d_6$, CD_3OD , CD_3COOD , CD_3CN , CDCl_3 and C_6D_6 (top).

sation from dichloromethane layered with pentane. The solid-state structure of $\text{Au}(\text{OCOCF}_3)_2(\text{tpy})$ (**62**, Figure 2.4) shows an elongation of the Au–O bond of the trifluoroacetate ligand *trans* to carbon compared to the trifluoroacetate ligand *trans* to nitrogen, 2.111(5) Å and 1.993(5) Å respectively, due to the greater *trans* influence of the tolyl group compared to the pyridine group. In addition, **62** shows similar bond lengths and angles to those reported for related cyclometalated gold(III) complexes,^{120–122} and has, as expected, close to square planar geometry with the normal deformations caused by the five-ring chelate structure. **62** has in particular very similar bond distances compared to the closely related complex $\text{Au}(\text{OAc})_2(\text{ppy})$ (**63**).¹²¹ The Au–C (1.995(7) Å) and Au–N (1.991(6) Å) bonds in **62** are slightly shorter than the corresponding ones in **63** (2.005(8) and 2.028(6) Å, respectively). This presumably reflects the greater *trans* influence of the acetate ligand over the trifluoroacetate, and supports the notion that the trifluoroacetate ligands will be more labile and therefore lead to enhanced reactivity. This is further supported by a longer Au–O bond distance for the Au–O bond *trans* to carbon in **62** than in $\text{Au}(\text{OAc})_2(\text{ppy})$ (**63**). Thus, the Au–O(3) distance in the trifluoroacetate ligand *trans* to carbon, is 2.111(5) Å in **62**, compared to 2.018(6) Å in **63**, and the Au–O(1) distance, to the trifluoroacetate ligand *trans* to nitrogen, is 1.993(5) Å *versus* 2.031(6) Å in **63**.

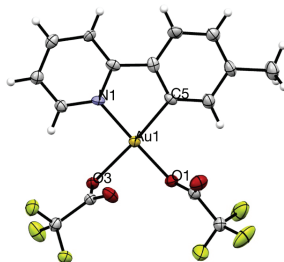


Figure 2.4: ORTEP view of the solid-state structure of $\text{Au}(\text{OCOCF}_3)_2(\text{tpy})$ (**62**) (106 K) with displacement ellipsoids at 50% probability. Selected bond distances (Å) and angles (deg): Au(1)–N(1), 1.991(6); Au(1)–C(5), 1.995(7); Au(1)–O(1), 1.993(5); Au(1)–O(3), 2.111(5); N(1)–Au(1)–C(5), 81.8(3); C(5)–Au(1)–O(1), 96.4(3); O(1)–Au(1)–O(3), 88.8(2); O(3)–Au(1)–N(1), 93.1(2); N(1)–Au(1)–O(1), 175.5(2); C(5)–Au(1)–O(3), 174.8(3).

In the solid-state structure of **62** there is an intermolecular Au...O interaction

between gold and the ether oxygen of the trifluoroacetate bonded *trans* to carbon in the C–N ligand (3.055 Å). Two and two molecules are in this way tightly associated. The shortest Au···Au distance is 4.243 Å, significantly longer than the sum of the van der Waals radii of 3.32 Å. There is also π -stacking apparent between one ‘dimer’ and another where the tolyl···pyridine distance is 3.759 Å. The interactions discussed are depicted in Figure 2.5.

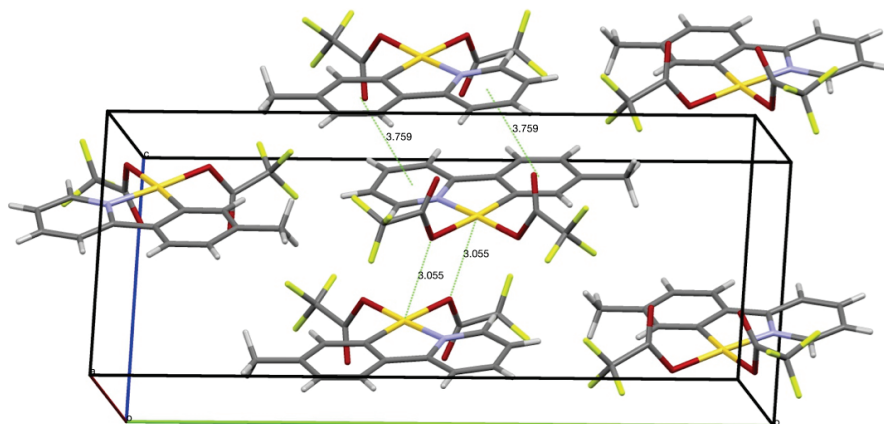


Figure 2.5: Interactions in the solid-state structure of $\text{Au}(\text{OCOCF}_3)_2(\text{tpy})$ (**62**).

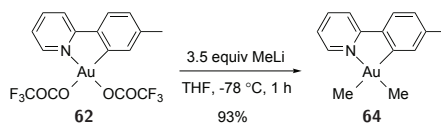
2.4 Alkylation and Arylation of Cyclometalated Gold(III) Complexes

The motivation for attempting alkylation was in part due to previous exploration in our group. A coordinatively labile monomethyl complex had previously been synthesised in low yields using SnMe_4 ,¹⁰⁴ as described in the introduction to this chapter.

2.4.1 Dialkylation And Diarylation

When $\text{Au}(\text{OCOCF}_3)_2(\text{tpy})$ (**62**) was treated with one equivalent of MeLi in toluene at room temperature, the initial light yellow solution turned black. The author

took this black colour as encouragement that something had happened. After removal of solvent, the black solid was suspended in dichloromethane and filtered through a pad of Celite to give a light yellow solution. The solvent was again removed and after several attempts at recrystallisation, a small amount of crystalline material that turned out to be the dimethylated $\text{AuMe}_2(\text{tpy})$ (**64**) was isolated in an extremely low yield. The procedure was repeated at 0 °C without improving the results but switching to a dry ice-acetone bath and using a higher excess of MeLi led to success. The solution stayed colourless upon addition of MeLi, but when allowed to warm up to room temperature the solution turned dark, almost black. The solvent was removed to give a white to grey powder. Removal of toluene *in vacuo* was cumbersome and THF was used as solvent instead. When using THF instead of toluene, the solution did not always turn dark upon warming to room temperature. Removal of solvent *in vacuo* afforded a grey powder that was redissolved in dichloromethane followed by one, or if needed two, filtrations through Celite. This gave a light yellow solution which yielded an analytically pure colourless powder of $\text{AuMe}_2(\text{tpy})$ (**64**) when solvent was removed. The reaction is depicted in Scheme 2.6.



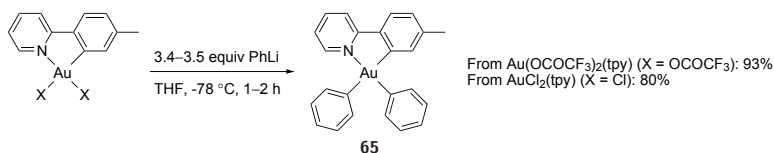
Scheme 2.6: Synthesis of $\text{AuMe}_2(\text{tpy})$.

To achieve perfectly clean product after filtration it seems necessary to allow the dichloromethane solution to turn dark or black before filtration through Celite. It is believed that small amounts of organogold are reduced by the excess MeLi, as gold nano particles are apparently formed when the solution is allowed to warm to room temperature. Attempts were made to add other quenching agents (e.g. isopropanol) before allowing the reaction to warm to room temperature, without much difference. However, the yield of the reaction is still high, even though some metallic gold formed by decomposition during work-up. Attempts with fewer equivalents of MeLi did not selectively yield a monoalkylated product, only mixtures. Since a good procedure to prepare **64** from $\text{Au}(\text{OCOCF}_3)_2(\text{tpy})$ (**62**) was

obtained, it was natural to see if it was possible to selectively synthesise **64** starting from $\text{AuCl}_2(\text{tpy})$ (**42**). With only a slight modification of the procedure (3.3 equiv MeLi, 3.5 h), **64** was obtained in 89% yield. Although longer reaction times seemed necessary from **42** compared to from **62**, it is probably not necessary with as much as 3.5 hours reaction time.

As the work-up procedure only requires a quick filtration through Celite, it is quite convenient but this also means that if impure starting material is used, the product will be impure too. Recrystallisation from dichloromethane layered with pentane is possible. Purification by column chromatography has not been investigated in any detail for the gold(III) complexes discussed herein.

Another complex made in an analogous fashion was $\text{AuPh}_2(\text{tpy})$ (**65**) by reacting PhLi with **62** (Scheme 2.7). The resulting solution after Celite filtration is quite dark. For an untrained eye, it is difficult to determine if the solution (or suspension) is purple from gold nanoparticles or if it is just the colour of **65** which is slightly purple, or more precisely maroon. To be certain that no metallic gold is present, an extra filtration can be performed.



Scheme 2.7: Synthesis of $\text{AuPh}_2(\text{tpy})$ from **62** or **42**.

A few other dialkylated and diarylated gold(III) complexes recently prepared by members of our research group are shown in Figure 2.6.^{123,124}

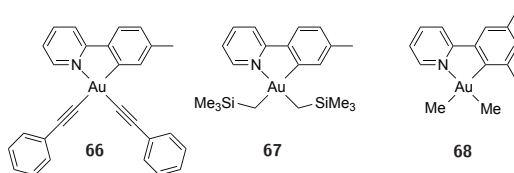


Figure 2.6: Other alkylated and arylated complexes that have recently been prepared in our laboratory.^{123,124}

2.4.1.1 Characterisation

AuMe₂(tpy) (**64**) was characterised by NMR, mass spectrometry and elemental analysis, and its solid-state structure was determined by single-crystal X-ray diffraction. As expected, the methyl group *trans* to carbon, the ligand with the stronger *trans* influence, appears at lower shift values than the methyl group *trans* to nitrogen, determined by ¹H–¹H NOESY spectroscopy. The ¹H NMR shifts for the methyl group *trans* to carbon and *trans* to nitrogen are 0.44 and 1.38 ppm, respectively, in chloroform-*d*, and 1.6 and 13.2 ppm in ¹³C NMR.

The solid-state structure of AuMe₂(tpy) (**64**) is shown in Figure 2.7. Consistent with the greater *trans* influence of the methyl group compared to the trifluoroacetate group in Au(OCOFCF₃)₂(tpy) (**62**), the Au–N bond is longer in AuMe₂(tpy) (**64**) (2.130(3) Å in **64** compared to 1.991(6) Å in **62**). The Au–N distance in **64** is however similar to other cyclometalated gold(III) complexes where a methyl group is *trans* to nitrogen (2.1092(19) and 2.1165(19) Å in AuMe(tpy)OTf (**55–OTf**) and AuMeOAc(tpy) (**69**), respectively).¹⁰⁴ The Au–C distance for the methyl *trans* to carbon is longer than the Au–C distance for the methyl *trans* to nitrogen in accordance with the stronger *trans* influence of the carbon *versus* the nitrogen of the chelating C–N ligand (2.134(4) Å *vs* 2.038(4) Å for *trans* to C and *trans* to N, respectively). The distance of 2.038(4) Å for Au–C(13), methyl *trans* to nitrogen, is within the range seen for other gold(III) methyl species where methyl

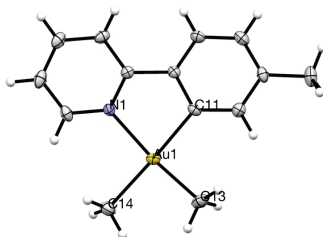


Figure 2.7: ORTEP view of the solid-state structure of AuMe₂(tpy) (**64**) (106 K) with displacement ellipsoids at 50% probability. Selected bond distances (Å) and angles (deg): Au(1)–N(1), 2.130(3); Au(1)–C(11), 2.062(4); Au(1)–C(13), 2.038(4); Au(1)–C(14), 2.134(4); N(1)–Au(1)–C(11), 80.01(13); C(11)–Au(1)–C(13), 93.86(16); C(13)–Au(1)–C(14), 89.13(17); C(14)–Au(1)–N(1), 97.04(15); N(1)–Au(1)–C(13), 173.78(14); C(11)–Au(1)–C(14), 176.03(17).

is *trans* to nitrogen (2.027(2) and 2.053(2) Å in AuMe(tpy)OTf (**55-OTf**) and AuMeOAc(tpy) (**69**), respectively).¹⁰⁴ The major intermolecular interaction in the solid-state structure of **64** is π -stacking between the aromatic rings; the distance between the tolyl and pyridine ring is 3.816 Å and the Au...pyridine ring distance is 3.821 Å. The shortest Au...Au distance is 4.955 Å, significantly longer than the sum of the van der Waals radii.

AuPh₂(tpy) (**65**) was characterised by ¹H, ¹³C NMR, mass spectrometry and elemental analysis. No crystals suitable for single crystal X-ray determination were obtained, although little effort was made to do so as the very similar complex AuPh₂(ppy) has been crystallographically characterised.¹²²

2.4.2 Monoalkylation And Monoarylation

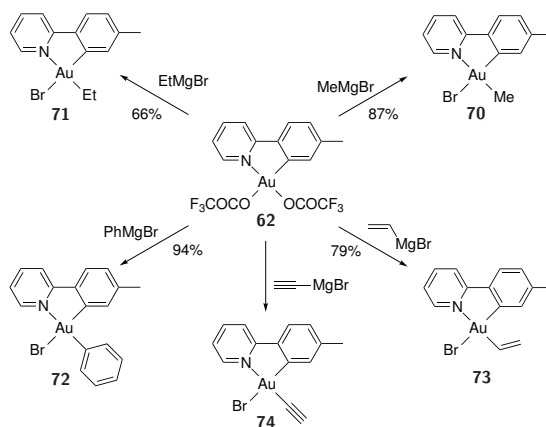
The next attempt made at alkylation and arylation was with Grignard reagents. Monoalkylation and arylation were achieved selectively, depicted in Scheme 2.8. In the work-up, it was necessary to wash with pH neutral water (neutralised with NaHCO₃) to remove magnesium salts and avoid decomposition, as the monoalkylated (as well as the dialkylated) complexes are sensitive to acid. It is worth noting that the alkyl or aryl group is situated *trans* to nitrogen, the ligand with the lowest *trans* effect. The trifluoroacetate ligand *trans* to carbon is replaced with a bromine, first suspected by the absence of fluorine by ¹⁹F NMR. As the procedure was high yielding, in the first attempt the material isolated after Celite filtration was clean by ¹H and ¹⁹F NMR (no signals in ¹⁹F) but was obtained in an amount twice as high as the theoretical yield. It was suspected that magnesium salts were the source of impurity. This issue was addressed by washing the isolated solid with water, which after the work-up yielded analytically pure material.

If the Grignard reagents are used in large excess, the dialkylated products are observable by ¹H NMR. Use of pure starting material in the reactions with Grignard reagents is crucial. Results from our group show that if impure starting material is used, it leads to a complex product mixture.¹¹¹ The synthesis of AuBrPh(tpy) (**72**) seems to be especially sensitive to the purity of **62**.¹¹¹ The elemental analysis for **72** was slightly off; 0.51% and 0.50% for carbon and hydrogen, respectively. However, it must be emphasised that the sample sent for elemental

analysis was not subjected to recrystallisation or any other extra purification.

Attempts at alkenylation and alkynylation with vinylmagnesium bromide and ethynylmagnesium bromide gave the desired products $\text{AuBr}(\text{CHCH}_2)(\text{tpy})$ (**73**) and $\text{AuBr}(\text{CCH})(\text{tpy})$ (**74**, Scheme 2.8) based upon the NMR data obtained as well as single crystal X-ray diffraction.

An attempt at monoalkylation of $\text{AuCl}_2(\text{tpy})$ (**42**) using 2.9 equivalents of methyl lithium led to a mixture of monomethylated (**70**) and dimethylated (**64**) product in a 8:2 ratio. Fine tuning the reaction conditions to achieve selective monoalkylation should be possible, but only limited investigations were performed.



Scheme 2.8: Monoalkylation of $\text{Au}(\text{OCOCF}_3)_2(\text{tpy})$, using 1.4–2.1 equiv Grignard reagents at -78°C for 1 h followed by 1 h at rt.

2.4.2.1 Characterisation

NOE interactions were observed between the Au–alkyl or Au–aryl and the hydrogen *ortho* to gold and tolylMe on the aryl ring, hence it could be determined that the alkyl or aryl is *cis* to carbon in the chelated C–N ligand. The resonances for the AuMe group in $\text{AuBrMe}(\text{tpy})$ (**70**) appear at 1.62 and 8.4 ppm in ^1H and ^{13}C NMR, respectively, which correspond well with the chemical shifts observed for the AuMe *cis* to carbon in $\text{AuMe}_2(\text{tpy})$ (**64**) of 1.38 and 13.2 ppm. The fourth ligand bound to gold(III) was determined by mass spectrometry by observing the

mass peak including the distinctive pattern of the two bromine isotopes.

Structures based on X-ray analyses were obtained for all the complexes depicted in Scheme 2.8 and are shown in Figure 2.8 and Figure 2.9, confirming the stereochemistry assigned by ^1H - ^1H NOESY. All seven complexes in Table 2.2 have close to square planar geometry as expected for gold(III) complexes (**75** is included in the table, but discussed in Section 2.4.3).

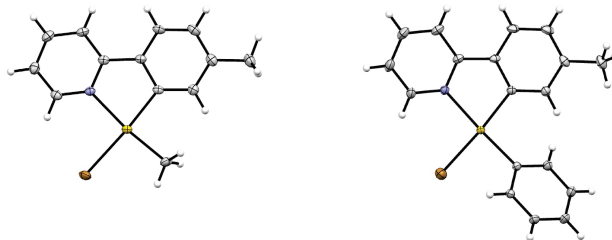


Figure 2.8: ORTEP view of the solid-state structures of AuBrMe(tpy) (**70**) and AuBrPh(tpy) (**72**) (100 and 293 K) with displacement ellipsoids at 50% probability. Selected bond distances (Å) and angles ($^\circ$) are given in Table 2.2.

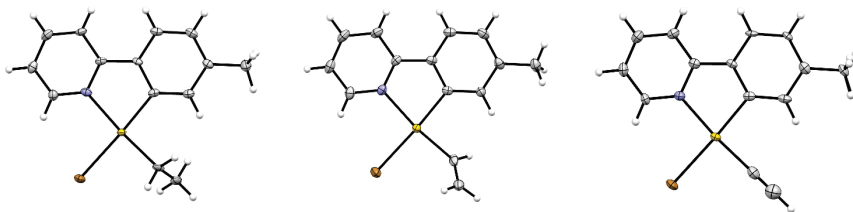


Figure 2.9: ORTEP view of the solid-state structures of AuBrEt(tpy) (**71**), AuBr(CH₂CH₂)(tpy) (**73**) and AuBr(CCH)(tpy) (**74**) (100 K) with displacement ellipsoids at 50% probability. Selected bond distances (Å) and angles ($^\circ$) are given in Table 2.2. A molecule of solvent (toluene) is omitted for clarity in the case of **74**.

Numerous attempts at growing X-ray quality crystals of **73** and **74** were performed. There is a good article describing crystal growth techniques for obtaining X-ray quality crystals of small molecules by Spingler *et al.*¹²⁵ The paper describes possible solvent combinations as well as techniques such as solvent layering and vapour diffusion. For **74**, crystal growth from toluene was successful. Toluene can *via* π - π stacking help stabilise a solid-state structure, and the methyl group can in

Table 2.2: Selected bond distances (\AA) and angles ($^\circ$) for AuMe₂(tpy) (**64**), AuBrMe(tpy) (**70**), AuBrPh(tpy) (**72**), AuBrEt(tpy) (**71**), AuBr(CHCH₂)(tpy) (**73**), AuBr(CCH)(tpy) (**74**)^a and *trans*-AuMePh(tpy) (**75**).

	64	70	72	71	73	74^a	75
Au-N	2.130(3)	2.1280(17)	2.121(3)	2.146(4)	2.136(4)	2.079(9)	2.118(5)
Au-C _{tolyl}	2.062(4)	2.023(2)	2.039(4)	2.029(5)	2.022(5)	2.047(10)	2.064(6)
Au-C _{transN}	2.038(4)	2.046(2)	2.015(3)	2.073(5)	2.037(6)	1.988(12)	2.006(6)
Au-Br	–	2.4964(2)	2.4774(5)	2.4899(5)	2.4881(6)	2.4977(11)	–
Au-C _{transC}	2.134(4)	–	–	–	–	–	2.152(7)
C _{transN} -C _X	–	–	–	1.464(8)	1.247(9)	1.039(17)	–
N-Au-C _{tolyl}	80.01(13)	81.26(7)	80.96(13)	81.32(18)	81.39(19)	81.5(4)	80.1(2)
N-Au-C _{transN}	173.78	173.54(8)	175.39(14)	173.34(18)	172.7(2)	174.6(4)	175.6(2)
N-Au-Br	–	95.00(5)	94.34(9)	95.41(11)	95.24(12)	95.9(2)	–
N-Au-C _{transC}	97.04(15)	–	–	–	–	–	95.6(2)
C _{transN} -Au-C _{tolyl}	93.86(16)	92.45(9)	95.31(14)	93.51(19)	91.5(2)	93.1(4)	96.4(3)
C _{tolyl} -Au-Br	–	175.83(6)	172.65(10)	175.41(14)	176.35(15)	177.3(3)	–
C _{tolyl} -Au-C _{transC}	176.03(17)	–	–	–	–	–	174.0(2)
C _{transN} -Au-Br	–	91.24(6)	89.64(11)	89.97(14)	91.92(16)	89.5(3)	–
C _{transN} -Au-C _{transC}	89.13(17)	–	–	–	–	–	88.1(2)
Au-C _{transN} -C _X	–	–	–	113.6(3)	127.3(5)	179.6(12)	–

C_{transN} indicates the C of the alkyl, aryl, vinyl or ethynyl group bound *trans* to N in the C-N chelate, whereas C_{transC} indicates the Me-group bound *trans* to the C of the tolyl. C_X indicates the C bonded to C_{transN} in **71**, **73** and **74**. The X-ray structures of **70–75** were obtained by Sigurd Øien at the University of Oslo. Crystal data and structure refinement are given in Experimental, Section 2.6. ^a **74** has toluene in the unit cell, **74**:0.5C₇H₈.

some cases give a more ordered system than if benzene is used. This was not the case for **74** as the tolyl is highly unordered, causing the need for restraints (in total 5-6 for the solvent and 2-6 for the ethynyl group). There is no π -stacking to be seen between the gold complex and the solvent molecule; the plane of the toluene moiety is almost perpendicular to the square plane of the gold(III) complex. The solid-state structure of AuBr(CCH)(tpy) (**74**) shows a linear coordination of the ethynyl group (Figure 2.9), a Au-C-C bond angle of $179.6(12)^\circ$. The corresponding bond angles in AuBr(CHCH₂)(tpy) (**73**) and AuBrEt(tpy) (**71**) are $127.3(5)^\circ$ and $113.6(3)^\circ$, respectively. The C-C bond length in the ethynyl group in **74** is $1.039(17)$ Å and in the vinyl group in **73** it is $1.247(9)$ Å, while in the ethyl group in **71** it is $1.464(8)$ Å. The Au-C_{transN} distance in **71** is $2.073(5)$ Å, $2.037(6)$ Å in **73** and $1.988(12)$ Å in **74**, due to the change in hybridisation of the carbon from sp^3 to sp^2 to sp .

As can be seen from Table 2.2 the Au-N distance in complexes **64** and **70-74** is within 2.079 - 2.146 Å which is longer than for Au(OCOCF₃)₂(tpy) (**62**, $1.991(6)$ Å) where the ligand *trans* to nitrogen is trifluoroacetate, a ligand with a smaller *trans* influence. The Au-C_{tolyl} distance in **64** and **75** (C_{tolyl} *trans* to Me) is longer than the Au-N distance in **70-74** (C_{tolyl} *trans* to Br), due to the stronger *trans* influence of the methyl group. The Au-C_{Me} distance in AuBrMe(tpy) (**70**) is slightly longer than in AuMe₂(tpy) (**64**), distances being $2.046(2)$ and $2.038(4)$ Å respectively. This could be due to the higher *cis* influence¹ of bromine compared to methyl, elongating the Au-C_{Me} in **70** compared to **64** but as the opposite effect is observed for the Au-N bond steric factors might dominate. The Au-Br bond length in **70-74** decrease in the order of **74** > **70** > **71** > **73** > **72**, while the Au-C_{tolyl} bond length decreases in the order **74** > **72** > **71** > **70** > **73**. In this series of complexes, the *cis* influence is thus highest for ethynyl. The Au-N bond length decreases in the order of **71** > **73** > **70** > **72** > **74**. In this series of complexes, the *trans* effect is (in decreasing order): Et > CHCH₂ > Me > Ph > CCH.

AuBrMe(tpy) (**70**) shows π -stacking in the the solid-state between the tolyl and the pyridine ring (distances of 3.660 and 3.688 Å) leading to Au...Au distances

¹The *cis* influence in *trans*-Pt(PPh₃)₂ complexes were found by Manassero *et al.* to be, in order of decreasing *cis* influence: I > Cl > SePh, SPh, SET > NO₃ > AcO, NO₂ > H > Me > Ph.^{126,127}

of 3.787 Å. The stacking is depicted in Figure 2.10.

The observed packing in **72** is different (Figure 2.11); there is no Au...Au interaction (Au...Au, 5.843 Å) as the solid-state structure shows Au...pyridine distances of 3.810 Å and π -stacking between the tolyl ring and the pyridine ring (tolyl...pyridine 3.823 Å). The phenyl ring alternates which direction it points as opposed to the AuMe group in **70**. This is likely to accommodate the more sterically bulky phenyl group. The phenyl ring is not fully perpendicular to the square plane by gold(III) and the four atoms bonded to it (torsion angle of 62.25°).

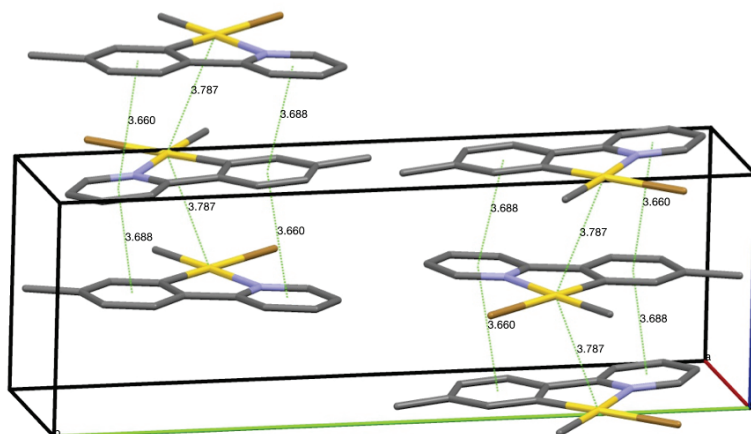


Figure 2.10: Packing in the solid-state structure of AuBrMe(tpy) (**70**).

In the solid-state structure of AuBrEt(tpy) (**71**), each gold atom shows π -stacking with one tolyl ring and one pyridine ring, Au...pyridine distances of 3.535 Å and Au...tolyl distances of 3.822 Å. The Au...Au distances are 5.505 Å. The stacking of **71** is depicted in Figure 2.12. AuBr(CHCH₂)(tpy) (**73**) shows the same stacking as in **71**; Au...pyridine distances of 3.689 Å and Au...tolyl distances of 3.742 Å and Au...Au distances of 5.383 Å. The packing in AuBr(CCH)(tpy) (**74**) is dominated by π - π stacking with tolyl...pyridine distances of 3.724 Å, which lead to a Au...tolyl stacking as well (3.761 Å). There are no aurophilic interactions (Au...Au distances of 5.298 Å).

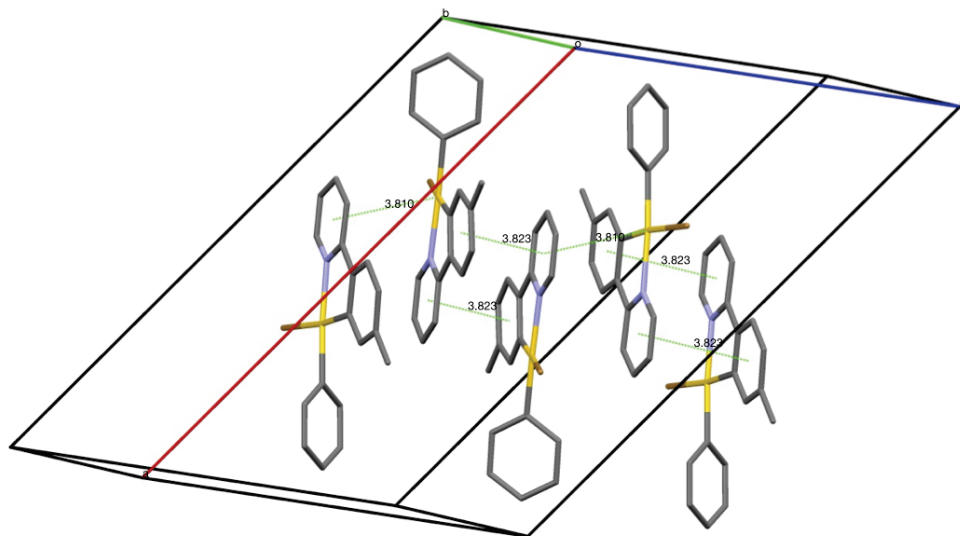


Figure 2.11: Packing in the solid-state structure of AuBrPh(tpy) (**72**).

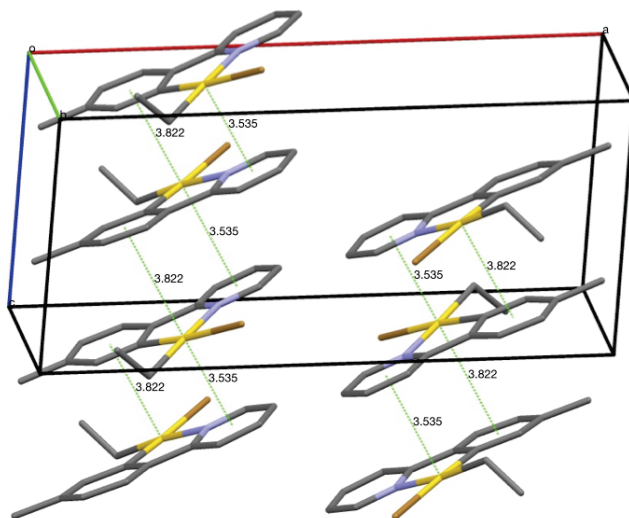
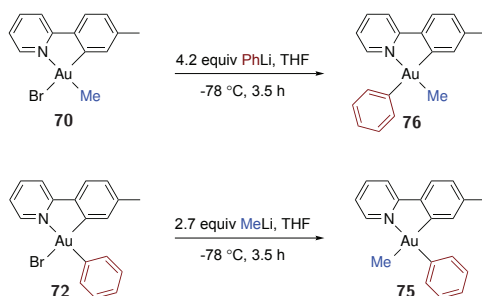


Figure 2.12: Packing in the solid-state structure of AuBrEt(tpy) (**71**).

2.4.3 Mixed Aryl And Alkyl Complexes

As mentioned, monoalkylated or -arylated cyclometalated gold(III) complexes were obtained using Grignard reagents. If the monoalkylated or -arylated complexes were subsequently reacted with a lithium reagent, a mixed complex could be obtained; one ligand methyl the other phenyl. The stoichiometry of the lithium reagent was important as too much yielded dialkylated product, especially in the case of *trans*-AuMePh(tpy) (**75**), where ‘*trans*’ refers to having the phenyl group *trans* to the nitrogen of the C–N chelating ligand.



Scheme 2.9: Arylation and alkylation of the monoalkylated Au(III) complexes yielded mixed Me/Ph products in a selective fashion.

2.4.3.1 Characterisation

The methyl or phenyl group from the monomethylated or -phenylated complexes remained in the same position *trans* to nitrogen and the methyl or phenyl group introduced by RLi ended up *trans* to carbon. The ^1H NMR shift for the methyl group in **75** and **76** were 0.54 and 1.45 ppm, respectively. The resonance with the lowest shift value is expected to be the complex where methyl is *trans* to the carbon of the chelating C–N ligand. The stereochemistry around gold of **76** was further confirmed by ^1H – ^1H NOESY NMR, showing an NOE interaction between the methyl group and the 6²-H in the tolyl-group. For *trans*-AuMePh(tpy) (**75**) the solid-state structure was determined by single-crystal X-ray diffraction, clearly showing that the correct stereochemistry was assigned (Figure 2.13).

trans-AuMePh(tpy) (**75**) gives a tetragonal crystal system, which is rather unusual. The solid-state structure of **75** (Figure 2.13) shows the torsion angle between the plane of the phenyl group and the square planar gold(III), to be 67.91° . The Au–C_{Me} bond length in **75** is 2.006(6) Å, similar to 2.0038(4) Å in AuMe₂(tpy) (**64**) indicating limited *cis* influence between phenyl and methyl. The Au–C_{Ph} distance in **75** is slightly shorter than in AuBrPh(tpy) (**72**), indicating a small *cis* influence, but the difference is only 0.009 Å.

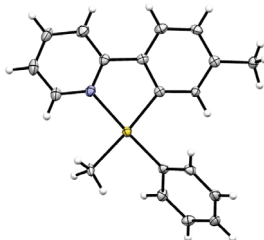


Figure 2.13: ORTEP view of the solid-state structure of *trans*-AuMePh(tpy) (**75**) (100 K) with displacement ellipsoids at 50% probability. Selected bond distances (Å) and angles ($^\circ$) are given in Table 2.2.

The packing in the tetragonal structure of **75** (Figure 2.14) is dominated by π -stacking, Au \cdots tolyl distances of 4.084 Å and pyridine \cdots tolyl distances of 4.160 Å. The shortest Au \cdots Au distance is 5.625 Å.

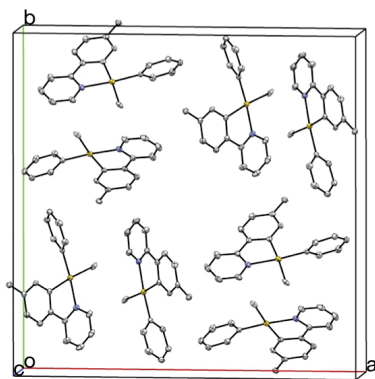


Figure 2.14: Packing in the solid-state structure of *trans*-AuMePh(tpy) (**75**).

2.5 Conclusions

In this chapter, the syntheses of several new cyclometalated gold(III) complexes have been shown. Selective monoalkylation or -arylation is the outcome when $\text{Au}(\text{OCOCF}_3)_2(\text{tpy})$ (**62**) is treated with Grignard reagents. However, treatment of $\text{Au}(\text{OCOCF}_3)_2(\text{tpy})$ (**62**) or $\text{AuCl}_2(\text{tpy})$ (**42**) with alkyl or aryl lithium reagents result in dialkylated or diarylated products. All reactions have good to excellent yields. Several of the cyclometalated gold(III) complexes discussed in this chapter show interesting reactivity which has been explored further and will be discussed in the following chapters. By the methods described in this chapter, the monoalkyl complex $\text{AuBrMe}(\text{tpy})$ (**70**) was obtained without use of toxic organotin reagents.

$\text{AuBr}(\text{CHCH}_2)(\text{tpy})$ (**73**) is an example of a gold(III) vinyl complex, which were discussed in Chapter 1 (Section 1.2) because vinyl gold complexes are proposed intermediates in gold catalysis. A gold(III) ethynyl complex was also prepared by the same method. Cyclometalated gold(III) complexes with one methyl and one aryl ligand were possible by monoalkylation or monoarylation with Grignard reagents, followed by arylation or alkylation by a lithium reagent.

2.6 Experimental

The syntheses of the gold(III) complexes mentioned in this chapter that have not been published in Paper I¹⁰⁶ (Appendix) are included here.

General Experimental Methods

$\text{Au}(\text{OAc})_3$ was purchased by Alfa Aesar. CH_2CHMgBr and HCCMgBr were purchased from Sigma-Aldrich and used as received. Acetic acid, CHCl_3 and NMR solvents were used as received. CH_2Cl_2 , Et_2O and THF were dried by use of the solvent purification system MB SPS-800 from MBraun. All reactions were performed with magnetic stirring, including microwave reactions. The microwave oven used was of the type Milestone MicroSYNTH with a rotor of the type SK-10. Unless otherwise stated, all reactions were performed anhydrous under argon, except when performed in the microwave. With the Grignard reagents, pH neutral distilled water neutralised with NaHCO_3 was used for washing. NMR spectra were recorded on a Bruker Avance DPX200 operating at 200 MHz (^1H) and AVII400 operating at 400 MHz (^1H). Mass spectrometry was performed

with a Waters Q-TOF-2 (ESI) instrument.

Au(OAc)₃(py) (57)

A solution of Au(OAc)₃ (0.096 g, 0.26 mmol, 1.0 equiv) and pyridine (22 μ L, 0.25 mmol, 1.0 equiv) in AcOH (15 mL) was heated in the microwave oven at 120 °C for 20 min to give a grey solution. After the solvent was removed *in vacuo*, the resulting solid was dissolved in CHCl₃, filtered through Celite and layered with Et₂O. Over night in the fridge, yellow crystals of **57** were formed in 70% yield (0.082 g). ¹H NMR (200 MHz, CDCl₃): δ 8.79 (dd, J = 6.7, 1.5 Hz, 2H), 8.08 (dddd, J = 7.7, 7.7, 1.5, 1.5 Hz, 1H), 7.71–7.54 (m, 2H), 2.09 (s, 3H), 1.97 (s, 6H). MS (ESI in CH₃CN): m/z 929.1 (15%, [2M+Na]⁺), 476.0 (100%, [M+Na]⁺), 394.1 (5%).

[Au(OAc)₂(bipy)][Au(OAc)₄] (59a)

A solution of Au(OAc)₃ (0.098 g, 0.25 mmol, 1.0 equiv) and 2,2'-bipyridine (0.041 g, 0.25 mmol, 1.0 equiv) in AcOH (10 mL) was heated in the microwave oven at 120 °C for 20 min. The light yellow solution was dried *in vacuo* and the crude product was recrystallised from CHCl₃ and Et₂O to yield 0.076 g (67%) as yellow plates. ¹H NMR (200 MHz, CD₃CN): δ 8.66–8.63 (m, 2H), 8.58–8.47 (m, 4H), 8.01–7.93 (m, 2H), 2.21 (s, 6H), 1.87 (s, 12H). MS (ESI+ in CH₃CN): m/z 471.1 (100%, M⁺), 457.1 (5%). MS (ESI- in CH₃CN): m/z 433.2 (100%, Au(OAc)₄⁻).

[Au(OAc)₂(bipy^{OMe})] [Au(OAc)₄] (59b)

By microwave: A solution of Au(OAc)₃ (0.098 g, 0.25 mmol, 1.0 equiv) and 4,4'-dimethoxy-2,2'-bipyridine (0.055 g, 0.26 mmol, 1.0 equiv) in AcOH (10 mL) was heated in the microwave oven at 120 °C for 20 min. This resulted in a yellow solution where solvent was removed *in vacuo*, the residue was taken up in CHCl₃ and filtered through Celite. The solution was concentrated *in vacuo*, layered with Et₂O and left in the fridge. This yielded crystals of **59b** in 83% yield (0.10 g). Thermal: A solution of Au(OAc)₃ (0.094 g, 0.25 mmol, 1.0 equiv) and 4,4'-dimethoxy-2,2'-bipyridine (0.055 g, 0.25 mmol, 1.0 equiv) in AcOH (9.0 mL) was heated in at 80 °C for 2.5 h. Solvent was removed *in vacuo*, the brown residue was taken up in CHCl₃ and filtered through Celite. The solvent was removed *in vacuo* and the product was washed with Et₂O. This yielded **59b** in 92% yield (0.11 g). ¹H NMR (200 MHz, CDCl₃): δ 9.45 (d, J = 2.9 Hz, 2H), 8.10 (d, J = 7.0 Hz, 2H), 7.16 (dd, J = 7.0, 2.8 Hz, 2H), 4.31 (s, 6H), 2.24 (s, 6H), 1.93 (s, 12H). MS (ESI+ in CH₃CN): m/z 531.1 (100%, M⁺), 454.1 (5%). MS (ESI- in CH₃CN): m/z

433.0 (30%, Au(OAc)₄⁻), 403.3 (5%), 266.9 (100%).

Au(OAc)₃(tpyH) (**60**)

A solution of Au(OAc)₃ (0.374 g, 1.00 mmol, 1.00 equiv) and 2-(*p*-tolyl)pyridine (175 μ L, 1.00 mmol, 1.00 equiv) in AcOH (30.0 mL) was heated in the microwave oven at 120 °C for 30 min. After the reaction, the light yellow solution was dried *in vacuo*, and the crude product was recrystallised from CHCl₃ and Et₂O to yield 0.225 g (42%) as yellow crystals. The product was slightly impure. ¹H NMR (200 MHz, CDCl₃): δ 9.21 (dd, *J* = 6.0, 1.2 Hz, 1H), 8.11–7.89 (m, 3H), 7.69–7.56 (m, 1H), 7.56–7.40 (m, 3H), 2.48 (s, 3H), 2.00 (s, 3H), 1.86 (s, 6H). MS (ESI in CH₃CN): *m/z* 566.1 (100%, [M+Na]⁺).

AuBr(CHCH₂)(tpy) (**73**)

A solution of **62** (0.101 g, 0.172 mmol, 1.0 equiv) in THF (10 mL) was cooled in a dry ice/acetone bath, and CH₂CHMgBr (1.0 M in THF, 0.24 mL, 0.24 mmol, 1.4 equiv) was added in one portion. The solution stayed light yellow after addition and was stirred for 1 h at -78 °C and then at rt for 1 h. While warming to ambient temperature, the reaction mixture cleared up to a light yellow solution and then turned black. THF was removed *in vacuo*. The resulting solid was dissolved in CH₂Cl₂ (30 mL) and washed with distilled water (pH = 7, 3 x 25 mL). The organic phase was dried over MgSO₄ and filtered through Celite to give a light yellow solution, and solvent was removed *in vacuo* to yield **73** as a light yellow powder in 79% yield (0.064 g). ¹H NMR (400 MHz, CD₂Cl₂): δ 9.54 (dd, *J* = 5.7, 1.5 Hz, 1H), 8.00 (ddd, *J* = 7.8, 7.8, 1.6 Hz, 1H), 7.91 (d, *J* = 8.1 Hz, 1H), 7.64 (d, *J* = 7.9 Hz, 1H), 7.48 (s, 1H), 7.46–7.41 (m, 1H), 7.20 (d, *J* = 7.9 Hz, 1H), 6.74 (dd, *J* = 16.5, 8.8 Hz, 1H), 6.11 (d, *J* = 8.8 Hz, 1H), 5.56 (d, *J* = 16.5 Hz, 1H), 2.41 (s, 3H). ¹³C NMR (101 MHz, CD₂Cl₂): δ 149.75, 142.79, 141.44, 137.11, 133.28, 129.06, 125.49, 124.38, 122.10, 120.15, 22.16. The quaternary C were not observed even with ns = 4k as the solubility was limited. X-Ray crystallographic data included in Table 2.6, *vide infra*.

AuBr(CCH)(tpy) (**74**)

The published procedure was followed,¹⁰⁶ except the product was not fully purified and hence only ¹H NMR is reported. ¹H NMR (400 MHz, CDCl₃): δ 9.90–9.66 (m, 1H), 8.07 (ddd, *J* = 8.1, 7.4, 1.6 Hz, 1H), 8.02 (dd, *J* = 1.7, 0.8 Hz, 1H), 7.89 (d, *J* = 7.9 Hz, 1H), 7.52 (d, *J* = 8.0 Hz, 1H), 7.45 (ddd, *J* = 7.4, 5.7, 1.5 Hz, 1H), 7.24–7.19 (m, 1H), 2.83 (s, 1H), 2.46 (s, 3H). X-Ray crystallographic data included in Table 2.7, *vide infra*.

***cis*-AuMePh(tpy) (76)**

A solution of AuBrMe(tpy) (**70**) (0.053 g, 0.12 mmol, 1.0 equiv) in THF (3.0 mL) was cooled in a dry ice/acetone bath, and then PhLi (0.90 mmol, 4.2 equiv) was added in one portion. The solution turned slightly yellow upon addition of PhLi, from an initial grey. The reaction mixture was stirred for 3.5 h at -78 °C and then allowed to warm up to rt. The resulting solid was dissolved in dry CH₂Cl₂ and filtered through Celite to give a yellow solution. CH₂Cl₂ was removed *in vacuo* to give a solid with a slightly purple colour (0.060 g). The product was slightly impure by ¹H NMR (hence higher weight of the product than it should, and likely salts present). ¹H NMR (400 MHz, CD₂Cl₂): δ 8.17 (d, *J* = 5.5 Hz, 1H), 7.94–7.86 (m, 2H), 7.74 (d, *J* = 8.1 Hz, 1H), 7.56 (s, 1H), 7.47 (d, *J* = 7.4 Hz, 2H), 7.28 (dd, *J* = 7.4, 7.4 Hz, 2H), 7.17–7.08 (m, 3H), 2.42 (s, 3H), 1.45 (s, 3H).

***trans*-AuMePh(tpy) (75)**

A solution of AuBrPh(tpy) (**72**) (0.056 g, 0.10 mmol, 1.0 equiv) in THF (3.0 mL) was cooled in a dry ice/acetone bath, and then MeLi (1.6 M in Et₂O, 0.18 mL, 0.29 mmol, 2.7 equiv) was added in one portion. There was no colour change upon addition of MeLi. The reaction mixture was stirred for 3.5 h at -78 °C and then allowed to warm to rt. The resulting grey solid was dissolved in dry CH₂Cl₂ and filtered through Celite to give a light yellow solution. CH₂Cl₂ was removed *in vacuo* to give a light yellow oil. The product (0.015 g, 30%) was obtained as a 1.0:0.3 mixture of **75** and the dialkylated product **64**. When the reaction was performed with 1.5 equiv of MeLi, the starting material:product ratio was 1.0:1.2 (by ¹H NMR). ¹H NMR (400 MHz, CD₂Cl₂): δ 8.76 (d, *J* = 5.6 Hz, 1H), 8.02–7.87 (m, 2H), 7.69 (dd, *J* = 8.2, 1.7 Hz, 1H), 7.40–7.32 (m, 3H), 7.21 (dd, *J* = 7.3, 7.3 Hz, 2H), 7.11 (d, *J* = 7.6 Hz, 1H), 7.03 (d, *J* = 8.0 Hz, 1H), 6.91 (s, 1H), 2.20 (s, 3H), 0.54 (s, 3H). X-Ray crystallographic data included in Table 2.8, *vide infra*.

Crystallographic Methods for 70–75

Crystals of **70–73** and **75** were obtained by crystallisation from dichloromethane layered with pentane in a freezer. Crystals of **74** were obtained by crystallisation from toluene in a freezer.

The data were acquired using a Bruker D8 Venture diffractometer with the APEX2 suite (v2013.6–2) (Bruker AXS Inc., Madison, Wisconsin, USA.), integrated with SAINT

V8.32B (*ibid.*), solved in the APEX2 suite and refined with SHELXL-2013.¹²⁸ The cif files were edited with enCIFer v1.4,¹²⁹ and molecular graphics were produced with Diamond v3.2i (Brandenburg, K. (2012). DIAMOND. Crystal Impact GbR, Bonn, Germany). In **74**, the solvent, toluene, is disordered and restraints were needed to ensure a convergent refinement.

Table 2.3: Crystal data and structure refinement for AuBrMe(tpy).

Complex	70	
Identification code	el-604_a	
Empirical formula	C ₁₃ H ₁₃ AuBrN	
Formula weight	460.12	
Temperature	100(2) K	
Wavelength	0.71073 Å	
Crystal system	Monoclinic	
Space group	P 2 ₁ /c	
Unit cell dimensions	a = 9.3840(5) Å	α = 90°
	b = 19.1314(11) Å	β = 109.4760(11)°
	c = 7.1463(4) Å	γ = 90°
Volume	1209.56(12) Å ³	
Z	4	
Density (calculated)	2.527 Mg/m ³	
Absorption coefficient	15.436 mm ⁻¹	
F(000)	848	
Crystal size	0.20 x 0.06 x 0.04 mm ³	
Theta range for data collection	2.302 to 34.969°	
Index ranges	-14 ≤ h ≤ 15	
	-30 ≤ k ≤ 30	
	-11 ≤ l ≤ 11	
Reflections collected	29255	
Independent reflections	5316 [R(int) = 0.0277]	
Completeness to theta = 25.242°	100.0%	
Max. and min. transmission	0.6270 and 0.1672	
Refinement method	Full-matrix least-squares on F ²	
Data / restraints / parameters	5316 / 0 / 147	
Goodness-of-fit on F ²	1.083	
Final R indices [I > 2σ(I)]	R ₁ = 0.0186, wR ₂ = 0.0385	
R indices (all data)	R ₁ = 0.0236, wR ₂ = 0.0397	
Extinction coefficient	0	
Largest diff. peak and hole	2.037 and -0.958 e.Å ⁻³	

X-Ray structure was obtained by Sigurd Øien, University of Oslo.

Table 2.4: Crystal data and structure refinement for AuBrEt(tpy).

Complex	71	
Identification code	EL-647_a	
Empirical formula	C ₁₄ H ₁₅ AuBrN	
Formula weight	474.15	
Temperature	100(2) K	
Wavelength	0.71073 Å	
Crystal system	Monoclinic	
Space group	P 2 ₁ /c	
Unit cell dimensions	a = 17.4594(12) Å	α = 90°
	b = 9.5449(7) Å	β = 95.1190(17)°
	c = 7.8849(5) Å	γ = 90°
Volume	1308.76(16) Å ³	
Z	4	
Density (calculated)	2.406 Mg/m ³	
Absorption coefficient	14.270 mm ⁻¹	
F(000)	880	
Crystal size	0.30 x 0.10 x 0.01 mm ³	
Theta range for data collection	2.342 to 30.033°	
Index ranges	-24<=h<=24	
	-13<=k<=13	
	-11<=l<=11	
Reflections collected	26931	
Independent reflections	3823 [R(int) = 0.0483]	
Completeness to theta = 25.242°	99.9%	
Max. and min. transmission	0.9296 and 0.2064	
Refinement method	Full-matrix least-squares on F ²	
Data / restraints / parameters	3823 / 0 / 156	
Goodness-of-fit on F ²	1.102	
Final R indices [I>2sigma(I)]	R ₁ = 0.0310, wR ₂ = 0.0630	
R indices (all data)	R ₁ = 0.0384, wR ₂ = 0.0653	
Extinction coefficient	0	
Largest diff. peak and hole	2.865 and -1.499 e.Å ⁻³	

X-Ray structure was obtained by Sigurd Øien, University of Oslo.

Table 2.5: Crystal data and structure refinement for AuBrPh(tpy).

Complex	72	
Identification code	EL605-P1_sym	
Empirical formula	C ₁₈ H ₁₅ AuBrN	
Formula weight	522.19	
Temperature	293(2) K	
Wavelength	0.71073 Å	
Crystal system	Monoclinic	
Space group	C2/c	
Unit cell dimensions	a = 20.7890(9) Å	$\alpha = 90^\circ$
	b = 13.4184(5) Å	$\beta = 127.876(3)^\circ$
	c = 13.8742(5) Å	$\gamma = 90^\circ$
Volume	3055.0(2) Å ³	
Z	8	
Density (calculated)	2.271 Mg/m ³	
Absorption coefficient	12.239 mm ⁻¹	
F(000)	1952	
Crystal size	0.139 x 0.099 x 0.097 mm ³	
Theta range for data collection	2.482 to 34.333°	
Index ranges	-32<=h<=32	
	-21<=k<=21	
	-21<=l<=22	
Reflections collected	45188	
Independent reflections	6402 [R(int) = 0.0353]	
Completeness to theta = 25.242°	99.9%	
Max. and min. transmission	0.9102 and 0.7231	
Refinement method	Full-matrix least-squares on F ²	
Data / restraints / parameters	6402 / 0 / 191	
Goodness-of-fit on F ²	1.066	
Final R indices [I>2sigma(I)]	R ₁ = 0.0278, wR ₂ = 0.0806	
R indices (all data)	R ₁ = 0.0320, wR ₂ = 0.0831	
Largest diff. peak and hole	2.659 and -4.128 e.Å ⁻³	

X-Ray structure was obtained by Sigurd Øien, University of Oslo.

Table 2.6: Crystal data and structure refinement for AuBr(CHCH₂)(tpy).

Complex	73	
Identification code	data_el-610_d	
Empirical formula	C ₁₄ H ₁₃ AuBrN	
Formula weight	472.13	
Temperature	100(2) K	
Wavelength	0.71073 Å	
Crystal system	Monoclinic	
Space group	<i>P</i> 2 ₁ / <i>c</i>	
Unit cell dimensions	a = 17.2353(10) Å	α = 90°
	b = 9.7537(6) Å	β = 94.524(2)°
	c = 7.5636(4) Å	γ = 90°
Volume	1267.54(13) Å ³	
Z	4	
Density (calculated)	2.474 Mg/m ³	
Absorption coefficient	14.731 mm ⁻¹	
F(000)	872	
Crystal size	0.20 x 0.10 x 0.04 mm ³	
Theta range for data collection	2.371 to 30.508°	
Index ranges	-24 ≤ h ≤ 24	
	-13 ≤ k ≤ 13	
	-10 ≤ l ≤ 10	
Reflections collected	25959	
Independent reflections	3873 [R(int) = 0.0327]	
Completeness to theta = 25.242°	99.9%	
Max. and min. transmission	0.7136 and 0.2445	
Refinement method	Full-matrix least-squares on F ²	
Data / restraints / parameters	3873 / 0 / 155	
Goodness-of-fit on F ²	1.189	
Final R indices [I > 2σ(I)]	R ₁ = 0.0307, wR ₂ = 0.0768	
R indices (all data)	R ₁ = 0.0336, wR ₂ = 0.0778	
Largest diff. peak and hole	4.082 and -1.655 e.Å ⁻³	

X-Ray structure was obtained by Sigurd Øien, University of Oslo.

Table 2.7: Crystal data and structure refinement for AuBr(CCH)(tpy).

Complex	74	
Identification code	data_EL717new2	
Empirical formula	C ₃₅ H ₂₂ Au ₂ Br ₂ N ₂	
Formula weight	1024.30	
Temperature	100(2) K	
Wavelength	0.71073 Å	
Crystal system	Monoclinic	
Space group	<i>C</i> 2/ <i>m</i>	
Unit cell dimensions	a = 21.0691(19) Å	α = 90°
	b = 6.6425(5) Å	β = 94.863(3)°
	c = 11.0452(9) Å	γ = 90°
Volume	1540.2(2) Å ³	
Z	2	
Density (calculated)	2.209 Mg/m ³	
Absorption coefficient	12.135 mm ⁻¹	
F(000)	948	
Crystal size	0.172 x 0.052 x 0.044 mm ³	
Theta range for data collection	2.565 to 25.023°	
Index ranges	-21 < h <= 24	
	-7 < k <= 7	
	-13 < l <= 13	
Reflections collected	6556	
Independent reflections	1492 [R(int) = 0.0558]	
Completeness to theta = 25.242°	97.5%	
Max. and min. transmission	1.0000 and 0.6697	
Refinement method	Full-matrix least-squares on F ²	
Data / restraints / parameters	1492 / 42 / 140	
Goodness-of-fit on F ²	1.067	
Final R indices [I > 2σ(I)]	R ₁ = 0.0345, wR ₂ = 0.0850	
R indices (all data)	R ₁ = 0.0382, wR ₂ = 0.0876	
Largest diff. peak and hole	5.330 and -0.869 e.Å ⁻³	

X-Ray structure was obtained by Sigurd Øien, University of Oslo. The unit cell contains 4 molecules of **74** and two molecules of toluene.

Table 2.8: Crystal data and structure refinement for AuMePh(tpy).

Complex	75	
Identification code	data_EL-609_a_a	
Empirical formula	$C_{19}H_{18}AuN$	
Formula weight	457.31	
Temperature	100(2) K	
Wavelength	0.71073 Å	
Crystal system	Tetragonal	
Space group	$I 4$	
Unit cell dimensions	a = 23.5247(11) Å	$\alpha = 90^\circ$
	b = 23.5247(11) Å	$\beta = 90^\circ$
	c = 5.7352(3) Å	$\gamma = 90^\circ$
Volume	3173.9(3) Å ³	
Z	8	
Density (calculated)	1.914 Mg/m ³	
Absorption coefficient	9.263 mm ⁻¹	
F(000)	1744	
Crystal size	0.175 x 0.174 x 0.163 mm ³	
Theta range for data collection	2.449 to 30.512°	
Index ranges	-33<=h<=22	
	-32<=k<=31	
	-8<=l<=7	
Reflections collected	12360	
Independent reflections	4794 [R(int) = 0.0228]	
Completeness to theta = 25.242°	99.4%	
Max. and min. transmission	0.7461 and 0.5696	
Refinement method	Full-matrix least-squares on F ²	
Data / restraints / parameters	4794 / 0 / 192	
Goodness-of-fit on F ²	1.156	
Final R indices [I>2sigma(I)]	R ₁ = 0.0200, wR ₂ = 0.0605	
R indices (all data)	R ₁ = 0.0207, wR ₂ = 0.0609	
Largest diff. peak and hole	1.936 and -0.617 e.Å ⁻³	

X-Ray structure was obtained by Sigurd Øien, University of Oslo.

Chapter 3

Reactivity of Cyclometalated Gold(III) Complexes

3.1 General Introduction

The results presented in this chapter are mainly unpublished and are included for the purpose of providing a greater picture of the reactivity of the cyclometalated gold(III) complexes presented in Chapter 2.

3.2 Reactivity of $\text{Au}(\text{OCOCF}_3)_2(\text{tpy})$

$\text{Au}(\text{OCOCF}_3)_2(\text{tpy})$ (**62**) was used to synthesise both mono- and dialkylated and -arylated complexes bearing the tpy ligand, discussed in Chapter 2. **62** reacted with ethylene, with formal insertion of ethylene observed, to be discussed in Chapter 4. Reactivity beyond alkylation/arylation and formal alkene/alkyne insertion will be discussed here.

As it was already observed that **62** in polar solvent has one sharp and one broad signal in ^{19}F NMR likely due to dissociation of a ligand, it was suspected that the complex could be reactive towards e.g. gases under higher pressure. At École Polytechnique Fédérale de Lausanne (EPFL), Switzerland facilities are available that are suitable for high pressure NMR (HP NMR) using sapphire NMR tubes that can withstand pressures up to 100 bar (for more experimental details, see

Experimental, Section 3.6). One of the complexes investigated using HP NMR was **62**. $\text{Au}(\text{OCOCF}_3)_2(\text{tpy})$ (**62**) in TFA-*d* does not react with carbon dioxide (40 bar, rt, 1 d), but it does however react with carbon monoxide (80 bar, rt, 1–3 d) forming two new species. As can be seen from the ^1H NMR spectra in Figure 3.1, the resolution is not optimal. The low resolution is in part due to the use of a

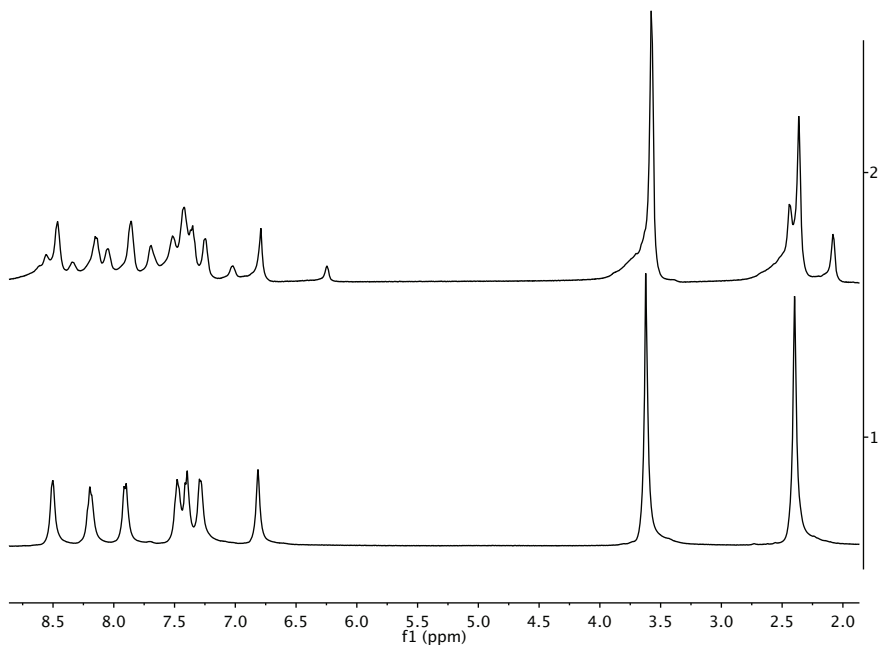


Figure 3.1: Reaction of $\text{Au}(\text{OCOCF}_3)_2(\text{tpy})$ (**62**) with CO (80 bar in TFA-*d*, 400 MHz). Bottom spectrum: Starting material, **62**, Top: After reaction with CO (rt, 3 d). ISTD ($\text{CH}_2\text{ClCH}_2\text{Cl}$) at ca 3.6 ppm, TFA-*d* at 11.5 ppm is omitted for clarity.

10 mm probe, but also as the facility usually obtains spectra in other solvents, the available shim files did not yield optimal resolution for dichloromethane- d_2 or TFA-*d*. Increase from a 5 mm probe, perhaps most commonly used in organic chemistry, to a 10 mm probe decreases the mass sensitivity.¹³⁰ Reaction of **62** with carbon monoxide in TFA-*d* led to formation of two new species seen by the appearance of two new singlets for the tolylMe and for the 6'-H (Ar-signal with lowest δ , Figure 3.1), but the main species was still the starting complex

62. Varying the temperature of the sample inside the probe of the NMR magnet from 0 °C to 59 °C did not change the product ratio. ^{13}C NMR did not shed any light upon the formed products and for the time being the nature of the two new species has not been determined. In 1930, Kharasch and Isbell showed that reaction of AuCl_3 with CO gave reduction to gold(I) with formation of $\text{Au}(\text{CO})\text{Cl}$ in up to 20% yield.¹³¹ Substantial decomposition to metallic gold was observed from AuCl_3 , although essentially quantitative yields were obtained from AuCl .¹³¹ $\text{Au}(\text{CO})\text{Cl}$ decomposed to metallic gold in the presence of alcohols, but was stable to acetic acid.¹³¹ In the case of **62** with CO, no metallic gold was observed, only a transparent yellow solution.

In dichloromethane- d_2 , **62** reacts with hydrogen (96 bar, rt, 1 d) to give reduction to metallic gold, observed by a gold coating of the sapphire NMR tube, see Figure 3.2. The thick coating in this case disabled the acquisition of a ^1H NMR spectrum. With a thin gold coating it is usually possible to acquire a decent ^1H NMR spectrum but in this case tuning and matching as well as locking on the solvent proved impossible. A change of solvent from dichloromethane- d_2 to TFA- d



Figure 3.2: Reduction of **62** with H_2 in a sapphire NMR tube led to gold coating.

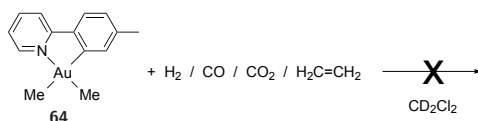
led to complete consumption of **62**, with formation of two new species observed by ^1H NMR when **62** was reacted with hydrogen (95 bar, rt, 2 d). Again, the two characteristic singlets for the tolylMe and 6'-H showed two new species. A slight coating on the tube walls indicated that some reduction to metallic gold took place here as well. It was not possible to deduce the nature of these species from the ^1H and ^{13}C NMR spectra.

3.3 Reactivity of $\text{AuMe}_2(\text{tpy})$

All the mono- and dialkylated species are sensitive to acid. In the case of $\text{AuMe}_2(\text{tpy})$ (**64**), the reactivity towards acids has been investigated in some depth and will be discussed in Section 3.3.3.

3.3.1 Reactivity Towards Gases

$\text{AuMe}_2(\text{tpy})$ (**64**) in dichloromethane- d_2 is unreactive towards gases such as hydrogen (96 bar, rt, 3–4 d), carbon monoxide (49 bar, rt, 2 d), carbon dioxide (30 bar, 50 °C, 18 h), and ethylene (48 bar, rt 3–4 d) (Scheme 3.1). These experiments were conducted using sapphire NMR tubes at EPFL in Lausanne.^{132–134}



Scheme 3.1: $\text{AuMe}_2(\text{tpy})$ in CD_2Cl_2 was unreactive towards high pressures of several gases (30–96 bar).

3.3.2 Reactivity Towards Oxygen Sources

$\text{AuMe}_2(\text{tpy})$ (**64**) is not particularly reactive towards oxygen. A J Young NMR tube with **64** in dichloromethane- d_2 was pressurised with 3 bar of oxygen and left at room temperature for a day without any reaction taking place. In benzene- d_6 , **64** pressurised with 3 bar of oxygen was quite stable at 80 °C for one day, 87% was still intact (by ISTD). After 2 days, more than half of the initial gold complex was

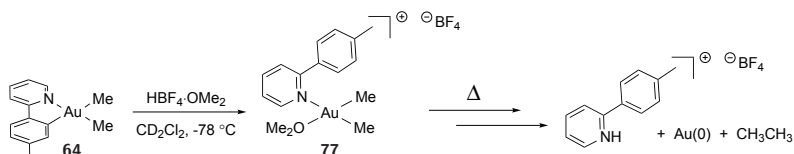
still in solution accompanied by apparent gold coating on the walls of the NMR tube. As no reaction took place, the radical initiator azobisisobutyronitrile (AIBN) was tried. AIBN is not compatible with halogenated solvents hence benzene-*d*₆ was used rather than dichloromethane-*d*₂. **64** in benzene-*d*₆, was added AIBN and pressurised with 3 bar oxygen. Neither standing at room temperature for 3 days nor heating at 60 °C for 6 hours gave any reaction. At 80 °C, **64** reacts with with AIBN and oxygen in benzene-*d*₆, and yielded what appeared to be two new gold complexes of unknown structure, based on the two sets of resonances in the aromatic region. The control experiment of **64** and AIBN in benzene-*d*₆ (80 °C, 7 d) showed no reaction between **64** and AIBN, but AIBN decomposes at higher temperatures to give many new resonances in ¹H NMR. The control experiment showed that **64** reacts with oxygen, in the presence of AIBN. Unfortunately, due to the decomposition of AIBN at higher temperatures, as expected for a radical initiator, it was difficult to determine the nature of the new gold species.

The experiments indicate that **64** has a high stability towards oxygen gas, consistent with what is observed handling the compound during work-up. Light however, is more of an issue, as the complex turns greyish to purple when left in the daylight over time. **64** in benzene-*d*₆ gave no immediate reaction with hydrogen peroxide at room temperature. No reaction was observed by ¹H NMR between **64** and water (in C₆D₆ or CD₂Cl₂ at rt). In both experiments, water was sparsely soluble in the organic solvent which means that mixing was not optimal.

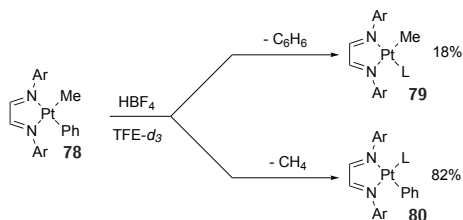
3.3.3 Reactivity Towards Acids

Whilst AuMe₂(tpy) (**64**) is unreactive towards several gases, it is however reactive towards acids. Addition of HBF₄ or HOTf to a solution of **64** at room temperature gave immediate protolytic cleavage of the Au-tpy bonds. If 2.2 equivalents of HOTf were added to a solution of **64** in dichloromethane-*d*₂ at -78 °C, selective protonolysis of the Au-C(*sp*²) bond was observed. The site of protonolysis was confirmed by the observed symmetry of the tolyl group, two inequivalent AuMe groups and the absence of methane. NOE interactions between the protons of one of the AuMe groups with the aromatic protons of tpyH suggest that tpyH is still coordinated to gold, now as a monodentate ligand bound through nitro-

gen. Presumably triflate occupies the fourth coordination site of gold(III). When $\text{HBF}_4 \cdot \text{OMe}_2$ is used instead, dimethyl ether occupies the fourth coordination site verified by NOE interactions between the AuMe and dimethyl ether, and between dimethyl ether and the tpyH. Below approximately -40°C only the sp^2 -C was cleaved, yielding $\mathbf{77}\text{-BF}_4$ (Scheme 3.2). This is the opposite of what has been observed for platinum(II).^{135,136} For the platinum complex $\text{Pt}(\text{N-N})\text{MePh}$ **78**, Bercaw *et al.* observed mainly protolytic cleavage of the sp^3 -C of the methyl group, rather than the sp^2 -C of the phenyl (Scheme 3.3).



Scheme 3.2: Protolytic cleavage of the Au-C(sp^2) bond of the tpy ligand in $\text{AuMe}_2(\text{tpy})$ at low temperature *via* $\mathbf{77}\text{-BF}_4$.



Scheme 3.3: Protonolysis of a platinum(II) complex,¹³⁵ L = TFE or H_2O .

If the gold(III) complex $\mathbf{77}\text{-BF}_4$ in dichloromethane- d_2 was allowed to warm to room temperature, it decomposed to ethane and metallic gold as well as 2-(*p*-tolyl)pyridinium (Scheme 3.2). It was verified by single-crystal X-ray diffraction that 2-(*p*-tolyl)pyridinium tetrafluoroborate was formed (Figure 3.3) and although not shown, the corresponding crystal structure with triflate as counteranion was also recorded. Ethane was presumably formed by reductive elimination from $\mathbf{77}\text{-BF}_4$ as reductive elimination of two ligands in a *cis* relationship usually happens readily for gold(III) alkyl complexes.¹³⁷⁻¹⁴⁰ The quite high stability of **64** is likely because the cyclometalated tpy ligand does not allow the necessary flexibility for

reductive elimination of ethane to occur. The necessary flexibility is present in **77-BF₄** where the tpy is only bound to gold through the nitrogen, hence reductive elimination to yield a gold(I) complex is feasible. Remember that gold(I) prefers a linear geometry, and tpy as a bidentate ligand is not able to accommodate this.

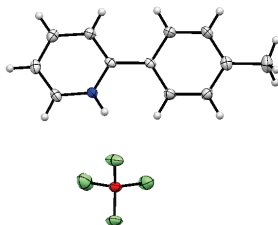
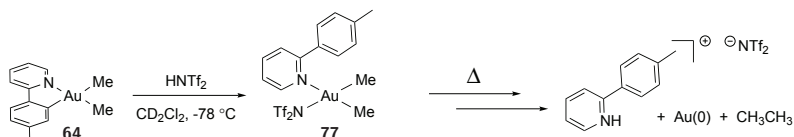


Figure 3.3: ORTEP view of 2-(*p*-tolyl)pyridinium tetrafluoroborate.

The decomposition of AuMe₂(tpyH)NTf₂ (**77-NTf₂**, Scheme 3.4) was studied by variable temperature ¹H NMR and showed that significant ethane extrusion took place between -10–0 °C, although it was evident at even lower temperatures (Figure 3.4, ethane at 0.85 ppm in CD₂Cl₂¹⁴¹). Between the 1st and 2nd spectrum in Figure 3.4, HNTf₂ was added, yielding 90–95% of AuMe₂(tpyH)NTf₂ (**77-NTf₂**, by ISTD). The sample was then left inside the NMR probe at -40 °C for 2 hours, which showed that **77-NTf₂** was stable at -40 °C. Increasing the temperature in the probe by 10 °C intervals showed that some ethane was formed already at low temperature but that somewhere between -10 and 0 °C, ethane formation started to dominate. From the protonation experiment it can be concluded that for short periods of time, handling of **77-NTf₂** at temperatures up to -10 °C is possible.

Reductive elimination from gold(III) alkyl complexes have been studied in depth in the 1970s by Kochi *et al.*⁷⁹ In several (trialkyl)gold(III)(triphenylphosphine) complexes, the methyl groups *cis* to each other were reductively eliminated to form the corresponding alkylgold(I) species *via* a dissociative mechanism that involved prior loss of the phosphine ligand.⁷⁹ One example of this reductive elimination is shown in Scheme 3.5, less than 5% of the cross-over product was obtained indicating an intramolecular mechanism.⁷⁹ Reductive elimination between alkyl groups in a *cis* relationship was observed. In the presence of excess triphenylphosphine the reductive elimination was significantly inhibited.⁷⁹



Scheme 3.4: Protolytic cleavage of the Au-C(*sp*²) of the tpy ligand in AuMe₂(tpy) at low temperature, here presumably *via* **77-NTf₂** that decomposes between -10 °C and 0 °C (Figure 3.4).

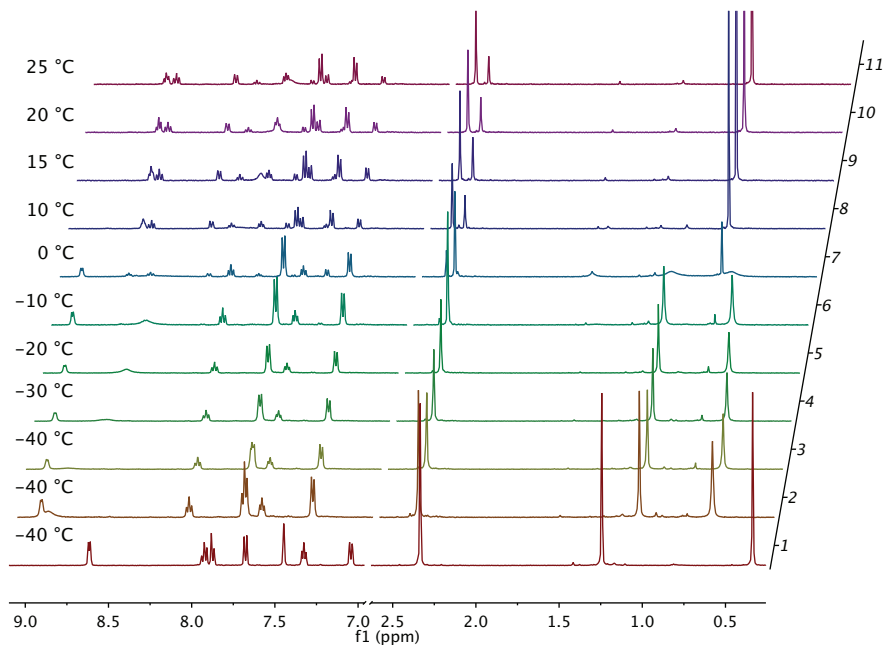
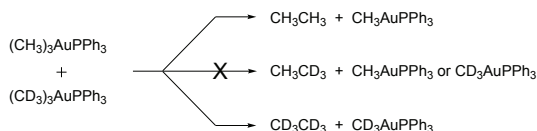
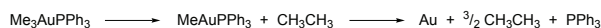


Figure 3.4: ¹H NMR (500 MHz, CD₂Cl₂) spectra showing decomposition of AuMe₂(tpyH)NTf₂ (**77-NTf₂**) with increasing temperature. Spectrum 1: Starting material, AuMe₂(tpy) (before acid addition), Spectrum 2: Immediately after acid addition, Spectrum 3: 2 h after acid addition. The region at 7.0–2.6 ppm contains only resonances from the ISTD CH₂ClCH₂Cl and residual solvent and is hence omitted to improve clarity, the ethane resonance is cut vertically in the top spectra. C₂H₆ in CD₂Cl₂ appears at 0.85 ppm at rt¹⁴¹ (C₂H₄ extrusion clearly visible in spectrum 6 and 7). All shifts are slightly temperature dependent.

The alkylgold(I)triphenylphosphine complex decomposed to metallic gold if excess triphenylphosphine was not added (Scheme 3.6). Kochi *et al.* claimed that alkenes derived from β -hydride elimination (e.g. ethylene when Et-groups are used) or alkanes derived from hydrogen transfer (e.g. methane in the case depicted in Scheme 3.6) are not important products in these reactions, leading to the conclusion that the decomposition of the gold(III)alkyl complexes happened *via* a dissociative mechanism.⁷⁹

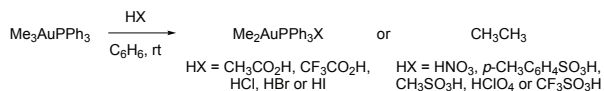


Scheme 3.5: Intramolecular reductive elimination in C₆D₆ at 80 °C with no cross-over, reported by Kochi *et al.*⁷⁹



Scheme 3.6: Decomposition of alkylgold(III) phosphine complexes without excess phosphine added, reported by Kochi *et al.*⁷⁹

Protonolysis of AuMe₂(tpy) (**64**) affords decomposition to metallic gold unless a stabilising ligand is added (*vide supra*). For the trialkylgold(III) complexes depicted in Scheme 3.7, protonolysis resulted in gold(III) complexes stable at room temperature when acids such as HCl, HBr, HI or acetic or trifluoroacetic acid were used, whereas with acids with less coordinating anions such as triflic acid, the gold(III) complex spontaneously eliminated ethane after formation of a new gold(III) alkyl complex.¹⁴²



Scheme 3.7: Protonolysis of Me₃AuPPh₃ with different acids gave methane and either a stable gold(III) alkyl complex or elimination of ethane, reported by Kochi *et al.*¹⁴²

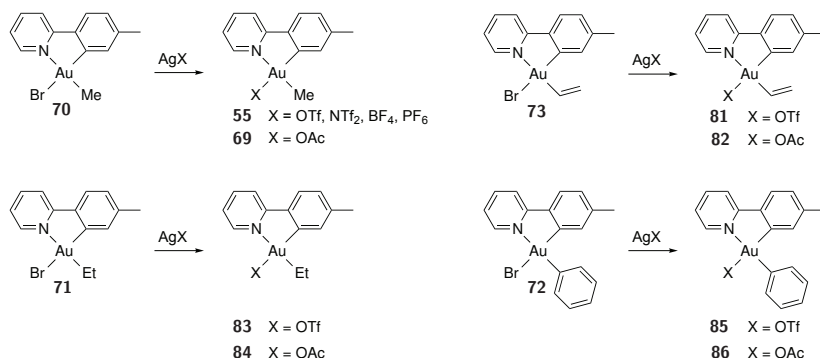
When AuMe₂(tpy) (**64**) was reacted with methyl triflate, ethane was observed by ¹H NMR. By electron ionisation mass spectrometry (EI MS), a fragment corresponding to tpy-Me was observed.

3.4 Reactivity of Monoalkylated and -Arylated Gold(III) Complexes

It was discovered that mildly acidic water gave slight decomposition of AuBrMe(tpy) (**70**) (Section 2.4.2). This instability towards acids was also observed for the other monoalkylated and monoarylated complexes of the type AuBrR(tpy).

3.4.1 Reactivity Towards Silver Salts

The monoalkylated species all react with silver(I) salts such as AgOAc, AgOTf, AgNTf₂, AgBF₄ and AgPF₆ and in the latter four cases, yielded a coordinatively labile ligand at gold(III). The initial screening was only performed on NMR scale, but the complexes AuMe(tpy)OTf (**55-OTf**) and AuPh(tpy)OTf (**85**) were synthesised from **70** and **72** on larger scale by another group member.¹¹¹ In this way it is possible to generate an ‘open’ coordination site at gold. A screening of **70**, **71**, **72** and **73** showed that all complexes reacted with AgOTf and AgOAc and the halide was abstracted (Table 3.1). The reactivity is shown in Scheme 3.8. Addition of AgOAc to **73** showed **82** and an additional minor species.



Scheme 3.8: *In situ* preparation of complexes of the type AuR(tpy)X with excess Ag(I) salts. In the case of wet solvents, H₂O can replace X.

Reaction of **70** with LiNTf₂ did not afford AuMe(tpy)NTf₂ (**55-NTf₂**), meaning the lithium salt could unfortunately not be used instead of the silver salt. A

desire to avoid silver in the reaction mixture, coupled with the high price of AgNTf₂ makes the lithium salt more desirable. Silver is known to be able to interact with gold, e.g. in gold(I) catalysis.^{143,144}

3.4.2 Reactivity Towards Gases

When AuMe(tpy)NTf₂ (**55-NTf₂**) generated *in situ* from AuBrMe(tpy) (**70**) and AgNTf₂ in dichloromethane-*d*₂ was pressurised with CO (40–45 bar, rt, 2 d), no reaction was observed.

3.4.3 Reactivity Towards Oxygen Sources

AuBrMe(tpy) (**70**) showed limited reactivity towards oxygen, similar to what was observed for AuMe₂(tpy) (**64**). In benzene-*d*₆, **70** was stable at 80 °C under 3 bar of oxygen for at least 25 days. A solution of **70** in dichloromethane-*d*₂ was pressurised with 3 bar oxygen and left at room temperature for a day without any reaction occurring. When AgPF₆ was added to the solution, abstraction of the halogen gave AuMe(tpy)PF₆ (**55-PF₆**). When pressurised with 3 bar oxygen, no reaction was observed at room temperature. AuBrMe(tpy) (**70**) was reacted with oxygen in the presence of AIBN to give subtle differences in the ¹H NMR spectrum (Figure 3.5) as well as the appearance of two new singlets at 3.74 ppm and 7.41 integrating to approximately 4 and 2, respectively, compared to the aromatic signals and the methyl groups. The same two singlets with similar intensities appeared when AuMe₂(tpy) (**64**) was treated with oxygen in the presence of AIBN, although a second species was also present in the reaction mixture of **64**. Neither of the two peaks were present when **64** was heated with AIBN as a control experiment. Unfortunately, we could not determine what this new species was and if it indeed was the same products starting from **70** as from **64**. It was clear that the aromatic regions were different, except for the singlet at 7.41 ppm, indicating different gold species at least. Attempts at growing crystals suitable for X-ray determination were however unsuccessful, both for the reaction from **70** and for the reaction from **64**.

Neither AuBrMe(tpy) (**70**) (CD₂Cl₂, 60 °C, 2 d) nor AuBrPh(tpy) (**72**) (C₆D₆, rt or CD₂Cl₂, 60 °C, 2–3 d) reacted with hydrogen peroxide.

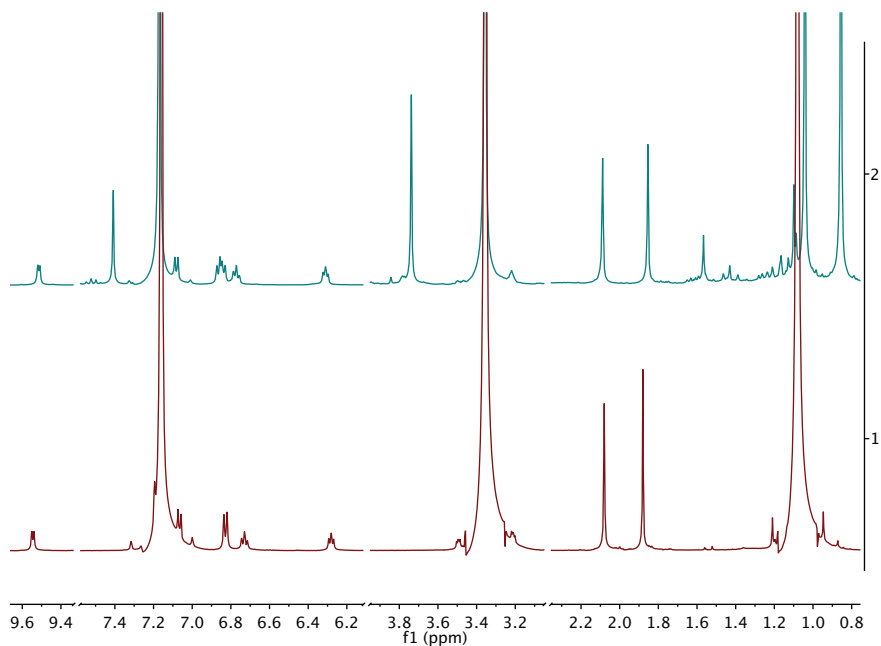
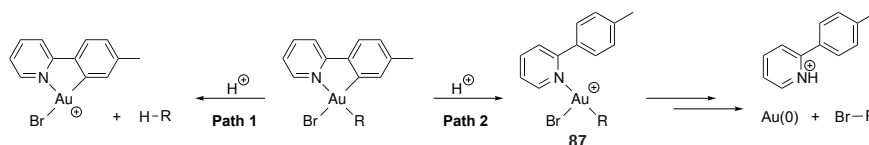


Figure 3.5: ^1H NMR (500 MHz, C_6D_6) of **70** with O_2 and AIBN (1,4-dioxane as ISTD, 3.36 ppm). Bottom: Before heating, Top: After heating. The spectra have been cut horizontally and the regions without any resonances are left out to improve clarity. Resonances at 0.8–1.6 ppm are due to AIBN.

3.4.4 Reactivity Towards Acids

Protonolysis of the gold(III) complexes of the type AuBrR(tpy) (**70–73**) can lead to cleavage of Au–C(*sp*²) in the tpy as was seen for AuMe₂(tpy) (**64**), but cleavage of Au–R can also happen (Scheme 3.9). When AuBrMe(tpy) (**70**) in dichloromethane-*d*₂ was reacted with triflic acid an immediate colour change was observed and apparently all starting material was consumed as determined by ¹H NMR. Two new species seem to have formed, based on the sets of aromatic signals, with no observed formation of methane. Similar reactivity was observed for AuBrPh(tpy) (**72**), as two new products were observed. A new peak was observed at 7.36 ppm which could correspond to benzene (benzene in CD₂Cl₂ are observed at 7.35 ppm, according to Fulmer *et al.*¹⁴¹) consistent with Path 1, Scheme 3.9. The sample was however not spiked with authentic sample of benzene. Methyl triflate reacts with **70** in dichloromethane-*d*₂ to form two new species, with no observed formation of ethane which could be expected if the methyl group was attacked. Two new species were also observed when **72** was reacted with methyl triflate, neither were toluene.



Scheme 3.9: Possible outcomes from protonolysis of the monoalkylated Au(III) complexes, AuBrR(tpy). Anions are omitted from the scheme. R = Me, Et, CHCH₂, Ph.

When AuBrEt(tpy) (**71**) was reacted with HBF₄·OEt₂, a small amount of what was likely bromoethane was observed, recognised by a quartet at 3.4 ppm and a triplet at 1.7 ppm.¹⁴⁵ Bromoethane integrated approximately 1:4 with the other product formed. There was only a hint of bromoethane formation when HOTf was used, and none when HCl(*aq*) was used. Formation of bromoethane is consistent with Path 2, Scheme 3.9.

AuBr(CHCH₂)(tpy) (**73**) gave some formation of what was likely bromoethylene when reacted with HBF₄·OEt₂ (Path 2, Scheme 3.9). Both shifts and coupling constants corresponded to bromoethylene (5.97, 5.84 and 6.44 ppm, *J* =

1.86, 7.12, 14.94 Hz in CDCl₃ according to literature).¹⁴⁵ There were some hints of bromoethylene formed in reaction with HOTf as well, but not conclusive.

AuBrPh(tpy) (**72**) likely produced benzene in reaction with HOTf, which point to protolytic cleavage of the Au-C_{Ph} bond by Path 1, Scheme 3.9. No bromobenzene was observed by ¹H NMR (expected for Path 2, Scheme 3.9). Some conclusions can be drawn from this series of experiments, although a thorough investigation has not been conducted. One, in **72** some protolytic cleavage of Au-C_{Ph} by HOTf likely took place to generate benzene (Path 1, Scheme 3.9) rather than protolytic cleavage of only the chelating ligand as there are two possible *sp*²-C in **72**. Two, protolytic cleavage of Au-C_{tolyl} in the chelating ligand likely happened, and that complex **87** formed was more unstable when the counteranion was BF₄⁻ rather than Cl⁻ or OTf⁻ which led to some decomposition presumably by reductive elimination of RBr by Path 2 in Scheme 3.9. BF₄ is a weakly coordinating ligand and likely stabilised **87** less than triflate or chlorine. In the case of HBF₄·OEt₂, the open coordination site drawn in **87** (Scheme 3.9) was likely occupied by water or ether, rather than BF₄. Three, protonolysis of AuBr(CHCH₂)(tpy) (**73**) produced bromoethylene (Path 2, Scheme 3.9), analogous to AuBrEt(tpy) (**71**), rather than Path 1 observed for AuBrPh(tpy) (**72**). To conclude whether or not bromomethane was produced in the case of AuBrMe(tpy) (**70**) is not possible without spiking the NMR sample with an authentic sample of bromoethane because it would only appear as a singlet. Table 3.1 summarises the reactivity of acids with the gold complexes discussed.

Table 3.1: Reactivity of monoalkyl and -aryl Au(III)-complexes towards acids.

	HCl(aq)	HBF ₄ ·OEt ₂	HOTf
AuBrMe(tpy) (70)	y (2:1)	y (5:1)	y
AuBrEt(tpy) (71)	y (4:1)	y, C ₂ H ₅ Br	y
AuBrPh(tpy) (72)	y (4:1)	n	y, C ₆ H ₆
AuBr(CHCH ₂)(tpy) (73)	y	y, C ₂ H ₃ Br	y

In CDCl₃ containing small amounts of H₂O. y = reaction observed, n = no reaction observed. Numbers in parentheses indicate *ca* ratio of product to starting material when reaction did not reach completion. Excess acid was added in all cases. CH₄/CH₃Br, C₂H₆/C₂H₅Br, C₆H₆/C₆H₅Br or C₂H₄/C₂H₃Br are indicated if observed.

3.4.5 Reactivity Towards Alkenes and Alkynes

When AuMe(tpy)NTf₂ (**55-NTf₂**) was generated *in situ* from AuBrMe(tpy) (**70**) and AgNTf₂, and was reacted with acetylene, a new species was produced and peaks at 6.3 and 6.0 ppm appeared in the ¹H NMR spectrum. The reaction did not reach completion over the course of 6 days, the solution still contained roughly equal amounts of unreacted **55-NTf₂** and the new species in solution.

When phenyl acetylene was added to **55-PF₆** in dichloromethane-*d*₂, the solution darkened immediately and all the starting material was consumed within the time it took to acquire a ¹H NMR spectrum (see Figure 3.6). Over time, the starting material (**55-PF₆**) reappeared together with the product that was initially formed, and the AuMe reappeared. The peaks corresponding to phenyl

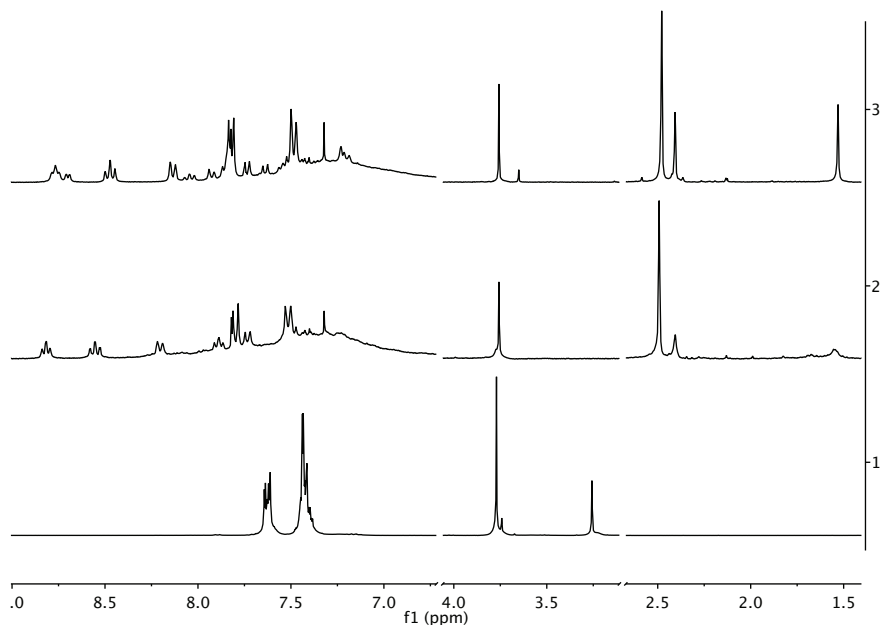


Figure 3.6: ¹H NMR (300 MHz, CD₂Cl₂) of AuMe(tpy)PF₆ (**55-PF₆**) with phenyl acetylene. Bottom: Phenyl acetylene, Middle: Shortly after addition, Top: After nearly 2 weeks. ISTD CH₂ClCH₂Cl at 3.7 ppm. The regions without any resonances are left out to improve clarity.

acetylene had disappeared already in the first spectrum (Figure 3.6).

Excess vinyl acetate was added to an *in situ* prepared sample of $\text{AuMe}(\text{tpy})\text{PF}_6$ (**55-PF₆**) in dichloromethane- d_2 . At room temperature (<1 h) apparently no reaction had taken place. However, heating the sample at 60 °C over night changed all resonances associated with the gold complex as well as the resonances from vinyl acetate. Interestingly, the singlet at 2.14 ppm for the methyl group in vinyl acetate was consumed. The organic product formed from vinyl acetate showed two doublets and one doublet of doublets (intensity 2:2:1). The full spectra are shown in Figure 3.7 and an enlargement is shown in Figure 3.8. The sample was heated at 60 °C for 3 days to form large amounts of material that deposited on the

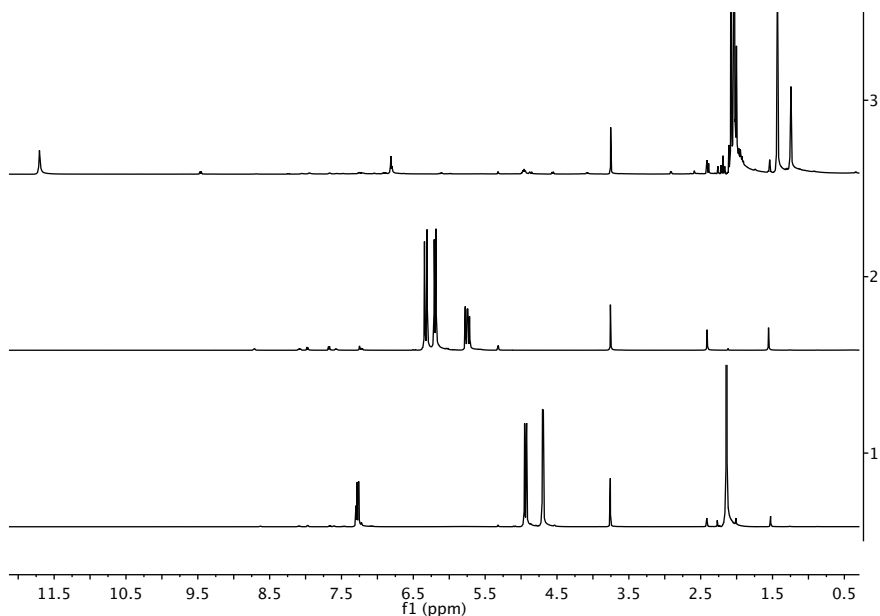


Figure 3.7: ^1H NMR (500 MHz, CD_2Cl_2) of $\text{AuMe}(\text{tpy})\text{PF}_6$ (**55-PF₆**) with vinyl acetate. Bottom: Shortly after addition (only minor changes compared to starting materials), Middle: Heating at 60 °C over night, Top: After 3 d at 60 °C. The intensities are comparable in all spectra. ISTD $\text{CH}_2\text{ClCH}_2\text{Cl}$ at 3.7 ppm. The spectra are clipped horizontally in the region 2.5–1.0 ppm.

tube walls. At that time, more or less all of the vinylic protons were consumed, a signal at 6.81 ppm was all that was left. The appearance of two singlets at 11.70 and 2.08 ppm suggested formation of acetic acid, confirmed by spiking the NMR sample with an authentic sample of acetic acid. The other products formed after heating for 3 days gave a large singlet at 2.04 and a doublet at 1.44 ppm, the structures were not confirmed. Crystals suitable for X-ray structure determination were unfortunately not obtained.

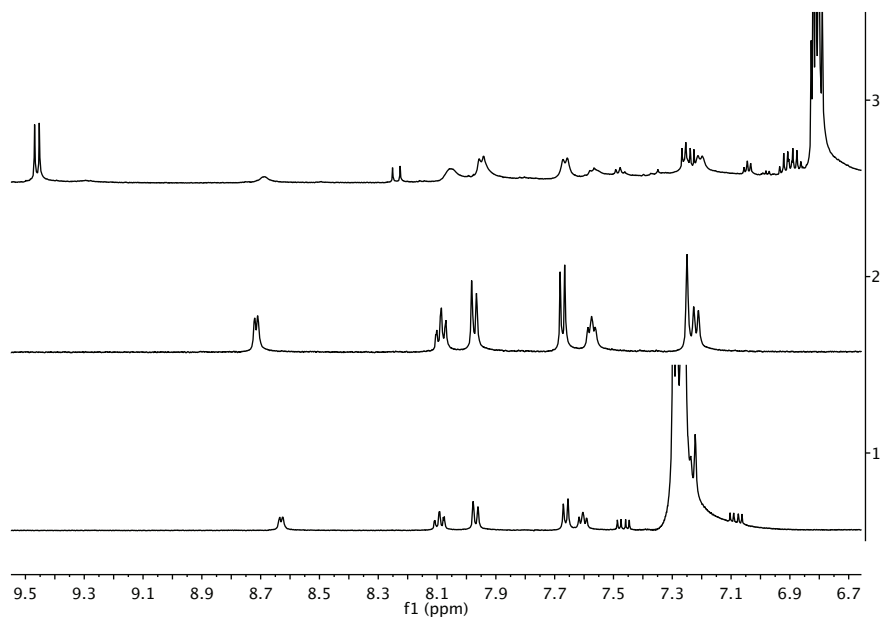


Figure 3.8: ^1H NMR (500 MHz, CD_2Cl_2) of $\text{AuMe}(\text{tpy})\text{PF}_6$ (**55-PF₆**) with vinyl acetate. Bottom: Shortly after addition (only minor changes compared to starting materials), Middle: Heating at 60 °C over night, Top: After 3 d at 60 °C. The intensities are comparable in all spectra. The spectra are clipped horizontally in the region 7.4–6.7 ppm. Only the aromatic region is shown, full spectra shown in Figure 3.7.

The work with $\text{AuR}(\text{tpy})\text{X}$ ($\text{R} = \text{Me}, \text{Ph}, \text{X} = \text{PF}_6, \text{BF}_4, \text{OTf}, \text{etc.}$) and alkenes and alkynes were mostly conducted at the University of Washington. The suspicion was that **55-X** catalysed polymerisation of alkenes and alkynes. The

reasons for believing this was that the olefins were consumed; the olefinic protons disappeared and signals appeared in the aliphatic region of the ^1H NMR spectrum. The other argument was that large amounts of material precipitated out of the solution during the course of the reaction. It was however not invested too much time and effort into these reactions. There is one example of polymerisation aided by gold(III) published by Díaz-Requejo, Pérez *et al.*¹⁴⁶ The main goal of the investigations was to observe a gold(III) alkene or alkyne complex and the fact that this was not the first observation of gold(III) catalysed polymerisation, if it was indeed polymerisation, were reasons to leave this part of the project.

3.5 Conclusions

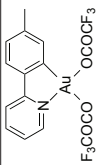
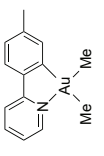
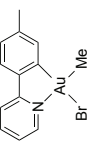
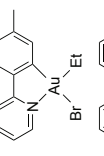
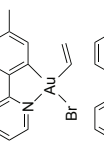
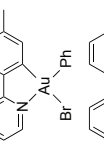
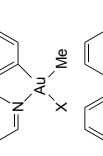
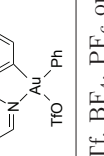
Table 3.2 shows a summary of the reactivity discussed in this chapter. It is not comprehensive, simply meant as an overview of what can be found in the text.

The cyclometalated gold(III) complexes were all insensitive to oxygen but some reacted when the radical initiator AIBN was added. The reactivity towards hydrogen peroxide and water is low, although complexes of the type $\text{AuR}(\text{tpy})\text{X}$ likely coordinates water instead of the X–ligand when exposed to water in the case of a weakly coordinating X (e.g. PF_6 , BF_4 , OTf^{111}). Of the complexes tested, only $\text{Au}(\text{OCOCF}_3)_2(\text{tpy})$ (**62**) reacted with carbon monoxide under high pressure. None of the complexes tested reacted with carbon dioxide under high pressure, although calculations suggested that $\text{AuMe}_2(\text{tpy})$ (**64**) should react with carbon dioxide.¹⁴⁷

Reactivity towards acid was observed for the mono- and dialkylated species. For $\text{AuMe}_2(\text{tpy})$ (**64**) protonation likely lead to reductive elimination with formation of ethane. The first step in the protonolysis was protolytic cleavage of the Au–C(sp^2) of the tpy ligand. Calculations performed by Dr. Ainara Nova suggested that $\text{AuMe}_2(\text{tpyH})\text{OTf}$ (**77–OTf**) was the kinetic product when $\text{AuMe}_2(\text{tpy})$ (**64**) was treated with HOTf, whereas the thermodynamic product was protolytic cleavage of the Au–Me bond *trans* to carbon to produce methane.¹⁴⁷ In the case of $\text{AuBrEt}(\text{tpy})$ (**71**) and $\text{AuBr}(\text{CHCH}_2)(\text{tpy})$ (**73**), RBr from the reductive elimination was observed and no formation of RH *via* direct protonation was seen.

Halide abstraction by a silver salt is feasible for all $\text{AuBrR}(\text{tpy})$ complexes

Table 3.2: Summary of reactivity discussed in this chapter.

[Au]	H ₂	O ₂	O ₂ +AIBN	H ₂ O ₂	CO	CO ₂	H ⁺	C ₂ H ₄	Ene/yne	AgX
	y				y	n		y ^a	y ^a	
	n	n	y	n	n	n	y	n		
	n	n	y	n	n		y			y
							y			y
										y
							y			y
	n			n	n			y		
										y

X = OTf, BF₄, PF₆ or NTf₂. y = reaction observed, n = no reaction observed, only the reactions performed are included (some are not discussed in the text). ^a Will be discussed in depth in Chapter 4.

investigated (R = Me, Et, CHCH₂, Ph). Alkenes and alkynes can react with the gold(III) complexes that seem to have a labile ligand, as in the case of AuR(tpy)X and also for Au(OCOCF₃)₂(tpy) (**62**, discussed in Chapter 4).

As is apparent from Table 3.2 there are parts of the reactivity of the synthesised cyclometalated gold(III) complexes that have not been investigated or only been investigated briefly. This chapter was meant as pointer to what has been investigated, but is by no means a comprehensive study.

3.6 Experimental

General Methods for HP NMR

HP NMR was conducted at EPFL in the group of Professor Paul Dyson under the guidance of Professor Gábor Laurenczy with financial support from COST (COST Action: CM1205) in the time period February 17th to March 2nd, 2014. An initial screening in hope of observing interesting reactivity of several of the synthesised gold(III) complexes was conducted together with M.Sc. Marte Sofie Holmsen, and will likely lead to further investigations. It was however not possible to characterise all products formed during the short period of time in Lausanne.

The sapphire NMR tubes used were a modification of what is discussed in these references.^{132–134} The sapphire NMR tubes used are shown in Figure 3.9 and can withstand pressures up to 100 bar. When working with the tubes under pressure it is crucial to have the protection around, as shown in the two rightmost pictures in Figure 3.9. To avoid breakage of the expensive tubes, they are secured tightly: the brass piece on the top is tightened as well as the white teflon ring on the middle of the protection. Inside the protection, the sapphire NMR tube sits in its own spinner. The whole assembly is mounted on top of the NMR magnet and the tube is inserted without exposing the operator to the unprotected pressurised tube.

The tubes were pressurised by opening a small valve on the top using spanners. To ensure that the tube was indeed pressurised and not leaking, it was weighed before and after the pressurisation. It was also possible to measure the pressure in the tubes digitally. Solvent volumes of 1.5–2.5 mL were used and required 10–30 mg Au–complex for each reaction (depending on the size of the tube). Spectra were acquired using a Bruker DRX 400 MHz spectrometer operating on 400 MHz (¹H) equipped with a 10 mm BBO probe.

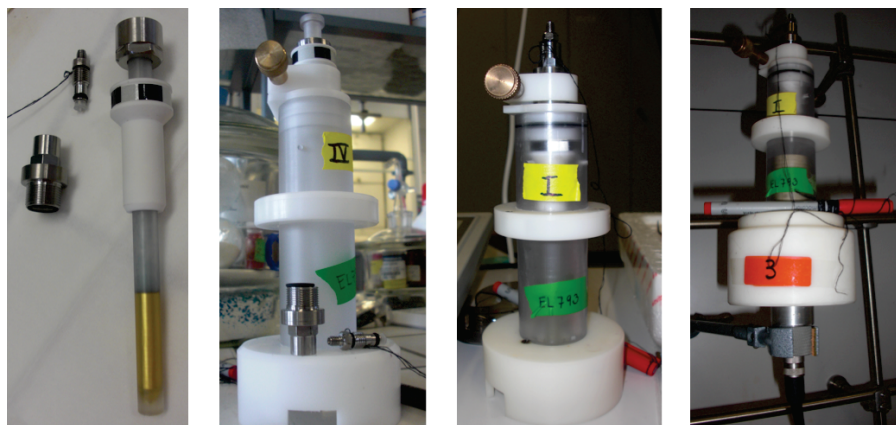


Figure 3.9: Sapphire tubes used for HP NMR. From left: Empty 10 mm sapphire NMR tube (here gold coated) with the necessary o-rings and seals, sapphire tube with protection ready for sample loading, closed tube with protection ready for transportation to/from the NMR instrument, and tube with protection in heating jacket.

General Experimental Methods for Experiments Conducted at The University of Oslo

Much of the protonolysis work was conducted at the University of Oslo. NMR spectra were recorded on a Bruker AVII400 or DRX500. A variable temperature BBO probe for the DRX500 was used when the variable temperature experiments were conducted.

General Experimental Methods for Experiments Conducted at The University of Washington

The NMR spectra were recorded on a Bruker AV300, AV300, AV500, or DRX500, operating at 300 or 500 MHz (^1H). NMR solvents were dried over CaCl_2 or Na .

A J Young NMR tube was loaded with Au-complex, ISTD added and solvent was vacuum transferred into the NMR tube. The second reagent was then added. A set-up where a J Young NMR tube could easily be pressurised with 5 bar of O_2 was utilised. In CD_2Cl_2 , 1,2-dichloroethane was used as an ISTD, in C_6D_6 , 1,4-dioxane was used (when AIBN was used, to avoid reaction with halogenated compounds). Standard Schlenk techniques and a N_2 -filled glove box were utilised. The hydrogen peroxide solution used was 30% H_2O_2 in H_2O .

AuMe₂(tpy) (64) + O₂

A J Young NMR tube with **64** and CD₂Cl₂ was pressurised with 3 bar of O₂. After 1 d at rt, only starting material was observed.

AuMe₂(tpy) (64) + O₂

A J Young NMR tube with **64** (3.5 mg), CH₂ClCH₂Cl (5 µL) and C₆D₆ was pressurised with 3 bar of O₂. The solution was heated at 80 °C for 2 d. After 1 d *ca* 87% of **64** was still present in solution, and no other species were observed although a slight purple coating was observed. After 2 d *ca* 48% of the starting complex was still in solution, the tube walls were strongly coated and the solution was still yellow. The appearance of a new set of resonances integrating 1:2 compared to **64**, no ethane observed.

AuMe₂(tpy) (64) + O₂ + AIBN

A J Young NMR tube with **64**, AIBN and C₆D₆ was pressurised with 3 bar of O₂. After 3 d at rt, only starting material was present. The tube was heated to 60 °C for 6 h without any reaction, followed by heating at 80 °C over night to form a new species. The nature of the Au-species was not determined. ¹H NMR (300 MHz, C₆D₆): δ 8.93 (d, *J* = 5.5 Hz, 1H), 8.62 (d, *J* = 4.7 Hz, 1H), 8.05 (d, *J* = 7.6 Hz, 2H), 7.41 (s, 2H), 7.39–7.28 (m, 1H), 7.15–7.05 (m, overlaps with solvent residual), 6.91–6.77 (m, 3H), 6.65 (dd, *J* = 6.1, 6.1 Hz, 1H), 3.74 (s, 3H), 2.12 (s, 3H), 2.10 (s, 3H). Resonances at 2–0 ppm are not included because of the decomposition products of AIBN.

AuMe₂(tpy) (64) + H₂O₂

64 (6 mg) in C₆D₆ was added excess H₂O₂(*aq*). No reaction observed by ¹H NMR.

AuMe₂(tpy) (64) + O₂ + AIBN

A reference ¹H NMR spectrum was recorded of **64**, AIBN, 1,4-dioxane (ISTD) and C₆D₆ in a J Young NMR tube. The tube was pressurised with 3 bar of O₂ and heated to 80 °C. Over night all the resonances had changed by ¹H NMR. 5 d at 80 °C did not yield further changes.

AuMe₂(tpy) (64) + AIBN

A reference ¹H NMR spectrum was recorded of **64**, AIBN, 1,4-dioxane (ISTD) and C₆D₆ in a J Young NMR tube. The tube was heated to 80 °C for 7 d. Resonances for **64** were unchanged, all AIBN resonances had changed.

AuMeOAc(tpy) (69)

To AuBrMe(tpy) (**70**) in CDCl₃ in an NMR tube was added excess AgOAc to generate AuMeOAc(tpy) (**69**) *in situ*. ¹H NMR (400 MHz, CDCl₃): δ 8.56 (d, *J* = 3.3 Hz, 1H), 7.95 (dd, *J* = 7.5, 7.5 Hz, 1H), 7.87 (d, *J* = 7.6 Hz, 1H), 7.58 (d, *J* = 7.6 Hz, 1H), 7.41 (dd, *J* = 5.9, 5.9 Hz, 1H), 7.28 (s, 1H), 7.12 (d, *J* = 7.6 Hz, 1H), 2.40 (s, 3H), 2.19 (s, 3H).

AuMe(tpy)OTf (55-OTf)

To AuBrMe(tpy) (**70**) in CDCl₃ in an NMR tube was added excess AgOTf to generate AuMe(tpy)OTf (**55-OTf**) *in situ*. ¹H NMR (400 MHz, CDCl₃): δ 8.86 (ddd, *J* = 5.6, 1.6, 0.8 Hz, 1H), 8.03 (ddd, *J* = 8.2, 7.5, 1.6 Hz, 1H), 7.93 (d, *J* = 8.1 Hz, 1H), 7.61 (d, *J* = 7.9 Hz, 1H), 7.54 (ddd, *J* = 7.3, 5.6, 1.4 Hz, 1H), 7.21 (s, 1H), 7.19 (ddd, *J* = 7.8, 1.7, 0.8 Hz, 1H), 2.42 (s, 3H).

AuMe(tpy)NTf₂ (55-NTf₂)

To AuBrMe(tpy) (**70**) in CD₂Cl₂ in an NMR tube was added excess AgNTf₂ to generate AuMe(tpy)NTf₂ (**55-NTf₂**) *in situ*. ¹H NMR (400 MHz, CD₂Cl₂): δ 8.72 (s, 1H), 8.07 (dd, *J* = 7.8, 7.8 Hz, 1H), 7.98 (d, *J* = 8.1 Hz, 1H), 7.69 (d, *J* = 7.9 Hz, 1H), 7.56 (dd, *J* = 6.6, 6.6 Hz, 1H), 7.28 (s, 1H), 7.24 (d, *J* = 8.0 Hz, 1H), 2.43 (s, 3H), 1.65 (s, 3H).

AuMe(tpy)PF₆ (55-AgPF₆)

To AuBrMe(tpy) (**70**) in CD₂Cl₂ in an NMR tube was added excess AgPF₆. A colourless precipitate formed immediately, and AuMe(tpy)PF₆ (**55-PF₆**) was generated *in situ*. ¹H NMR (300 MHz, CD₂Cl₂): δ 8.69–8.60 (m, 1H), 8.07 (ddd, *J* = 8.1, 7.4, 1.6 Hz, 1H), 7.94 (d, *J* = 8.1 Hz, 1H), 7.64 (d, *J* = 8.2 Hz, 1H), 7.58 (ddd, *J* = 7.2, 5.6, 1.3 Hz, 1H), 7.26–7.14 (m, 2H), 2.41 (s, 3H), 1.53 (s, 3H).

AuEtOAc(tpy) (84)

To AuBrEt(tpy) (**71**) in CDCl₃ in an NMR tube was added excess AgOAc to generate

AuEtOAc(tpy) (**84**) *in situ*. ^1H NMR (400 MHz, CDCl_3): δ 8.53 (d, $J = 3.7$ Hz, 1H), 7.92 (dd, $J = 7.8, 7.8$ Hz, 1H), 7.86 (d, $J = 8.2$ Hz, 1H), 7.59 (d, $J = 7.9$ Hz, 1H), 7.38 (dd, $J = 6.5, 6.5$ Hz, 1H), 7.35 (s, 1H), 7.13 (d, $J = 7.3$ Hz, 1H), 2.42 (s, 3H), 2.26 (q, $J = 7.8$ Hz, 2H), 2.21 (s, 3H), 1.33 (t, $J = 7.6$ Hz, 3H).

AuEt(tpy)OTf (**83**)

To AuBrEt(tpy) (**71**) in CDCl_3 in an NMR tube was added excess AgOTf to generate AuEt(tpy)OTf (**83**) *in situ*. ^1H NMR (400 MHz, CDCl_3): δ 8.91–8.83 (m, 1H), 7.99 (dd, $J = 7.5, 7.5$ Hz, 1H), 7.92 (d, $J = 7.5$ Hz, 1H), 7.63 (d, $J = 7.9$ Hz, 1H), 7.52 (dd, $J = 6.3, 6.3$ Hz, 1H), 7.32 (s, 1H), 7.19 (d, $J = 7.4$ Hz, 1H), 2.46 (s, 3H), 2.41 (q, $J = 7.7$ Hz, 2H), 1.41 (t, $J = 7.6$ Hz, 3H).

Au(CHCH₂)OAc(tpy) (**82**)

AuBr(CHCH₂)(tpy) (**73**) in CDCl_3 in an NMR tube was added excess AgOAc to generate Au(CHCH₂)OAc(tpy) (**82**) *in situ*. From ^1H NMR the desired complex was formed, but in addition another species was present. Shifts are not reported as the shifts overlap.

Au(CHCH₂)(tpy)OTf (**81**)

To AuBr(CHCH₂)(tpy) (**73**) in CDCl_3 in an NMR tube was added excess AgOTf to generate Au(CHCH₂)(tpy)OTf (**81**) *in situ*. ^1H NMR (400 MHz, CDCl_3): δ 8.44 (s, 1H), 8.01 (dd, $J = 8.8, 8.8$ Hz, 1H), 7.90 (d, $J = 8.4$ Hz, 1H), 7.57 (d, $J = 8.2$ Hz, 1H), 7.49–7.43 (m, 1H), 7.37 (s, 1H), 7.17 (d, $J = 7.9$ Hz, 1H), 6.55 (dd, $J = 16.5, 8.7$ Hz, 1H), 5.95 (d, $J = 8.7$ Hz, 1H), 5.59 (d, $J = 16.2$ Hz, 1H), 2.41 (s, 3H).

AuPhOAc(tpy) (**86**)

To AuBrPh(tpy) (**72**) in CDCl_3 in an NMR tube was added excess AgOAc to generate AuPhOAc(tpy) (**86**) *in situ*. ^1H NMR (400 MHz, CDCl_3): δ 8.61–8.53 (m, 1H), 7.99 (dd, $J = 8.0, 8.0$ Hz, 1H), 7.89 (d, $J = 8.2$ Hz, 1H), 7.64–7.51 (m, 3H), 7.48–7.37 (m, 1H), 7.22 (s, 3H), 7.08 (d, $J = 7.9$ Hz, 1H), 6.73 (s, 1H), 2.20 (s, 1H), 2.07 (s, 3H).

AuPh(tpy)OTf (**85**)

To AuBrPh(tpy) (**72**) in CDCl_3 in an NMR tube was added excess AgOTf to generate AuPh(tpy)OTf (**85**) *in situ*. ^1H NMR (400 MHz, CDCl_3): δ 8.97 (d, $J = 3.9$ Hz, 1H),

8.07 (dd, $J = 7.8, 7.8$ Hz, 1H), 7.95 (d, $J = 8.1$ Hz, 1H), 7.61–7.55 (m, 4H), 7.29 (s, 3H), 7.18–7.06 (m, 1H), 6.65 (d, $J = 2.8$ Hz, 1H), 2.21 (s, 3H).

AuBrMe(tpy) (70) + O₂ + AIBN

A J Young NMR tube with **70**, AIBN, 1,4-dioxane and C₆D₆ was pressurised with 3 bar of O₂. The solution was heated at 80 °C for 1 d. A slight shift was observed for AuMe and tolylMe, and appearance of a new resonance at 3.7 and 7.4 ppm. ¹H NMR (500 MHz, C₆D₆): δ 9.51 (d, $J = 5.3$ Hz, 1H), 7.41 (s, 2H), 7.08 (d, $J = 7.8$ Hz, 1H), 6.85 (dd, $J = 13.5, 7.8$ Hz, 2H), 6.77 (dd, $J = 7.3, 7.3$ Hz, 1H), 6.31 (dd, $J = 6.5, 6.5$ Hz, 1H), 3.74 (s, 3H), 2.09 (s, 3H), 1.85 (s, 3H). The signals further upfield are not included, as AIBN decomposition overlaps with possible AuMe, two large peaks at 1.04 (s, 11H) and 0.86 (s, 13H) from AIBN.

AuBrMe(tpy) (70) + O₂

A J Young NMR tube with **70** (2.2 mg) and CD₂Cl₂ was pressurised with 3 bar of O₂. After 25–30 d at 80 °C, the solution was still clear and no apparent changes in the ¹H NMR were observed.

AuMe(tpy)PF₆ (55–PF₆) + O₂

To a J Young NMR tube with **70** and CD₂Cl₂ was added excess AgPF₆ to generate **55–PF₆** *in situ*. The tube was then pressurised with 3 bar of O₂. A ¹H NMR spectrum was acquired showing only **55–PF₆**.

AuBrMe(tpy) (70) + H₂O₂

To a J Young NMR tube with **70**, CH₂ClCH₂Cl and CD₂Cl₂ was added excess H₂O₂ (*aq*) and heated to 60 °C for 2 d. No reaction observed by ¹H NMR.

AuBrMe(tpy) (70) + HOTf

To a J Young NMR tube with **70** dissolved in CD₂Cl₂ was added HOTf with immediate change of colour from colourless to light yellow and then to light brown. The appearance of new species was observed, and no methane. Major species: ¹H NMR (500 MHz, CD₂Cl₂): δ 12.10–11.80 (m, 1H), 8.77–8.50 (m, 2H), 8.11 (ddd, $J = 8.6, 1.7, 1.7$ Hz, 1H), 8.03 (dddd, $J = 7.6, 6.0, 1.5, 1.5$ Hz, 1H), 7.30 (d, $J = 1.1$ Hz, 2H), 2.44 (s, 3H),

2.38 (s, 3H).

AuBrMe(tpy) (70) + MeOTf

To a J Young NMR tube with **70** in CD_2Cl_2 was added MeOTf. The solution turned yellow immediately, then light brown. Product not determined. ^1H NMR (500 MHz, CD_2Cl_2): δ 8.04 (ddd, $J = 7.8, 7.8, 1.7$ Hz, 1H), 7.94 (ddd, $J = 8.2, 1.1, 1.1$ Hz, 2H), 7.64 (d, $J = 7.9$ Hz, 1H), 7.48 (dd, $J = 8.1, 1.3$ Hz, 2H), 7.42 (ddd, $J = 7.3, 5.6, 1.4$ Hz, 1H), 7.23–7.13 (m, 4H), 7.09 (dd, $J = 7.4, 7.4$ Hz, 1H), 6.53 (s, 1H), 2.18 (s, 6H).

AuBrPh(tpy) (72) + H_2O_2

To **72** and $\text{CH}_2\text{ClCH}_2\text{Cl}$ in C_6D_6 was added excess $\text{H}_2\text{O}_2(aq)$. No reaction observed at rt by ^1H NMR.

AuBrPh(tpy) (72) + H_2O_2

To **72** and $\text{CH}_2\text{ClCH}_2\text{Cl}$ in CD_2Cl_2 was added excess $\text{H}_2\text{O}_2(aq)$. The solution was heated at 60 °C for 2–3 d with no change according to ^1H NMR, the solution was still clear.

AuBrPh(tpy) (72) + HOTf

To a J Young NMR tube with **72** in CD_2Cl_2 was added HOTf. Immediate colour change from colourless to yellow and later dark brown, accompanied by precipitation. A resonance corresponding well with benzene was observed.

AuBrMe(tpy) (70) + AgPF_6 + Acrylonitrile

To a J Young NMR tube with **70** in CD_2Cl_2 was added excess AgPF_6 to generate AuMe(tpy)PF_6 (**55-PF₆**) *in situ* followed by addition of acrylonitrile. Apparently no reaction neither at rt nor at 60 °C for 7 d.

AuBrMe(tpy) (70) + AgPF_6 + Vinyl acetate

To a J Young NMR tube with **70** in CD_2Cl_2 was added excess AgPF_6 to generate AuMe(tpy)PF_6 (**55-PF₆**) *in situ* followed by addition of vinyl acetate. Apparently no reaction had happened within 30–45 min at rt. The sample was heated at 60 °C overnight. Both resonances for vinyl acetate and the resonances for **55-PF₆** changed significantly. The sample was heated at 60 °C for 3 d, at that time the vinylic resonances from

vinyl acetate had been consumed. The walls of the tube were covered with deposited matter. The sample was spiked with acetic acid confirming that one of the products were acetic acid. First Au-product formed: ^1H NMR (500 MHz, CD_2Cl_2): δ 8.72 (d, $J = 5.3$ Hz, 1H), 8.09 (ddd, $J = 7.8, 7.8, 1.7$ Hz, 1H), 7.97 (d, $J = 8.1$ Hz, 1H), 7.67 (d, $J = 7.9$ Hz, 1H), 7.57 (dd, $J = 6.6, 6.6$ Hz, 1H), 7.25 (s, 1H), 7.22 (d, $J = 8.2$ Hz, 1H), 2.41 (s, 3H), 1.56 (s, 3H). First vinyl product (integrals with respect to Au-complex present): ^1H NMR (500 MHz, CD_2Cl_2): δ 6.33 (d, $J = 17.9$ Hz, 40H), 6.20 (d, $J = 11.8$ Hz, 40H), 5.75 (dd, $J = 17.8, 11.8$ Hz, 20H). Only the first product is reported.

Chapter 4

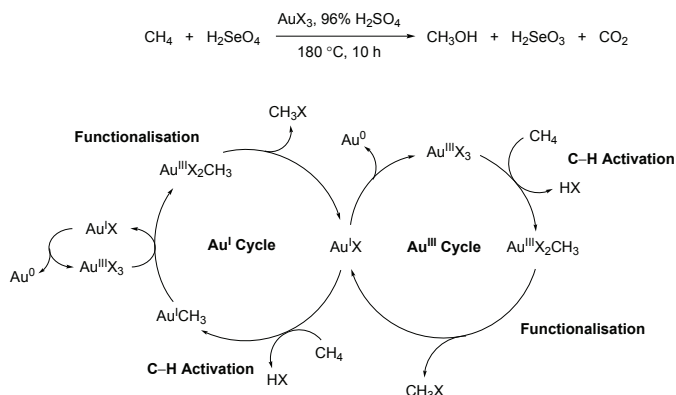
Alkene and Alkyne Insertion

4.1 General Introduction

The work presented in this chapter is mainly found in Paper II¹⁰⁷ (Appendix), but some additional unpublished results are included as well.

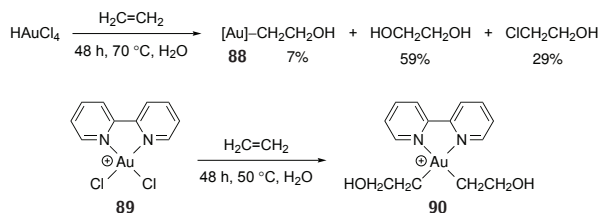
Activation of small organic molecules has great practical value.^{103,148} Functionalisation of methane from natural gas is highly desirable.¹⁴⁸ The so-called Shilov system where a platinum(II) complex is used to activate methane to methanol has received extensive attention.¹⁴⁸ The reaction is catalytic but uses stoichiometric amounts of expensive platinum(IV) as oxidant. Later, Periana *et al.* showed that oxidation of methane to methanol is possible using gold (Scheme 4.1).³³ In sulfuric acid, the reaction was stoichiometric in gold while addition of selenic acid could oxidise the gold(0) formed and thus give a catalytic cycle. The proposed catalytic cycle for the oxidation of methane to methanol by gold is depicted in Scheme 4.1, which gave turnover numbers up to 30.³³ The work by Periana *et al.* demonstrated that cationic gold can catalyse activation of alkanes increasing the interest for catalysis by gold.²⁶

There is little work reported on addition of water to an alkene in the presence of gold(III).^{40,149,150} Only a few literature examples reporting reactions of gold(III) with simple alkenes exist and mechanistic studies are lacking.⁹⁴ Atwood *et al.* recently published reactivity of gold(III) complexes with one atmosphere of ethylene or propylene in water at room temperature and at 70 °C.¹⁰³

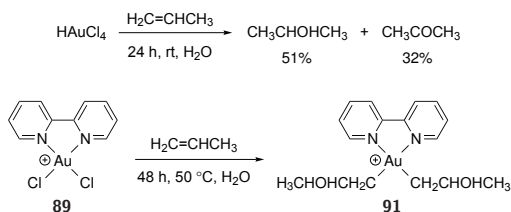


Scheme 4.1: Conversion of methane to methanol in the presence of gold and the proposed catalytic cycle, by Periana *et al.* X = HSO₄.³³

When the gold(III) complex was HAuCl₄ or AuCl₃P(*m*-C₆H₄SO₃Na)₃, Atwood *et al.* observed formation of organic products (alcohols and aldehydes/ketones), and reduction to metallic gold. If AuCl₂(bipy)X (**89**, X = Cl⁻ or PF₆⁻) was used instead, gold(III) β-hydroxy complexes Au(bipy)(CH₂CH₂OH)₂X (**90**) and Au(bipy)(CH₂CHOHCH₃)₂Cl (**91**) were observed. The complexes were characterised by NMR and HR MS, but not isolated.¹⁰³ Atwood *et al.* argued that since gold is less susceptible to β-hydride elimination it enabled the isolation of the β-hydroxyalkyl complexes **90** and **91** that otherwise, for other metals, are isolated by blocking the coordination site required for β-hydride elimination.¹⁰³



Scheme 4.2: Selected examples of reaction of Au(III) complexes with ethylene by Atwood *et al.*¹⁰³ Counteranion Cl⁻ or PF₆⁻.



Scheme 4.3: Selected examples of reaction of Au(III) complexes with propylene by Atwood *et al.*¹⁰³ Counteranion Cl⁻ or PF₆⁻.

The organic products observed in the reaction using ethylene reported by Atwood *et al.* were ethylene glycol, 2-chloroethanol and acetaldehyde.¹⁰³ The amount of ethylene glycol formed seemed to be related to the amount of metallic gold formed. Scheme 4.2 shows selected experiments with ethylene. When HAuCl₄ or AuCl₃P(*m*-C₆H₄SO₃Na)₃ were treated with propylene, the organic products were acetone and isopropanol, consistent with Markovnikov attack by OH⁻ on coordinated propylene. In the same reaction using AuCl₂(bipy)⁺ (**89**) full conversion to Au(bipy)(CH₂CHOHCH₃)⁺ (**91**) was seen.¹⁰³ Selected experiments with propylene are shown in Scheme 4.3.

4.2 Initial Trials

Inspired by the work of Atwood *et al.* describing the reaction of simple gold(III) complexes with ethylene and propylene at moderate temperatures and pressures,¹⁰³ the two cyclometalated gold(III) complexes AuMe(tpy)(OTf) (**55-OTf**) and Au(OCOCF₃)₂(tpy) (**62**) were tested in reaction with ethylene. Each vessel was equipped with small spheres to ensure solvent, ethylene and water to mix. The solvents tested with **55-OTf** were TFE, nitromethane, acetone and methanol. **62** was tested in TFE and methanol. Solutions of the gold(III) complexes in the respective solvents containing 50 mM water were pressurised with ethylene and heated (Scheme 4.4). Water was not chosen as a solvent for the testing as complexes **55-OTf** and **62** are quite insoluble in water. The solubility in alcohols is also limited but sufficient for obtaining homogenous solutions of all samples prepared. It was observed that the solution of **62** in methanol had already turned

slightly purple before pressurisation with ethylene. As mentioned in Chapter 2, **62** is not stable in methanol over time and the observed purple colour was likely metallic gold.

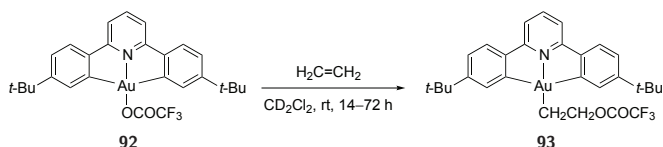


Scheme 4.4: Attempt on Au(III) catalysed ethylene functionalisation with 10 mol% **55-OTf** or **62** with respect to H_2O . Solvents were TFE, MeNO_2 , acetone and MeOH for **55-OTf**, and TFE and MeOH for **62**. Ethylene pressures of 5, 10, 15 and 20 bar.

After 3–4 days, the solutions were analysed directly by ^1H NMR of the protic solution where a capillary containing benzene- d_6 had been added for locking and referencing purposes. It was in this way possible to analyse all the solutions resulting from the 24 runs. What was quite unexpected was that $\text{AuMe}(\text{tpy})\text{OTf}$ (**55-OTf**) was apparently stable in all four solvents even at elevated temperatures with water added. However, based on experiments where water was added to **55-OTf** it was likely that water occupies the coordination site *trans* to carbon instead of triflate.¹¹¹

The results that were most intriguing were the change in the ^1H NMR for all the resonances of $\text{Au}(\text{OCOCF}_3)_2(\text{tpy})$ (**62**) in TFE and methanol. The experiment was repeated with **62** in TFE with one atmosphere of ethylene by bubbling the gas through the solution. The ^1H NMR spectrum corresponded with the spectra obtained from the high pressure reactions. Higher pressures of ethylene had only minor impact on the products formed, consistent with the work by Atwood *et al.*¹⁰³

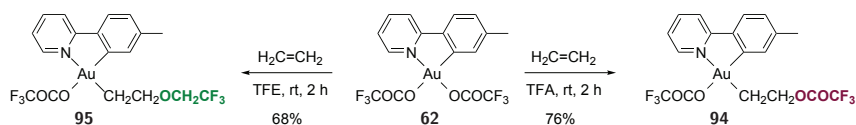
Bochmann *et al.* very recently showed that ethylene slowly inserted into the Au(III)– OCOCF_3 bond of **92** (Scheme 4.5),¹⁰⁹ a complex bearing a related ligand to the tpy system used in the work described in this thesis. Comparing the ^1H NMR spectra obtained by Bochmann *et al.* to what was obtained for **62** in the reaction with ethylene, it was postulated that a similar insertion reaction had taken place.



Scheme 4.5: Formal ethylene insertion into a Au–OCOCF₃ bond reported by Bochmann *et al.*¹⁰⁹

4.3 Formal Ethylene Insertion

When ethylene was bubbled through a solution of Au(OCOCF₃)₂(tpy) (**62**) in TFA at room temperature, an almost immediate change of colour from light yellow to colourless was observed. Ethylene inserted into the Au–O bond of the trifluoroacetate ligand *trans* to nitrogen forming Au(CH₂CH₂OCOCF₃)(OCOCF₃)(tpy) (**94**, Scheme 4.6). When the reaction was followed by ¹H NMR in TFA-*d*, full conversion of **62** to **94** was completed within <5 min seen from the appearance of two new triplets with coupling constants of 7.9 Hz at 4.79 and 2.40 ppm for the two methylene groups. Complex **94** was obtained in 76% isolated yield. Interestingly, the formal ethylene insertion takes place *trans* to nitrogen, the weakest *trans* effect side of the chelating C–N ligand. Recall from Chapter 2 (Section 2.3) that the trifluoroacetate ligand *trans* to carbon likely dissociates and reassociates in solution shown by ¹⁹F NMR.



Scheme 4.6: Formal ethylene insertion in Au(OCOCF₃)₂(tpy) to yield **94** and **95** in TFA and TFE, respectively.

If however TFE, was used as the protic solvent instead of TFA, a different product was formed. With TFE as the solvent, Au(CH₂CH₂OCH₂CF₃)(OCOCF₃)(tpy) (**95**) was observed, with only a small amount of **94** formed (Scheme 4.6). When the procedure was performed in TFE-*d*₃, the conversion to **96**ⁱ was completed in *ca* 30

ⁱCompound number **95** is used for Au(CH₂CH₂OCH₂CF₃)(OCOCF₃)(tpy) formed in TFE, compound number **96** is used for Au(CH₂CH₂OCD₂CF₃)(OCOCF₃)(tpy) formed in TFE-*d*₃.

min, seen by the appearance of two new triplets with coupling constants of 7.8 Hz for the methylene protons at 3.97 and 2.26 ppm (methylene unit from TFE- d_3 not observed in deuterated solvent as it is then ^1H NMR silent). $\text{Au}(\text{OCOCF}_3)_2(\text{tpy})$ (**62**) does not react with TFE unless ethylene is present, confirmed by heating **62** in TFE at 50 °C for 4 days in a J Young NMR tube. The reaction to form **96** proceeded slower than the reaction to form **94** in the two solvents TFE- d_3 and TFA- d , respectively. Monitoring the reactions from **62** to **94** and **96** by ^1H NMR is convenient as the singlet for the Ar-H *ortho* to gold and methyl in the tolyl group (6'-H), the aromatic signal at the lowest ppm value, shifts significantly to higher ppm values ($\Delta\delta$ between 0.65 and 0.31 ppm depending on complex and solvent) when **62** is converted to **94** or **96**. In TFE- d_3 solution on NMR scale, >99.5% **96** was observed (and <0.5% **94**) whereas when attempting to isolate pure **95** on a larger scale, **94** was always present in a small amount (*ca* 5%). To drive the formation towards **95** rather than **94**, redissolving the product mixture in TFE was tried several times followed each time by solvent removal *in vacuo*, without any change of the ratio between **95** and **94**. This result suggests both a formal insertion and a nucleophilic attack by the solvent (TFA or TFE).

Once the identities of the products that resulted from the reactions in TFA and TFE were determined, it was quite convenient to determine the ratios of the two. However, initially it was not as simple. When the spectra of **94** and **95** were stacked (Figure 4.1), the differences in chemical shifts are small making it difficult to be certain that the extra peaks observed were not simply due to TFE or TFA residual solvent, free or somehow coordinated. To establish that there were in fact two different products formed, a sample containing **94** was mixed with a sample containing **95** (bottom spectrum, Figure 4.1). Several of the aromatic resonances in this mixture look like apparent triplets (or as in an aromatic ring; doublet of doublets with two similar coupling constants). The NMR sample was then spiked with some of **94** (top spectrum, Figure 4.1). The following change in the aromatic region made the conclusion clear; two different species were present.

In a non-coordinating solvent such as dichloromethane- d_2 , only 40% conversion of **62** to **94** was seen after 2 hours at room temperature versus full conversion in TFA- d after few minutes. After approximately 24 hours the yield of the reaction in dichloromethane- d_2 was 94% (measured by ISTD). The rate of reaction

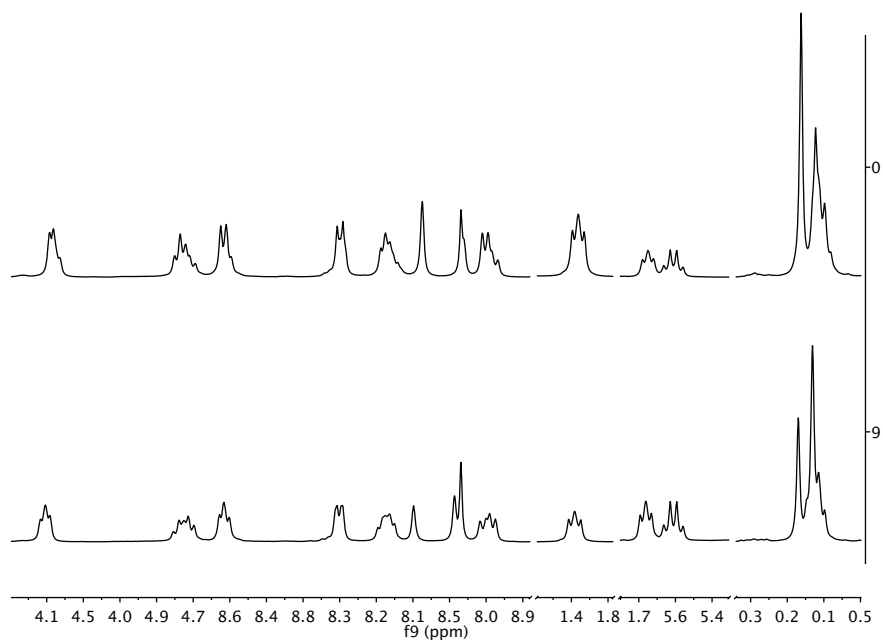


Figure 4.1: ^1H NMR (500 MHz, CDCl_3) spectra showing product mixtures of **94** and **95**. Bottom: 1:1 mixture of **94** and **95**, Top: NMR sample spiked with **94**.

for conversion of **62** to **94** in dichloromethane- d_2 is similar to the rate observed by Bochmann *et al.* in the reaction showed in Scheme 4.5.¹⁰⁹ Both complexes **94** and **95** are stable in dichloromethane- d_2 solution over the course of several weeks (monitored by ^1H NMR). The stability of **94** in TFA- d is somewhat lower; decomposition was observed within a day and approximately 25% of **94** had decomposed over the course of 5 days.

4.3.1 Characterisation

The structures of **94** and **95** were confirmed by NMR spectroscopy, mass spectrometry and X-ray crystallography. Elemental analysis was only performed for **94** as it was apparent from ^1H NMR that isolated material of **95** contained traces of **94**, even after several attempts at recrystallisation or redissolving in TFE, the ratio did not change significantly. It was hypothesised that there might be an equilibrium between the two products and that it would be possible to drive the equilibrium towards **95** by stirring the mixture in TFE, but unfortunately upon removal of solvent there was always small amounts of **94** left, the same being the case after recrystallisation.

The masses obtained from high resolution mass spectrometry corresponded to the fragments $[\text{M} - \text{OCOCF}_3]^+$ (for both **94** and **95**), $[\text{M} - \text{CH}_2\text{CH}_2\text{OCOCF}_3]^+$ (for **94**) and $[\text{M} - \text{CH}_2\text{CH}_2\text{OCH}_2\text{CF}_3]^+$ (for **95**). ^1H - ^1H NOESY clearly showed that the ethylene unit had inserted *cis* to carbon of the chelating C-N ligand. It was necessary to use quite long relaxation delays in ^{13}C NMR to observe all four carbons coupling to ^{19}F (in the COCF_3 and CH_2CF_3 -groups) as they are split into quartets. For **95** this was especially tricky due to the 5% or so of **94** present in all attempts at isolating **95**. For **94** a relaxation delay of 30 s and a number of scans of >5k was needed to clearly distinguish the different carbon atoms. This was however a short delay compared to what was necessary for **95**; relaxation delay of 60 s and 6k scans. The $^1J(^{13}\text{C}-^{19}\text{F})$ coupling constants for the CF_3 -groups were 280–290 Hz in the two complexes, whereas the $^3J(^{13}\text{C}-^{19}\text{F})$ coupling constants were 34–42 Hz, with the lowest observed for the OCH_2CF_3 -group in **95** (Table 4.1).

The solid-state structures of **94** and **95** are shown in Figure 4.2. The Au-N bond length in **94** and **95** is approximately 0.1 Å longer than in **62**, likely due

Table 4.1: ^1H and selected ^{13}C NMR shifts in ppm with coupling constants in parenthesis for complexes $\text{Au}(\text{OCOCF}_3)_2(\text{tpy})$ (**62**), $\text{Au}(\text{CH}_2\text{CH}_2\text{OCOCF}_3)(\text{OCOCF}_3)(\text{tpy})$ (**94**) and $\text{Au}(\text{CH}_2\text{CH}_2\text{OCH}_2\text{CF}_3)(\text{OCOCF}_3)(\text{tpy})$ (**95**) in CD_2Cl_2 .

δ	62	94	95
6-CH	8.42 (5.8 Hz)	8.38 (5.5, 1.7, 0.8 Hz)	8.32 (5.5, 1.7, 0.8 Hz)
4-CH	8.19 (7.7 Hz)	8.04 (7.6, 7.6, 1.7 Hz)	8.00 (8.2, 7.5, 1.6 Hz)
3-CH	7.92 (8.0 Hz)	7.93 (8.2 Hz)	7.90 (8.2 Hz)
3'-CH	7.50–7.42	7.64 (7.9 Hz)	7.60 (7.9 Hz)
5-CH	7.50–7.42	7.48 (7.2, 5.6, 1.3 Hz)	7.44 (7.5, 5.5, 1.3 Hz)
4'-CH	7.23 (7.8 Hz)	7.22 (7.8, 1.6, 0.8 Hz)	7.18 (8.0, 1.7, 0.9 Hz)
6'-CH	6.71	7.36	7.24
CH₂O	–	4.83–4.69	3.95–3.92
CH₂CF₃	–	–	3.90 (8.8 Hz)
ArCH₃	2.37	2.45	2.40
AuCH₂	–	2.43–2.36	2.37–2.31
CO	161.4 (37.9 Hz)	161.6 (37.1 Hz)	161.5 (36.8 Hz)
CO/H₂	160.9 (39.3 Hz)	161.2 (41.8 Hz)	68.3 (33.6 Hz)
CF₃ (<i>trans</i> to C)	118.4 (289.4 Hz)	118.3 (290.0 Hz)	118.4 (290.0 Hz)
CF₃ (<i>trans</i> to N)	116.2 (288.1 Hz)	115.1 (285.9 Hz)	124.9 (279.6 Hz)

to the stronger *trans* influence of the alkyl ligands in **94** and **95** compared to the trifluoroacetate ligand in **62**. The bond angles around gold are fairly similar for the three complexes **62**, **94** and **95**, with no more than 4.3° deviation between the three structures, **94** being more similar to **62** than what **95** is. The dominating factors regarding the packing in the crystal structures of **94** and **95** are π -interactions. **94** shows a Au- π stacking where the Au...tolyl distance is 3.570 Å. **95** shows a quite strong π -stacking between the aromatic rings with a distance between the tolyl and the pyridine of 3.696 Å. There appears to be no Au...Au interactions in the crystal structures; the shortest Au...Au distance in **94** and **95** are 4.825 and 4.831 Å, respectively, significantly longer than the sum of the van der Waals radii.

The bond lengths and angles of **94** and **95** are compared to **62** and **93**¹⁰⁹ in Table 4.2. All four complexes are close to square planar as expected for gold(III) and show fairly similar solid-state structures. The bond lengths and angles in **94** and **95** correspond well with what is reported for (C-N-C)Au-CH₂CH₂OCOCF₃ (**93**) by Bochmann *et al.*, although bond angles, as can be seen from Table 4.2, are slightly different due to the tridentate C-N-C ligand in **93**¹⁰⁹ versus the bidentate tpy in **94** and **95**.

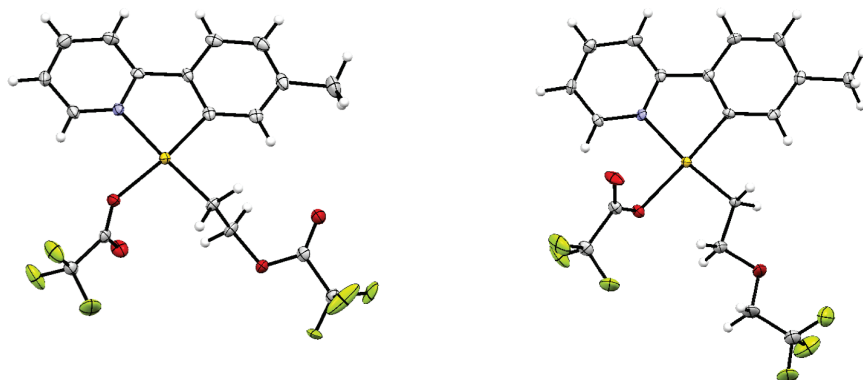


Figure 4.2: ORTEP view of the solid-state structures of **94** (left) and **95** (100 K) with 50% probability displacement ellipsoids. Selected bond distances (Å) and angles (°) are shown in Table 4.1. The CF_3 -group in **94** on the ligand where ethylene inserted is disordered with a 1:1 population of two orientations, here only one orientation is shown.

Table 4.2: Selected bond distances (Å) and angles (°) from the X-ray structures of complexes **62**, **94**, **95** and **93** (reported by Bochmann *et al.*¹⁰⁹).

Bond lengths/angles	62	94	95	93
Au–N	1.991(6)	2.098(2)	2.107(4)	2.048(10)
Au–C	1.995(7)	1.993(3)	2.006(4)	2.089(10) & 2.063(10)
Au–X	1.993(5)	2.042(3)	2.040(4)	2.055(11)
Au–O _{transC}	2.111(5)	2.104(2)	2.110(3)	–
C–Au–X	96.4(3)	95.12(12)	92.09 (18)	97.8(5) & 100.2(4)
N–Au–C	81.8(3)	81.80(11)	81.48(17)	81.1(4) & 80.9(4)
N–Au–O _{transC}	93.1(2)	92.90(9)	94.68(14)	–
N–Au–X	175.5(2)	176.80(11)	173.52(16)	178.4(4)
C–Au–O _{transC}	174.8(3)	174.42(10)	175.61(16)	162.0(4)
X–Au–O _{transC}	88.8(2)	90.20(10)	91.77(16)	–

X is the ligand *trans* to N; OCOCF_3 in **62**, alkyl in **94** and **95**. *transC* indicates ligand *trans* to C. The X-ray structure of **93** has 3 AgOAc molecules in the unit cell.

4.4 Mechanistic Investigations

It is beneficial to investigate the mechanism of operation for gold catalysed reactions. Computational methods have been used to shed some light on the preferred mechanisms of several reactions.^{151–156} However much effort is still being dedicated to isolate some of the intermediates^{56,80,94,157} and investigate the elementary steps^{137,158–164} proposed with either experimental or computational methods.^{74,165} Coordination of olefins to gold(III) is assumed to be a key step in the catalytic functionalisation of olefins,^{56,94} followed by the addition of a nucleophile.¹⁶⁶ For the latter step, both intra- and intermolecular addition have been proposed.^{74,165} The intermolecular process has more experimental^{167,168} and computational support,^{169–172} but there is not a clear explanation of why this mechanism should be the preferred route for all systems. In addition, the recent observation of a *syn* insertion of alkynes and allenes into a Au–Si bond¹⁵⁹ suggests that direct insertion of olefins into other Au–X bonds should not be directly discarded. The reversibility of hydroamination of alkenes have been studied for a gold(I) complex by Toste *et al.* where the authors postulated an *anti* addition of an amine which was reversible until the protodeauration step.¹⁷² For gold(III) there appear to be no similar studies, intriguing further investigations of the reversibility of the reaction going from **62** to **94**.

4.4.1 Reversibility of Nucleophilic Attack

Having established that two slightly different products formed depending on whether the solvent was TFA or TFE, it was hypothesised that an equilibrium between the two products **94** and **95** might be present. It was also of interest to know which of the two complexes **94** and **95** would form in a solvent mixture containing approximately equal amounts of TFA and TFE and hence approximately equal amounts of the two possible nucleophiles.

Au(OCOCF₃)₂(tpy) (**62**) was dissolved in a 1:1 mixture (v/v) of TFA and TFE, and ethylene was bubbled through the reaction mixture. After solvent removal, the resulting product mixture contained approximately 85% of **94** and 15% of **95**, as analysed by ¹H NMR in chloroform-*d* (bottom spectrum, Figure 4.3). The

question remained if **95** could be converted to **94**, and *vice versa*. The resulting product mixture (85:15, **94**:**95**) was dissolved in TFA and stirred at room temperature for nearly 2 days. After solvent removal *in vacuo*, the product mixture was analysed and by ^1H NMR, the sample contained solely **94** (middle spectrum, Figure 4.3). The mixture containing now solely **94** was dissolved in TFE and stirred for 1 day at room temperature before removing the solvent. Analysis by ^1H NMR gave a composition of **95** and **94** of 93–94% and 6–7%, respectively (top spectrum, Figure 4.3). The experiment showed that **94** could be converted to **95** and back to **94** again.

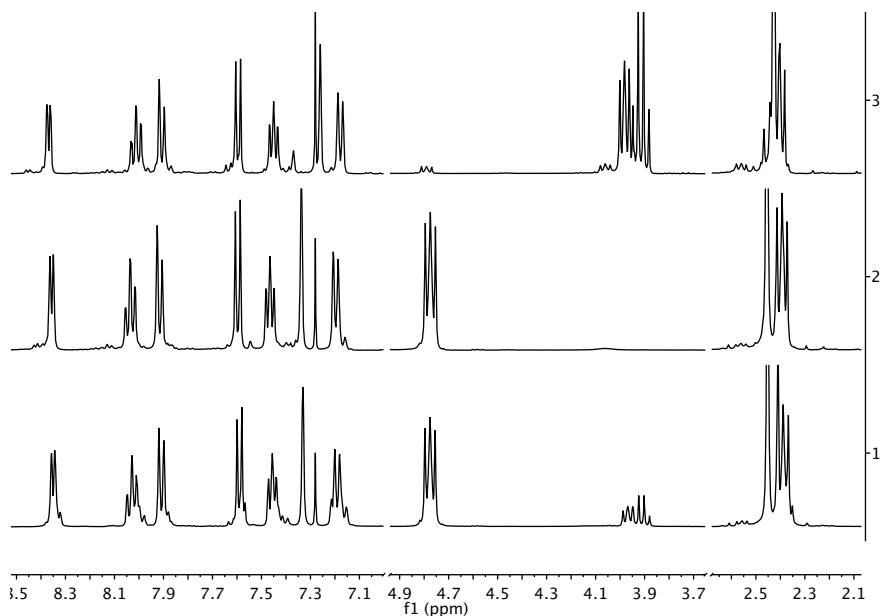
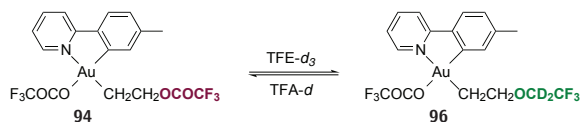


Figure 4.3: ^1H NMR (400 MHz, CDCl_3) spectra showing the equilibrium observed between **94** and **95**. Bottom: In a 1:1 mixture of TFA:TFE, 85% **94** and 15% **95** resulted, Middle: Mixture from bottom spectrum stirred in TFA (rt, <2 d), **94** only observed product, Top: Mixture from middle spectrum stirred in TFE (rt, 1 d), 93–94% **95** and 6–7% **94**. The tolylMe has been clipped horizontally to improve the clarity.

To obtain a more quantitative result in this respect, isolated **95** was dissolved in TFA-*d* at room temperature, and within few minutes reacted to form solely **94** (before a ^1H NMR spectrum was acquired). The same was true for **94**; when **94** was dissolved in TFE- d_3 , it reacted to form **96** (Scheme 4.7). For full conversion of **94** to **96** in TFE- d_3 , some heating was necessary (50 °C over night). At room temperature, only 40–45% conversion of **94** to **95** was observed when **94** was dissolved in TFE- d_3 . It was most likely not necessary to heat **94** in TFE- d_3 at 50 °C for 16.5 hours.

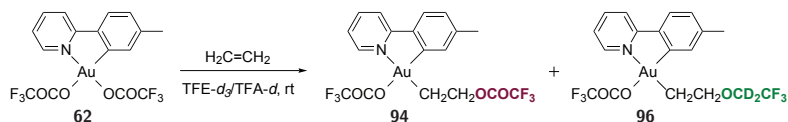


Scheme 4.7: Equilibrium observed between **94** and **96** in TFA-*d* and TFE- d_3 , respectively.

The equilibrium between **94** and **96** depicted in Scheme 4.7 was investigated by ^1H NMR by varying the TFA-*d*/TFE- d_3 concentrations (Figure 4.4). In a 1:1 mixture of TFA-*d*:TFE- d_3 (v/v), a product ratio of **94** and **96** of approximately 9:1 resulted after allowing the solution to equilibrate. The spectra shown in Figure 4.4 are recorded after equilibrium was reached (after a few h). The ratio between **94** and **96** did however change only slightly from the first spectrum recorded after ethylene insertion was completed. The average equilibrium constant for the interconversion of **94** to **96** is approximately 0.18, found from Equation 4.1, and the average $\Delta G^\circ = 1.1$ kcal/mol. The equilibrium constant showed remarkably small variation upon changing the solvent composition and suggests a slight thermodynamic preference of **94** over **96**. The K_{eq} and ΔG° calculated from the measurements are given in Table 4.3. However, accurate integrals in the ^1H NMR spectrum are hard to obtain with such small amounts of one of the species.

$$K_{eq} = \frac{[\mathbf{96}][TFA]}{[\mathbf{94}][TFE]} \quad (4.1)$$

Complex **94** dominates in solution even when there is more TFE- d_3 present, suggesting that **94** is thermodynamically more stable than **96**. To test this hypothesis, **62** was reacted with ethylene in dichloromethane- d_2 with 1.2 equivalents



Scheme 4.8: Products **94** and **96** formed in different ratios depending on the ratios of TFA-*d* and TFE-*d*₃.

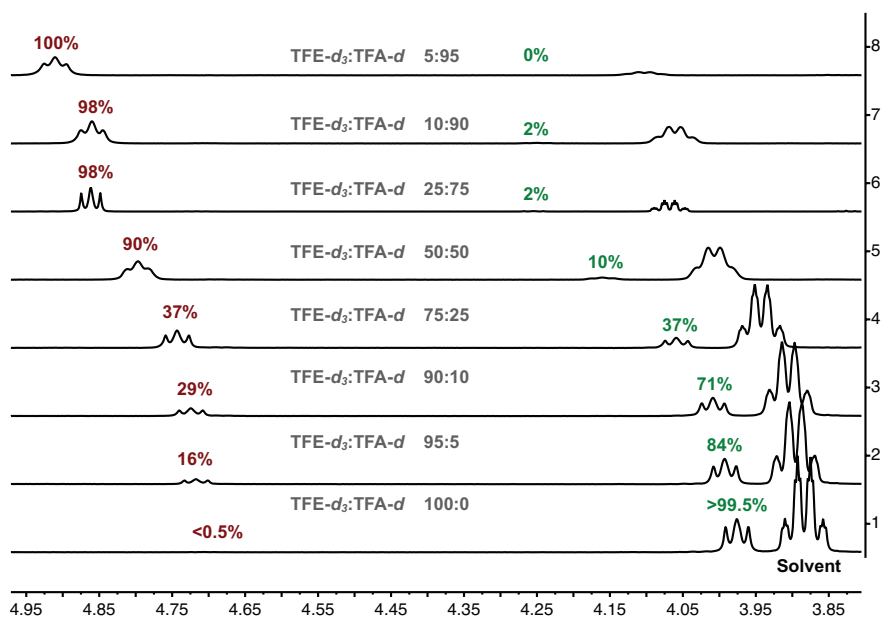


Figure 4.4: ¹H NMR (500 MHz) of **94** (maroon, triplet to the left) and **96** (green, triplet to the right) in variable concentrations of TFE-*d*₃ and TFA-*d* (v/v, written in the middle of the spectra). The peaks shown arise from the CH₂-group next to O in **94** and **96** respectively. The apparent quartet to the right labeled 'solvent' (3.9 ppm in the bottom spectrum) is due to TFE. In the top spectrum there is exclusively **94** formed, whereas in the bottom spectrum there is almost exclusively **96**. All peaks shift slightly with varying solvent composition.

Table 4.3: Concentration of **94** and **96** with varying concentration of TFE- d_3 and TFA- d (v/v) as well as calculated K_{eq} and ΔG° [kcal/mol].

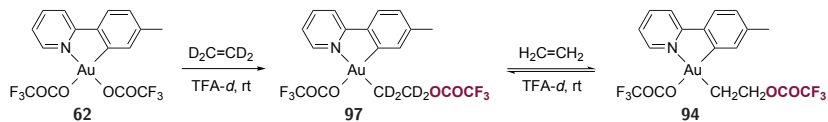
TFE- d_3 [%]	TFA- d [%]	94 [%]	96 [%]	K_{eq}	ΔG°
5	95	0	100	–	–
10	90	2.2	97.8	0.20	0.95
25	75	1.8	98.2	0.05	1.77
50	50	10.3	89.7	0.11	1.31
75	25	36.9	63.1	0.19	0.98
90	10	71.2	28.8	0.27	0.78
95	5	84.2	15.8	0.28	0.75
100	0	99.8	0.2	–	–

For calculating the K_{eq} and ΔG° the numbers in this table were used, although the uncertainty associated with measuring the integrals does not allow for accurate concentrations.

of TFE present in the solution. This should ensure that the concentration of the two nucleophiles $^- \text{OCOCF}_3$ and TFE should be approximately equal assuming full dissociation of the trifluoroacetate ligand. Full conversion to **94** was seen within a day or so. There was no sign of complex **95** after 5 days, confirmed by spiking the NMR sample with an authentic sample of **95**. In the aprotic solvent dichloromethane- d_2 , **94** is thus clearly thermodynamically preferred over **95**.

4.4.2 Reversibility of Ethylene Insertion

Interconversion of **94** and **95** indicates that the nucleophilic addition of $^- \text{OCOCF}_3$ or TFE to coordinated ethylene is reversible, but coordination of ethylene could still be irreversible. To investigate whether ethylene insertion is reversible or not, ethylene- d_4 was added to a solution of $\text{Au}(\text{OCOCF}_3)_2(\text{tpy})$ (**62**) in TFA- d at room temperature (see Scheme 4.9 and Figure 4.5). The expected shifts for the insertion complex **97** were observed in ^1H NMR (middle spectrum Figure 4.5, for structure of **97**; see Scheme 4.9). Then unlabelled ethylene was bubbled through the solution of **97**. After 5 minutes, signals for the two CH_2 -groups appeared in the ^1H NMR spectrum. The top spectrum in Figure 4.5 shows the NMR spectrum recorded after the sample was left over night, as that was when the highest ratio of **94** to **97** was seen (1:4). Attempts at reforming complex **62** from **94** failed. A solution of **94** in TFA- d was purged with argon gas, and a solution of **94** in



Scheme 4.9: Reaction of ethylene- d_4 with **62** gave full conversion to **97** which was treated with unlabelled ethylene to form significant amounts of **94** (**97:94**, 4:1).

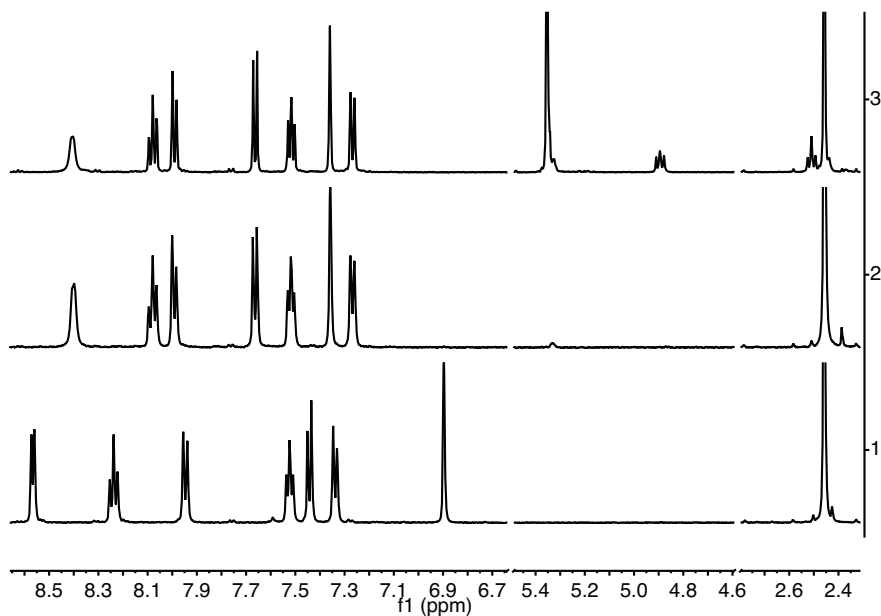


Figure 4.5: ^1H NMR spectra (TFA- d_4 , 600 MHz) of the reaction of $\text{Au}(\text{OCOCF}_3)_2(\text{tpy})$ (**62**) with ethylene- d_4 followed by reaction with unlabelled ethylene. Bottom: Starting material $\text{Au}(\text{OCOCF}_3)_2(\text{tpy})$ (**62**). Middle: After reaction with ethylene- d_4 ; $\text{Au}(\text{CD}_2\text{CD}_2\text{OCOCF}_3)(\text{OCOCF}_3)(\text{tpy})$ (**97**). Top: After reaction with unlabelled ethylene; $\text{Au}(\text{CH}_2\text{CH}_2\text{OCOCF}_3)(\text{OCOCF}_3)(\text{tpy})$ (**94**) formed in addition to **97** as is apparent from the two triplets at 4.9 and 2.5 ppm. Notice that parts of the spectra have been omitted to improve the clarity.

dichloromethane- d_2 was subjected to several freeze-pump-thaw cycles. There was however no sign of **62** by ^1H NMR. The experiments show that ethylene insertion is indeed reversible, however being unable to reform **62** leaves the question open with respect to whether ethylene- d_4 /ethylene exchange takes place *via* **62** or *via* some other intermediate.

4.4.3 External Versus Internal Nucleophilic Addition of Trifluoroacetate

Both internal or external attack by trifluoroacetate at ethylene coordinated to gold are possible pathways to form **94** (Figure 4.6). For further investigation into the mechanism, the ethylene insertion was conducted with *cis*-dideuterioethylene. There are two possible diastereomeric outcomes of the reaction between **62** and *cis*-dideuterioethylene, the *threo* and the *erythro* isomers (Figure 4.7) resulting from intermolecular or intramolecular addition of trifluoroacetate, respectively.

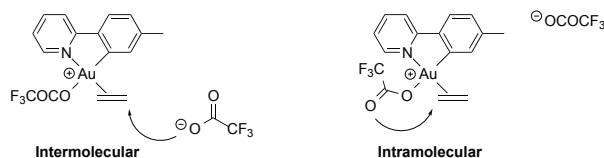


Figure 4.6: Inter- *vs* intramolecular attack by $^-\text{OCOCF}_3$ at coordinated ethylene.

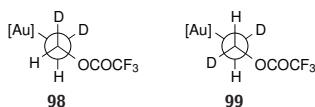
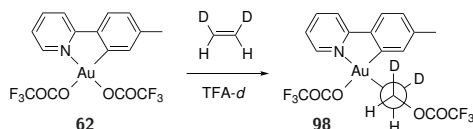


Figure 4.7: Possible diastereomers in the reaction of *cis*-dideuterioethylene with **62**; *threo* **98** and *erythro* **99** resulting from external or internal attack on ethylene, respectively.

The coupling constants for the possible product complexes *threo* (**98**) and *erythro* (**99**) should give insight into whether there is an external or internal attack on ethylene. According to Bercaw *et al.*, the coupling constants $^3J(^1\text{H}-^1\text{H})$ for the *threo* and *erythro* products in the Pt(IV) complex $[\text{Pt}(\text{CHDCHD})\text{Cl}_5]_2^-$ are 6 and

8 Hz, respectively.¹⁷³ For a mercury complex, the *erythro* product gave a coupling constant of 8.4 Hz (in CD₃OD).¹⁷⁴ For Au(CHDCHDOCOCF₃)(OCOCF₃)(tpy) (**98**), the spectra showed two doublets as expected and the observed coupling constant in the reaction depicted in Scheme 4.10 was approximately 6 Hz (6.1 and 5.7 Hz in TFA-*d* and CD₂Cl₂, respectively), corresponding with a *threo* orientation. Observation of the *threo* product **98** supports an external nucleophilic attack by ⁻OCOCF₃ or TFE on ethylene.



Scheme 4.10: Reaction of *cis*-dideuterioethylene with **62** gave the *threo* product **98** consistent with external nucleophilic attack.

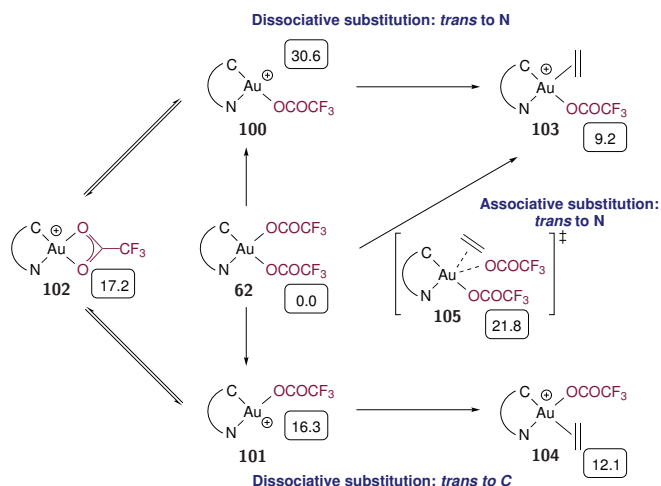
Complex **98**, resulting from the reaction with *cis*-dideuterioethylene (Scheme 4.10), was monitored over time. No interconversion from the *threo* diastereomer to the *erythro* diastereomer was observed in dichloromethane-*d*₂ over the course of several days. No interconversion was observed in TFA-*d* after one day (due to slow decomposition in TFA-*d* **98** cannot be monitored for long periods of time).

4.4.4 DFT Calculations on the Reaction Mechanism

To support the experimental findings and gain deeper insight into the mechanism, a mechanistic study of the ethylene insertion into the Au-OCOCF₃ bond in **62** was performed using DFT calculations. The DFT calculations were performed by Dr. Ainara Nova (University of Oslo). The first step that can be envisioned in the formal ethylene insertion discussed in this chapter, is either direct insertion or dissociation of one ⁻OCOCF₃ ligand followed by ethylene coordination to gold. All attempts to find a transition state (TS) for the direct insertion of ethylene into the Au-O bonds were unsuccessful, and hence the substitution of ⁻OCOCF₃ by ethylene was explored (Scheme 4.11). This substitution process can be either dissociative or associative.

4.4.4.1 Ethylene Coordination to Gold

Both the dissociative and the associative pathways are shown in Scheme 4.11. Dissociation of the ${}^{-}\text{OCOCF}_3$ *trans* to nitrogen yields intermediate **100** 30.6 kcal/mol higher in energy than the reactants (**62** and ethylene), while dissociating the ligand *trans* to carbon leads to **101**, 16.3 kcal/mol higher in energy than **62** and ethylene (Scheme 4.11). Due to the higher *trans* effect of carbon *versus* nitrogen in the tpy ligand, this is as expected. **100** and **101** can interchange through **102** where the trifluoroacetate ligand is η^2 -bound to gold (17.2 kcal/mol, Au–O distances of 2.08 and 2.39 Å for the O *trans* to N and *trans* to C, respectively), only slightly uphill from **101**. Dissociation of the ${}^{-}\text{OCOCF}_3$ ligand *trans* to carbon is feasible at room temperature in TFE according to the calculations, which is in accordance with the broad peak observed in ${}^{19}\text{F}$ NMR in polar solvents corresponding to the trifluoroacetate group *trans* to carbon, as discussed in Chapter 2 (Section 2.3). The high energy of **100** (30.6 kcal/mol above reactants) however makes **100** unlikely to be



Scheme 4.11: Ethylene addition by dissociative (*trans* to N or C) of ${}^{-}\text{OCOCF}_3$ or associative (*trans* to N) substitution in **62**. The numbers indicated are free energies in kcal/mol in TFE (dielectric continuum). The energies of ${}^{-}\text{OCOCF}_3$ and ethylene have been included in the calculations where needed, hence all values refer to the same overall composition.

a kinetically competent intermediate at room temperature.

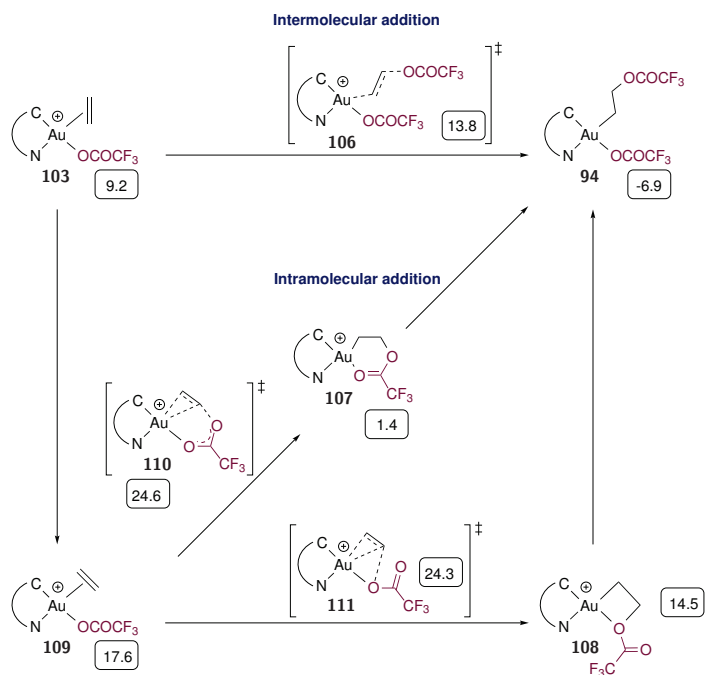
Coordination of ethylene to **100** and **101** to yield **103** at 9.2 kcal/mol and **104** at 12.1 kcal/mol above **62** and ethylene. The energies show a thermodynamic preference for coordination of ethylene *trans* to nitrogen, the ligand with the weaker *trans* influence, corresponding well with the only observed product in the reaction being the complex where ethylene insertion has taken place *trans* to nitrogen. Formation of **103** *via* **100** in a dissociative fashion seems unlikely due to the high energy of **100** of 30.6 kcal/mol. An associative pathway from **62**, still *trans* to nitrogen, going through the TS **105** of 21.8 kcal/mol is however reasonable for a reaction taking place at room temperature. Associative substitution *trans* to carbon was calculated to be 17.8 kcal/mol above reactants (**62** + ethylene, Scheme 4.13).

4.4.4.2 Nucleophilic Addition to Coordinated Ethylene

Having found a pathway leading to an intermediate where ethylene is coordinated *trans* to nitrogen (intermediate **103**) that is feasible at room temperature, the next step is the nucleophilic attack by ${}^{-}\text{OCOCF}_3$ or TFE at ethylene coordinated to gold. Inter- and intramolecular addition of ${}^{-}\text{OCOCF}_3$ or TFE to ethylene coordinated to gold can be envisioned *via* one of the three TS depicted in Scheme 4.12.

There are two pathways from **103** to obtain the product **94** that can be envisioned; intermolecular addition of ${}^{-}\text{OCOCF}_3$ *via* **106** or intramolecular addition either *via* an intermediate with a 6-membered ring **107** or a 4-membered ring **108** (Scheme 4.12). The intermolecular addition where dissociated ${}^{-}\text{OCOCF}_3$ attacks ethylene coordinated to gold is calculated to occur *via* TS **106** at only 13.8 kcal/mol, making this a fast process at room temperature consistent with what is observed experimentally. The product **94** has an associated free energy 6.9 kcal/mol lower than the reactants (**62** + ethylene). The geometry of TS **106** is depicted in Figure 4.8.

From the calculations performed, it is suggested that more than one step is required for the intramolecular addition. It seems as though it is necessary for the coordinated ethylene to reorient its coordination from the preferred orientation, where the C=C bond is perpendicular to the C–Au–N plane in **103**, to having a



Scheme 4.12: Inter- and intramolecular nucleophilic addition of ${}^{-}\text{OCOCF}_3$ to **103**. The numbers indicated are free energies in kcal/mol in TFE. The energies of ${}^{-}\text{OCOCF}_3$ and ethylene have been included in the calculations where needed, hence all values refer to the same overall composition.

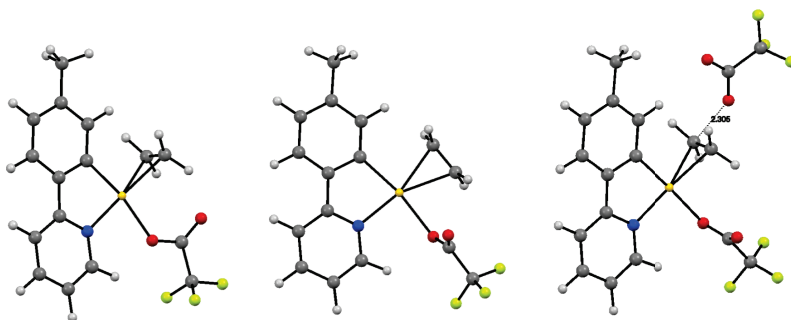
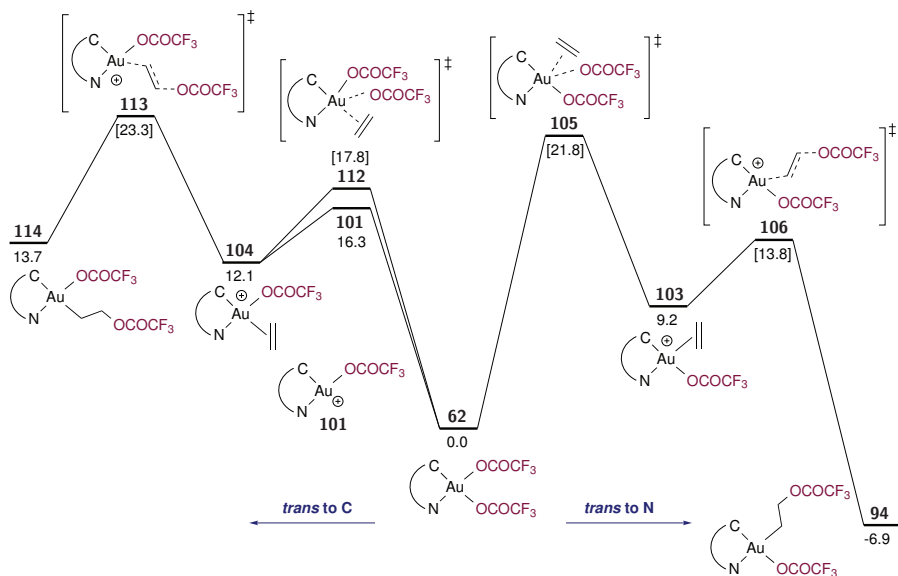


Figure 4.8: Intermediates **103** (left, ethylene coordinated perpendicular to the C–Au–N plane) and **109** (parallel with the plane, higher in energy), and TS **106** (right, C⋯O distance of 2.305 Å).

parallel orientation as in **109**. This reorientation has an energy cost of 8.4 kcal/mol (17.6 kcal/mol in **109** vs 9.2 in **103**, respectively). When ethylene has reoriented its coordination to gold, two pathways *via* a 6-membered or a 4-membered intermediate were found. The pathway *via* the 6-membered intermediate **107** at 1.4 kcal/mol has an associated TS **110** located 24.6 kcal/mol higher in energy than the reactants. The 4-membered intermediate **108** is formed *via* the TS **111** at 24.3 kcal/mol. The two pathways for intramolecular addition have similar energy barriers, both have transition states with associated free energies of 24–25 kcal/mol above reactants. For ease of visualisation, the geometries of coordinated ethylene in **103** and **109** are depicted in Figure 4.8

The difference of 8.4 kcal/mol between **103** and **109** depending on the orientation of coordinated ethylene is what accounts for most of the higher energy barrier



Scheme 4.13: Visualisation of the energetically accessible pathways for ethylene coordination and subsequent product formation by ethylene addition *trans* to C or N where the latter forms the observed product. The numbers indicate free energies in kcal/mol with respect to **62** + ethylene. The energies of OCOCF_3 and ethylene have been included in the calculations where needed, hence all values refer to the same overall composition.

of an intramolecular addition (*via* TS **110** or **111**) *versus* an intermolecular addition, making the intermolecular addition kinetically much more favourable. These computational findings are in complete agreement with the experiment where *cis*-dideuterioethylene and **62** formed only the *threo* product **98**, clearly demonstrating the intermolecular addition of ${}^{-}\text{OCOCF}_3$.

The computational results point to the idea that if there exist systems in which the coplanar orientation of the alkene and the nucleophile is preferred, an intramolecular addition could be the favoured mechanism. In addition, in systems with no steric limitations both intra- and intermolecular additions could be possible mechanisms.

Addition of ethylene *trans* to carbon is calculated to give a final product 13.7 kcal/mol above reactants in energy (**114**, Scheme 4.13). The endergonic nature of addition *trans* to carbon is consistent with the only observed product is where ethylene has inserted *trans* to nitrogen, yielding **94**.

4.4.4.3 Nucleophilic Attack by TFE

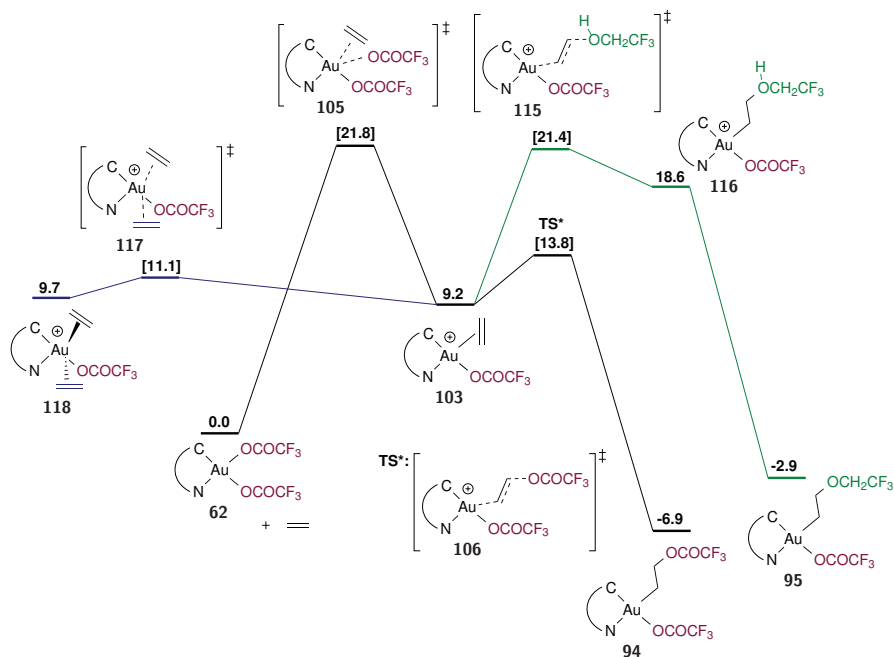
As the reader might recall, if **62** is reacted with ethylene in TFE rather than in TFA, **95** is formed instead of **94**. Having established that the likely mechanism of formation of **94** *via* external nucleophilic attack by ${}^{-}\text{OCOCF}_3$ by both experimental and computational means, the next consideration was the mechanism of formation of **95** by nucleophilic attack by TFE.

Due to the large difference in energy between the inter- and intramolecular addition of ${}^{-}\text{OCOCF}_3$ (Scheme 4.12), only the intermolecular addition was considered for nucleophilic addition of TFE. An analogous intermediate of **109** (Scheme 4.12) with OCH_2CF_3 coordinated *trans* to carbon could be envisioned, but was not computed as it seemed less likely.

Intermolecular addition of TFE to **103** yields the cationic intermediate **116** *via* the TS **115** (Scheme 4.14). Fast deprotonation gives the product **95**, 2.9 kcal/mol lower in energy than reactants (**62** + ethylene).

As seen from the higher energy barrier in Scheme 4.14 and the 4.0 kcal/mol lower energy (in TFE) of **94** compared to **95**, **94** is both kinetically and thermodynamically preferred over **95** in the solvent TFE, thus nucleophilic addition of

$^-OCOCF_3$ is both kinetically and thermodynamically preferred over nucleophilic addition of TFE (in TFE). The same thermodynamic preference is observed in gas phase by 2.7 kcal/mol ($\Delta\Delta G^\circ(95 - 94) = 2.7$ kcal/mol) and 5.2 kcal/mol in dichloromethane ($\Delta\Delta G^\circ(95 - 94) = 5.2$ kcal/mol). The calculated thermodynamic preference of **94** over **95** is consistent with the experiment conducted where **62** in dichloromethane- d_2 with 1.2 equivalents of TFE was reacted with ethylene to form **94** as the sole product and with the experimentally found ΔG° of 1.1 kcal/mol.



Scheme 4.14: Energy profile for the for addition of $^-OCOCF_3$ (in black) and TFE (in green) to **62**. Addition of ethylene to **103** is indicated in blue. All energies of minima and TS (in brackets) are free energies in kcal/mol in TFE. The energies of ethylene, $^-OCOCF_3$ and TFE have been included in the calculations where needed, hence all values refer to the same overall composition. The exchange of two ethylene molecules is possible by the low energy barrier to give pentacoordinated bis(ethylene) intermediate **118** (in blue).

4.4.4.4 Solvent Effects

All the calculations were performed in TFE as a dielectric continuum ($\epsilon = 26.74^{175}$). In TFE, **94** is both kinetically and thermodynamically preferred over **95**, however experimentally the observed product in TFE- d_3 is always **96** (**95** and **96** differ only by $\text{OCH}_2\text{CF}_3/\text{OCD}_2\text{CF}_3$). This is explained by the large excess of TFE- d_3 compared to TFA/ ${}^-\text{OCOCF}_3$ present in a 20 mM solution of **62** in TFE- d_3 where the only source of ${}^-\text{OCOCF}_3$ is what stems from **62** itself (hence only 20 mM).

The consumption of **94** was faster in TFA- d (ca 5 min) and TFE- d_3 (ca 30 min) than in dichloromethane- d_2 (ca 1 d). The free energy of TS **105** in dichloromethane (25.1 kcal/mol) is 3.3 kcal/mol higher in energy compared to the same TS in TFE (21.8 kcal/mol). TS **105**, which the calculations predict to be the rate determining step, is higher in energy in dichloromethane, accounting for the lower reaction rate in dichloromethane compared to in TFE. The more polar solvent TFE stabilises TS **105** better, the calculated energy difference is thus reasonable. Higher polarity cannot alone account for the difference in reaction rate as dichloromethane and TFA have similar polarities ($\epsilon = 8.93$ and 8.42^{175} respectively) even though the reaction is significantly faster in TFA. TFA should however be able, through stabilisation by hydrogen bonding, to assist in the departure of ${}^-\text{OCOCF}_3$. It is worth remembering that both TFA and TFE are reactants in the reaction of **62** with ethylene, hence as solvents they are not innocent. Specific hydrogen bond interactions could have implications for the energies calculated but were not considered in the calculations.

4.4.4.5 Reversibility

The energy barriers for nucleophilic attack by ${}^-\text{OCOCF}_3$ or TFE at coordinated ethylene in Scheme 4.14 are low and the reactions are only slightly exothermic, making a reversible reaction reasonable, consistent with the experimentally observed reversibility. **94** and **95** can interchange easily *via* intermediate **103**, recall that if **95** is dissolved in TFA- d it immediately reacts to form **94** and that if **94** is dissolved in TFE- d_3 it gradually reacts to form **96**. The other step confirmed experimentally to be reversible, was coordination of ethylene as reaction of the tetradeuterated **97** (from reaction with $\text{D}_2\text{C}=\text{CD}_2$) in TFA- d with $\text{H}_2\text{C}=\text{CH}_2$

forms some of the unlabelled complex **94** (Scheme 4.9). The pentacoordinated bis(ethylene) intermediate **118** where two ethylenes are coordinated to gold has an associated free energy of 9.7 kcal/mol, only slightly higher than **103** (9.2 kcal/mol) and a barrier from **103** to **118** of only 1.9 kcal/mol (Scheme 4.14). Thus, ethylene exchange *via* this pathway is preferable when compared to going all the way back to **62**. This is supported by the fact that **62** was not observed after the initial reaction and it was not possible to reform **62** by purging a solution of **94** in TFA-*d* with argon or by several freeze-pump-thaw cycles on a solution of **94** in dichloromethane-*d*₂.

4.4.5 Attempts at Achieving a Catalytic Process

Only one insertion was observed using ethylene, and always with ethylene inserting into the Au–O bond *trans* to nitrogen. Adding triflic acid (HOSO₂CF₃) to a solution of **94** in TFA-*d* in an attempt to make the transformation catalytic and force the protodeauration step did not succeed. It seemed as though the only change triflic acid induced was faster decomposition. To quench any water present, trifluoroacetic anhydride was added in a few experiments. This however had little effect upon the stability of **94** in TFA-*d* and no further reactivity was observed.

As described in Chapter 3, HP NMR using sapphire NMR tubes were used to study several of the gold(III) complexes described in this thesis. **62** was studied at high pressure of ethylene yielding the expected **94**. With an ethylene pressure of 60 bar followed by heating at 50 °C for one day, **94** in TFA-*d* did not yield a catalytic process as desired. The reason not to use higher ethylene pressures than 60 bar at room temperature was that heating was desirable. Higher reaction temperature was believed to affect the reaction more than a small pressure increase. Another reason for trying higher pressures of ethylene was the desire to observe any intermediates in the reaction, e.g. ethylene coordinated to gold(III) in some respect. As functionalisation of ethylene with, for example CO, would be highly desirable, 78 bar of CO was added to a solution of **94** in TFA-*d* containing some ethylene in the solution. No reactivity seemed to be the outcome of the experiment.

A suggestionⁱⁱ that was undertaken was to add iodine in an attempt to move to a

ⁱⁱIn a discussion with A. S. K. Hashmi, Universität Heidelberg.

catalytic transformation. This did indeed lead to further reactivity, see Figure 4.9. The two apparent triplets associated with the two methylene groups in **94** (from inserted ethylene) disappeared over time accompanied by the appearance of two new triplets. The two new triplets appeared at 4.56 and 3.28 ppm, and was believed to be 1,2-diiodoethane (Scheme 4.15). The control experiment of ethylene and

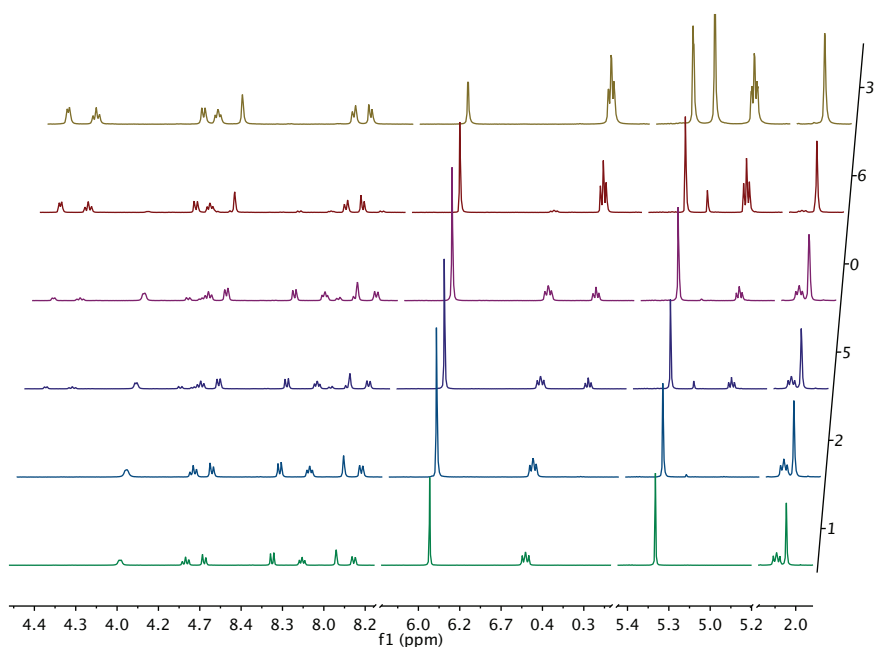
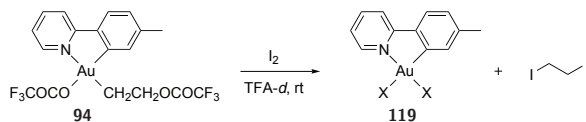


Figure 4.9: ^1H NMR (500 MHz, $\text{TFA-}d$) spectra showing the reaction of **94** with I_2 in $\text{TFA-}d$ (solvent residual omitted for clarity, $\text{CH}_2\text{ClCH}_2\text{Cl}$ as ISTD at 3.7 ppm). Spectrum 1: Before addition of I_2 , Spectrum 2: After addition of I_2 . Going up the series, the reaction time increases. Parts of the spectra have been omitted to improve clarity.

iodine in $\text{TFA-}d$, without any gold(III) complex added, quickly revealed that gold was not needed in the transformation of ethylene to 1,2-diiodoethane. Colourless crystals suitable for X-ray crystal determination were grown from the mixtures resulting from the reactions undertaken both in the presence and absence of gold. Both solid-state structures were found to be 1,2-diiodoethane. In the resulting gold(III) complex **119**, tpy is still bonded in a bidentate fashion (7 Ar-H, still



Scheme 4.15: Reaction of **94** with I_2 . X = I or $OCOCF_3$.

nonsymmetric), iodine likely occupied one or both of the other coordination sites (denoted as X in Scheme 4.15). As the control experiment had revealed that gold was not necessary for the transformation, the investigations were left at this point.

4.4.6 Different Solvents

In addition to TFA, TFE and dichloromethane- d_2 , methanol, water, acetonitrile and THF were also investigated briefly.

As described in Section 4.2, $Au(OCOCF_3)_2(tpy)$ (**62**) in methanol was reacted with ethylene. The nucleophilic attack has in this case likely happened by methanol, analogous to attack by trifluoroethanol. The assumed gold(III) product **120** is shown in Figure 4.10

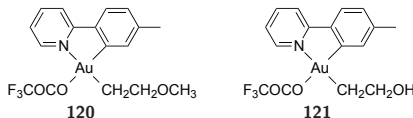


Figure 4.10: Assumed products from the reaction between **62** and ethylene in MeOH (**120**) and H_2O (**121**).

Water was not the most suitable solvent for the reaction due to the insolubility of both starting material **62** and product, and to complicate matters, bubbling ethylene into a suspension of **62** in water created large amounts of foam. As solubility is not a requirement for a reaction to take place, some investigations were still initiated, but without success. The suspension quickly started to bubble out of the vent needle, even when a condenser was mounted on the top of the round bottom flask. The resulting foaming suspension did not seem to have reacted even after several days (then bubbling of ethylene was only taking place in portions to prevent all the solvent from escaping through the vent needle). Due to the

foam created, it was not convenient to perform this reaction in standard glassware but it was thought a closed system with the ability to tolerate higher pressures might overcome this issue. A teflon liner for a Parr reactor was loaded with **62** and water and pressurised with ethylene followed by heating at 50 °C for 3 days. Evaporation of the solvent yielded three different products by ^1H NMR (Figure 4.11). One product was **94**, but the main product of the reaction was likely

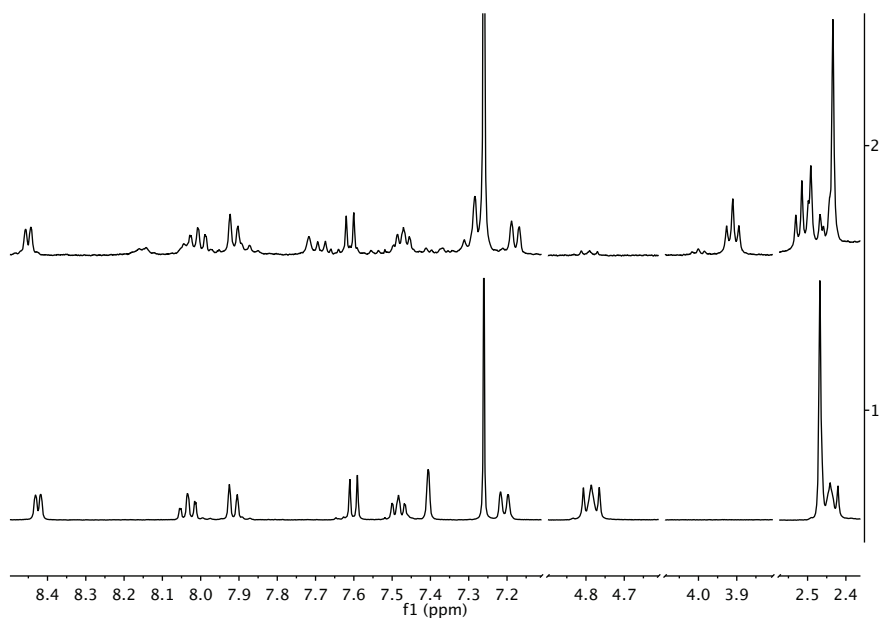


Figure 4.11: ^1H NMR (400 MHz, CDCl_3) spectrum showing the product of the reaction of **62** with ethylene in H_2O (top) compared to **94** (bottom). Parts of the spectra have been omitted to improve clarity.

formed by nucleophilic attack by water at coordinated ethylene (**121**, Figure 4.10). The second ligand was likely still trifluoroacetate, as the ^{19}F showed one major resonance and several minor (integrating to *ca* 10% of the major). The resonances observed in the ^1H NMR spectrum in Figure 4.11 (top) show a greater resemblance to **95**; H-6' (singlet, 7.3 ppm) has higher ppm value than **62**, but lower than in **94**. The triplet for the methylene unit furthest away from gold appeared at lower

ppm values consistent with alcohol/ether rather than acetate as in **94**. Attempts at crystal growth did not succeed.

In acetonitrile however, full conversion was seen after almost 2 days. The first spectrum acquired (bottom spectrum, Figure 4.12) showed mainly starting material **62**, but also a product that was not **94** as is formed in TFA-*d* or dichloromethane-*d*₂. Over the course of two days at room temperature, the first product formed reacted to form a new species (top spectrum, Figure 4.12). On NMR scale, the sole product formed after 2 days differed from **94**. At preparative scale, the formation of **94** was observed, in addition to the product observed at NMR scale. Attempts to purify the crude mixture by crystallisation gave some

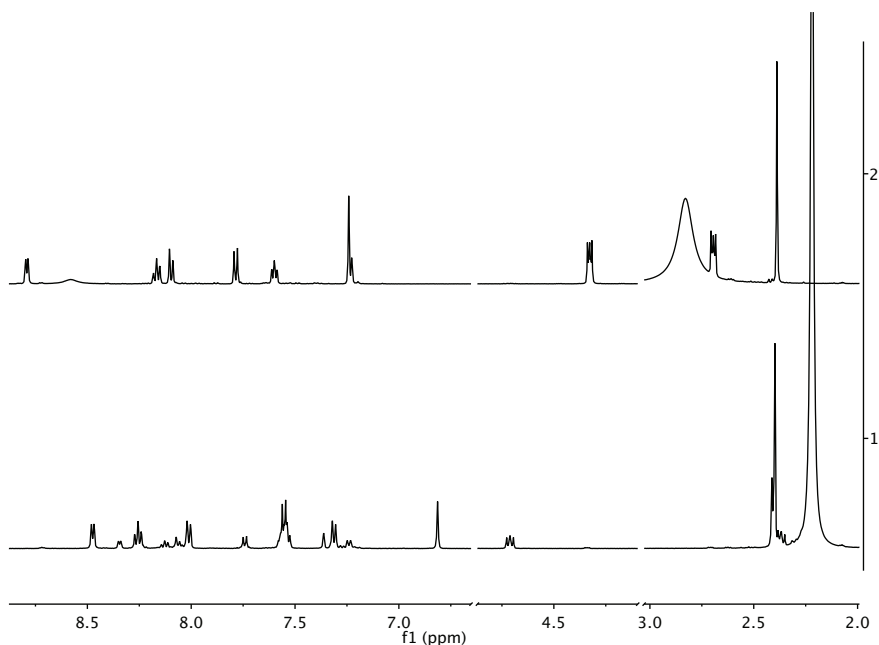


Figure 4.12: ¹H NMR (500 MHz, CD₃CN) spectra of the reaction of **62** with ethylene in CD₃CN. Bottom: 30 min after ethylene addition (1. product:**62**, 0.3:1), Top: After 2 d at rt, 2. product. Parts of the spectra have been omitted to improve clarity.

crystals, but the crystals selected for X-ray structure determination proved to be **94** and hence gave no indication of what the other product might be. Based on

the appearance of the ^1H NMR spectrum in acetonitrile- d_3 , a product similar in structure to **94** is formed. The identity of the product was not found as attempts at preparative scale reactions led to isolation of mixtures or **94**.

The reaction between **62** and ethylene in THF- d_8 proceeds slower even than in dichloromethane- d_2 . Another factor other than the reaction time is also apparent from the spectra shown in Figure 4.13; there are two products formed. The mixture shown (top spectrum, Figure 4.13) contains two products and the starting material in approximately 1:2:1 ratio (observing the doublets at 8.5 and 7.2 ppm). The nature of the two products was not determined.

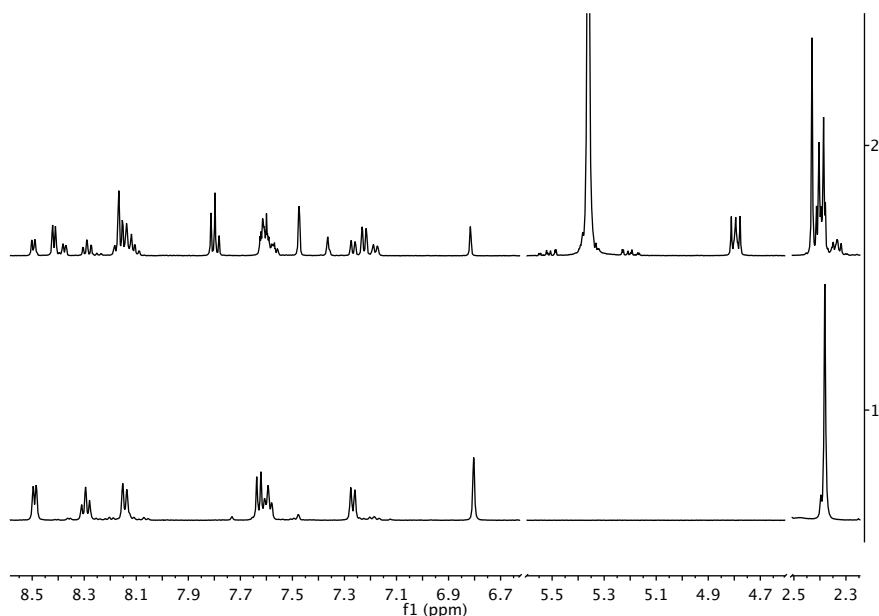


Figure 4.13: ^1H NMR (500 MHz, THF- d_8) spectra of the reaction of **62** with ethylene in THF- d_8 . Bottom: **62** in THF- d_8 before ethylene added, Top: Approx. 22 h after addition of ethylene. Parts of the spectra have been omitted to improve clarity.

Choice of solvent for the reaction between $\text{Au}(\text{OCOCF}_3)_2(\text{tpy})$ (**62**) and ethylene had a strong influence on the observed reaction rate in addition to determining

the product. Increasing solvent polarity and hydrogen bonding ability gave higher observed reaction rates (at least in a qualitative fashion).

4.5 Other Alkenes and Alkynes

Thorough investigation has so far only been conducted for ethylene, but several other compounds have been tested as well. Some alkenes, such as 1,5-cyclooctadiene (cod) and 1,5-hexadiene gave formal insertion as well.¹⁷⁶ As the tested alkenes gave exiting results, of course alkynes were of interest. $\text{Au}(\text{OCOCF}_3)_2(\text{tpy})$ (**62**) reacted quickly with ethynyltrimethylsilane (in TFA-*d*, rt) and 1,2-bis(trimethylsilyl)ethyne (TFA-*d*, rt) but led to mixtures of products. It seems as though all the alkenes and

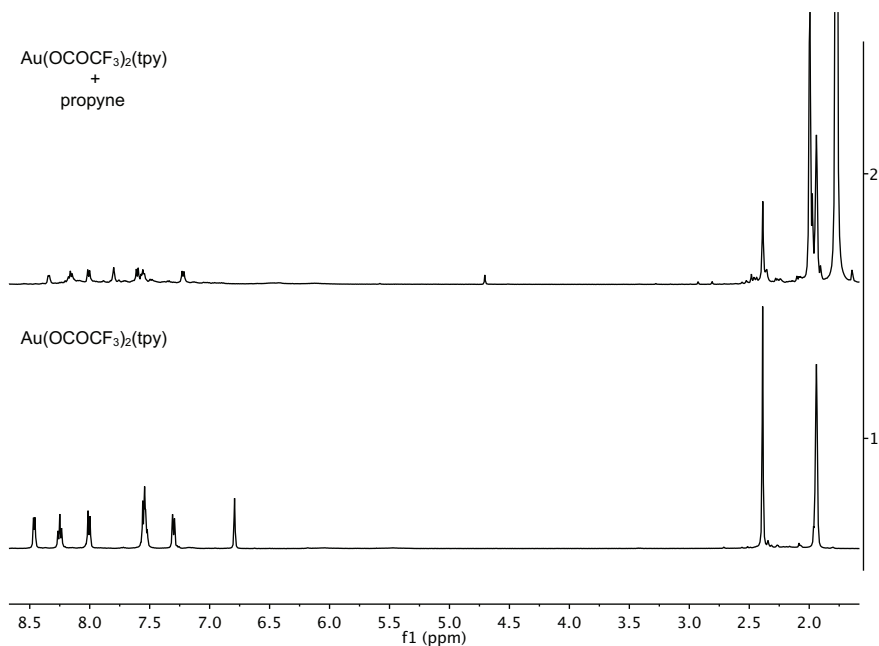


Figure 4.14: ¹H NMR spectrum (CD_3CN , 500 MHz) of **62** reacted with propyne (s at 1.77 ppm and q at 1.98 ppm). The resonances corresponding to propyne have been clipped horizontally to improve the clarity.

alkynes tested so far give quite apparent colour change upon reaction, a feature especially helpful when performing NMR tube experiments.

4.5.1 $\text{Au}(\text{OCOCF}_3)_2(\text{tpy})$ with Propyne

Propyne reacts quickly with $\text{Au}(\text{OCOCF}_3)_2(\text{tpy})$ (**62**) in acetonitrile- d_3 or TFA- d . The reaction in acetonitrile- d_3 is not particularly clean, but one major product is observed (Figure 4.14). The singlet at 4.7 ppm is an impurity, it was present in the reference spectrum of propyne in acetonitrile- d_3 . In TFA- d however, the spectra looked slightly more messy (Figure 4.15), but the extra singlet at 4.8 ppm likely caused by a vinylic proton is worth noticing. As the mechanism to form **94** described in Section 4.4 was shown to proceed *via* an *anti* addition of $^-\text{OCOCF}_3$

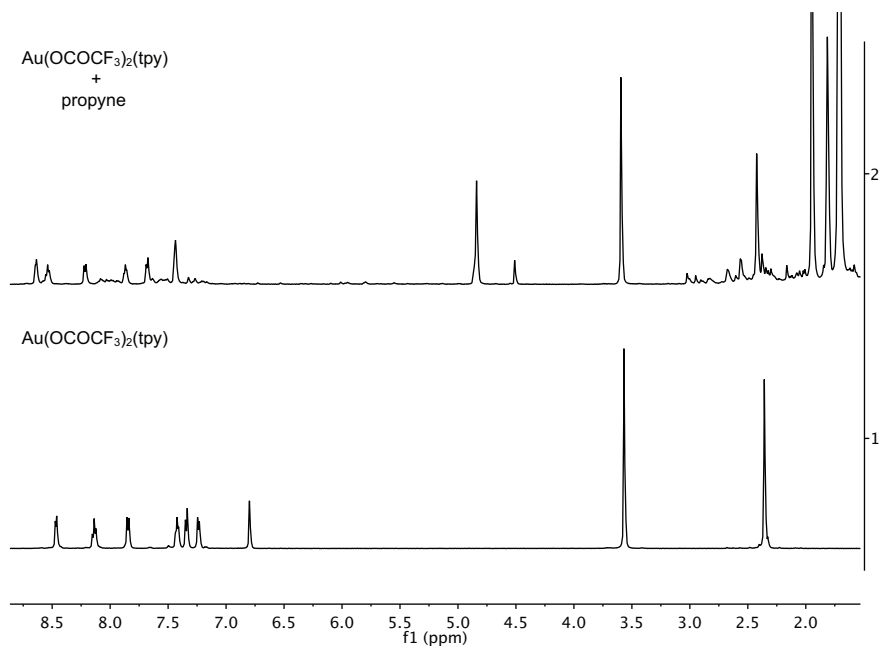


Figure 4.15: ^1H NMR spectrum (TFA- d , 500 MHz) of **62** reacted with propyne (s at 1.71 ppm and 1.94 ppm). The signals corresponding to propyne have been clipped horizontally to improve the clarity. $\text{CH}_2\text{ClCH}_2\text{Cl}$ as ISTD (3.7 ppm).

to coordinated ethylene, it seems reasonable to assume that this was also the case when ${}^{-}\text{OCOCF}_3$ adds to coordinated propyne. In the case of propyne, insertion can lead to a product where the methyl group is attached to the carbon adjacent to gold (**122**, Figure 4.16), or adjacent to oxygen of the trifluoroacetate group (**123**). The latter is perhaps the more likely product as the assumed vinylic proton is quite shielded (4.5–5 ppm), consistent with a vinylic proton adjacent to gold rather than adjacent to trifluoroacetate.

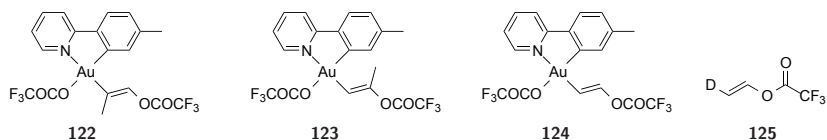


Figure 4.16: Proposed Au-complexes from the reaction between **62** and propyne (**122** and **123**) and acetylene (**124**) in $\text{TFA-}d$, and a possible organic product in the reaction with acetylene (**125**).

4.5.2 $\text{Au}(\text{OCOCF}_3)_2(\text{tpy})$ with Acetylene

Acetylene under high pressure is explosive, hence experiments involving acetylene (containing acetone) were only performed by bubbling the gas into a solution of $\text{Au}(\text{OCOCF}_3)_2(\text{tpy})$ (**62**) in $\text{TFA-}d$. The solution changed from light yellow to orange after the acetylene addition, and later turned brown. Acetylene reacted with **62** in $\text{TFA-}d$ to form a new gold species, presumably a vinyl complex and an organic product. It was quite apparent that an additional species was growing in, and by far more than one equivalent compared to the starting gold(III) complex. It was evident that some catalytic transformation was indeed taking place, as the signals for this species in the ${}^1\text{H}$ NMR spectrum now integrated to about 16:1 compared to the gold(III) complex, also referenced to an internal standard. The signals for the gold(III) complex clearly shifted in the ${}^1\text{H}$ NMR spectrum and a new signal appeared at about 6.3 ppm integrating to 1–2 compared to the aromatic signals in the tpy ligand. The two large doublets at 7.2 and 5.2 ppm with coupling constants of approximately 13.8 Hz, integrating 1:1 with each other and 16:1 compared to the gold(III) complex were observed and were especially of interest. The spectrum acquired shortly after addition of acetylene showed two or more

new species (Figure 4.17) and 2 days after addition one new presumably gold(III) complex and one organic product were formed (top spectrum, Figure 4.17). A ^1H - ^1H COSY experiment revealed that the resonance at 6.3 ppm coupled to one of the aromatic protons and that the two large doublets coupled to each other. The gold(III) complexes formed in the reaction is presumably **124** (Figure 4.16) formed by *anti* addition of $^-\text{OCOCF}_3$ to coordinated acetylene. The organic product formed in the reaction with acetylene, has a coupling constant of 13.8 Hz, reasonable for a *trans* coupling. The reaction was undertaken in deuterated solvent, hence one possible product would be deuterated vinyl trifluoroacetate (**125**, Figure 4.16) that could fit well with the chemical shifts observed.

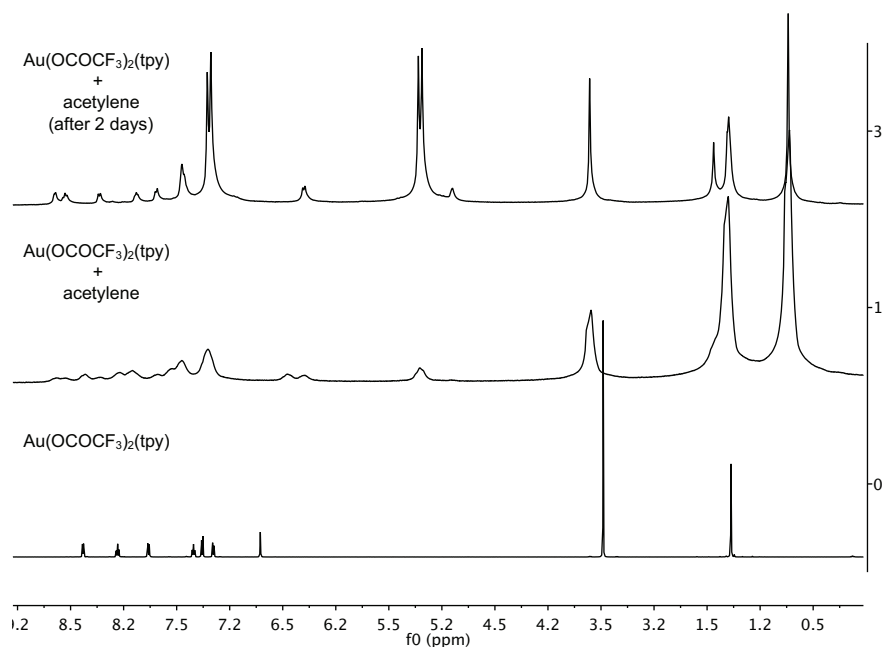


Figure 4.17: ^1H NMR spectrum ($\text{TFA-}d$) of **62** reacted with acetylene. Bottom spectrum is acquired at 600 MHz instrument with a 5 mm probe whereas the two top spectra are acquired on a 400 MHz instrument with a 10 mm probe.

The reaction was also performed in dichloromethane- d_2 yielding a large number of resonances in the aromatic and aliphatic regions that were difficult to interpret.

The protic TFA-*d* might aid the catalytic transformation as such catalytic activity seemed absent in the aprotic dichloromethane-*d*₂. The control experiment showed that acetylene stays intact in TFA-*d* over the course of several days, which indicate that Au(OCOCF₃)₂(tpy) (**62**) was required for the transformation to take place.

4.6 Conclusions

Reaction of ethylene with Au(OCOCF₃)₂(tpy) (**62**) in TFA-*d* and dichloromethane-*d*₂ gave Au(CH₂CH₂OCOCF₃)(OCOCF₃)(tpy) (**94**) whereas in TFE-*d*₃ the reaction gave Au(CH₂CH₂OCD₂CF₃)(OCOCF₃)(tpy) (**96**). As the concentration of TFE-*d*₃ is much higher than the trifluoroacetate concentration when the reaction is performed in TFE-*d*₃ as the solvent, nucleophilic addition of the alcohol (TFE) takes place rather than by the trifluoroacetate. **94** is however thermodynamically preferred over Au(CH₂CH₂OCH₂CF₃)(OCOCF₃)(tpy) (**95**), demonstrated both experimentally and computationally.

The mechanism for the formal insertion of ethylene into the Au–O bond consistent with both experimental and computational methods consists of the associative substitution of the trifluoroacetate ligand *trans* to nitrogen by ethylene followed by the intermolecular addition of trifluoroacetate to the coordinated ethylene. The intermolecular nature of the formal insertion was established by using *cis*-1,2-dideuterioethylene as a mechanistic probe.

The formal insertion of ethylene is reversible, shown by exchange of ethylene-*d*₄ (inserted to form **97**) by ethylene to form substantial amounts of **94**. The pathway for the ethylene exchange is expected to happen *via* the pentacoordinated gold species Au(CH₂CH₂)₂(OCOCF₃)(tpy)⁺ (**118**) found computationally.

The formal insertion of ethylene can take place in several solvents with; TFA, TFE, dichloromethane, methanol, THF, water and acetonitrile investigated. The nature of the nucleophile, and hence the product, has not been fully determined in all cases. The reactivity towards unsaturated compounds extends further than just ethylene; propyne, acetylene, cod and 1,5-hexadiene are mentioned in this chapter. The alkynes seem especially interesting as a catalytic transformation appear to take place.

4.7 Experimental

General Experimental Methods

Au(OCOCF₃)₂(tpy) (**62**) was synthesised as described in Paper I¹⁰⁶ (Appendix). Pressurised reactions were conducted at SINTEF using a system containing 4 x 6 wells that were added small teflon spheres, to enable good mixing when displaced on a shaker board. Each well contained 2 mL solvent. NMR solvents were used as received. NMR spectra were recorded on Bruker Avance AVII400, DRX500, and AV600 instruments operating at 400, 500 and 600 MHz (¹H). For experiments with acetylene, sample volumes of 1.5–2.5 mL were used and the spectra were acquired using a Bruker DRX400 spectrometer operating on 400 MHz (¹H) equipped with a 10 mm BBO probe. The acetylene used contained acetone. Ethylene was from Hydrogas. The remaining experiments described in this chapter are included in Paper II¹⁰⁷ (Appendix).

AuMe(tpy)OTf (**55-OTf**)

The synthesis was based on the procedure to make **55-OTf** from AuClMe(tpy) (**56**),¹⁰⁴ and was performed by Eline Aa. Tråseth (University of Oslo). AuBrMe(tpy) (**70**) was stirred with AgOTf (1.9 equiv) in TFE at rt for 2 d.¹¹¹

High Pressure Reactions With Ethylene

6 stock solutions, each of 12.0 mL of solvent containing 10.75 μ L H₂O (50.0 mM) and 30–40 mg of either AuMe(tpy)OTf (**55-OTf**) or Au(OCOCF₃)₂(tpy) (**62**) were prepared. This corresponded to *ca* 10 mol% catalyst loading with respect to H₂O. 2.0 mL of stock solution was added to each reaction vessel, see Figure 4.18. The green teflon rubber seals that are depicted in the middle of Figure 4.18 were present to ensure a perfect seal, the picture shows the wells before closing. After use, several of the green rubber seals were slightly destroyed and in some samples the o-rings had fallen into the solution.

Au(OCOCF₃)₂(tpy) (**62**) + Ethylene in MeOH

The reaction set-up (*vide supra*) was used. This gave **120**, chemical shifts are not reported because the complex was recorded in protic TFE with C₆D₆ as an internal reference which give shifts that are difficult to compare.

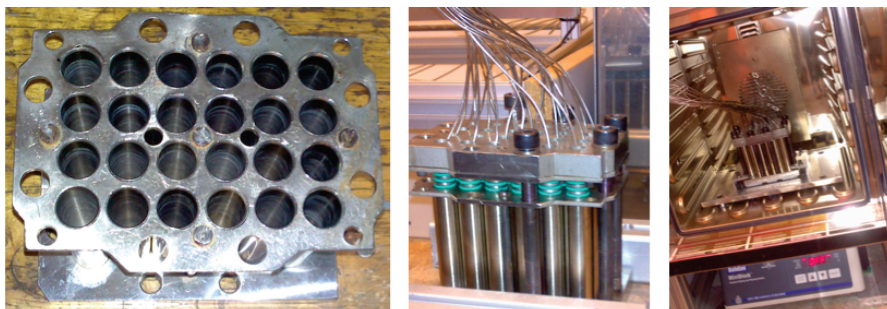


Figure 4.18: Setup used at SINTEF for reactions under pressure. Left: 4 x 6 wells used, Middle: Before sealing, green tefflon rubber prevents leakage, Right: Oven with shaker.

Table 4.4: Reaction setup. AuMe(tpy)OTf (**55-OTf**), Au(OCOCF₃)₂(tpy) (**62**).

P/S	S ₁ -55-OTf	S ₂ -55-OTf	S ₃ -55-OTf	S ₄ -55-OTf	S ₅ -62	S ₆ -62
5 bar	TFE	MeNO ₂	Acetone	MeOH	TFE	MeOH
10 bar	TFE	MeNO ₂	Acetone	MeOH	TFE	MeOH
15 bar	TFE	MeNO ₂	Acetone	MeOH	TFE	MeOH
20 bar	TFE	MeNO ₂	Acetone	MeOH	TFE	MeOH

P = pressure, S = solution.

Reversibility of Attack by ⁻OCOCF₃ and ⁻OCH₂CF₃ (Figure 4.3)

62 was dissolved in a 1:1 mixture (v/v) of TFA and TFE and stirred in the dark at rt, solvent was removed *in vacuo* and the solid was dissolved in CDCl₃ and analysed by ¹H NMR (spectrum 1, Figure 4.3). This yielded *ca* 85% **94** and 15% **95**. The NMR sample was added back to the reaction mixture, dried *in vacuo*, and TFA added. The solution was stirred in the dark for 2 d, solvent was removed *in vacuo* and the solid was analysed by ¹H NMR (spectrum 2, Figure 4.3). Now, only **94** was observed by ¹H NMR. Again, the NMR sample was added back to the bulk reaction mixture, the solvent was removed *in vacuo*, TFE was added and the solution was stirred in the absence of light at rt over night. Solvent was removed *in vacuo* and the resulting solid analysed by ¹H NMR (spectrum 3, Figure 4.3). The composition was now 93–94% **95** and 6–7% **94**.

General Method for NMR Experiments

A J Young NMR tube was loaded with, Au(III) complex (*ca* 5 mg), ISTD ($\text{CH}_2\text{ClCH}_2\text{Cl}$, 1.0 μL) and solvent (0.5 mL), and a reference spectrum was acquired after mixing. Gas was bubbled through the solution for 30–60 s. In TFA-*d* or TFE-*d*₃ when ethylene was used, this led the light yellow solution to turn colourless. A ¹H NMR spectrum was acquired within 5–10 min.

Au(OCOCF₃)₂(tpy) (62) + Ethylene + I₂

62 in TFA-*d* was added ethylene followed by excess I₂ and monitored over time. The reported NMR data were acquired *ca* 2 d after addition. ¹H NMR (500 MHz, TFA-*d*): δ 8.73 (d, *J* = 6.0 Hz, 1H), 8.60 (dddd, *J* = 8.0, 8.0, 1.9, 1.9 Hz, 1H), 8.08 (d, *J* = 8.1 Hz, 1H), 8.01 (ddd, *J* = 6.8, 6.8, 3.0 Hz, 1H), 7.89 (s, 1H), 7.35 (d, *J* = 8.0 Hz, 1H), 7.27 (dd, *J* = 7.9, 2.0 Hz, 1H), 4.56 (td, *J* = 7.0, 1.8 Hz, 4H), 3.47 (d, *J* = 2.0 Hz, 3–4H), 3.28 (td, *J* = 7.0, 2.0 Hz, 4H), 2.36 (s, 3H).

Au(OCOCF₃)₂(tpy) + Ethylene in CH₃CN

Full conversion after 2 d at rt. ¹H NMR (500 MHz, CD₃CN): δ 8.79 (d, *J* = 5.4 Hz, 1H), 8.17 (ddd, *J* = 7.8, 7.8, 1.5 Hz, 1H), 8.10 (d, *J* = 8.1 Hz, 1H), 7.79 (d, *J* = 8.3 Hz, 1H), 7.60 (ddd, *J* = 7.2, 5.6, 1.4 Hz, 1H), 7.24 (s, 1H), 7.23 (d, *J* = 1.7 Hz, 1H), 4.35–4.30 (m, 2H), 2.72–2.67 (m, 2H), 2.39 (s, 3H). Large, br, s at 2.83 ppm integrating to *ca* 20.

Au(OCOCF₃)₂(tpy) (62) + Ethylene in H₂O

A reaction vessel for a Parr reactor was loaded with **62** (0.100 g, 0.170 mmol) and H₂O (52 mL), then pressurised with ethylene (10 bar) and heated to 50 °C while stirring. The pressure increased to 12 bar. Due to insensitivity of the equipment, the reaction mixture experienced T up to 70 °C for shorter periods of time. The reaction was stirred for 3 d. Unfortunately the power at SINTEF shut down some time during the reaction time leading to the temperature falling from 50 °C to rt. The reaction mixture had turned purple, but little material had precipitated. Solvent was removed *in vacuo* and gave a colourless solid. Major product, **121**: ¹H NMR (400 MHz, CDCl₃): δ 8.45 (dd, *J* = 5.8, 1.4 Hz, 1H), 8.01 (ddd, *J* = 7.9, 7.9, 1.6 Hz, 1H), 7.91 (d, *J* = 8.1 Hz, 1H), 7.61 (d, *J*

= 7.9 Hz, 1H), 7.51–7.43 (m, 1H), 7.28 (s, 1H), 7.18 (d, $J = 8.1$ Hz, 1H), 3.91 (t, $J = 6.4$ Hz, 2H), 2.56–2.48 (m, 2H), 2.43 (s, 3H).

Au(OCOCF₃)₂(tpy) (62) + Ethylene in THF

Major product: ¹H NMR (500 MHz, THF-*d*₆): δ 8.44–8.40 (m, 1H), 8.21–8.07 (m, 2H), 7.81 (d, $J = 7.9$ Hz, 1H), 7.66–7.54 (m, 2H), 7.49–7.43 (m, 1H), 7.22 (ddd, $J = 7.9, 0.7, 0.7$ Hz, 1H), 4.83–4.77 (m, 2H), 2.43 (s, 3H), 2.41–2.38 (m, 2H). Minor product: ¹H NMR (500 MHz, THF-*d*₆): δ 8.40–8.35 (m, 1H), 8.21–8.05 (m, 2H), 7.81 (d, $J = 7.9$ Hz, 1H), 7.36 (s, 1H), 7.18 (dd, $J = 8.0, 1.5$ Hz, 1H), 3.79 (t, $J = 7.7$ Hz, 2H), 2.40 (s, 3H), 2.37–2.29 (m, 2H). Resonances are slightly overlapping for starting material, major product and minor product, hence the integrals are likely overestimated in some cases.

Au(OCOCF₃)₂(tpy) (62) + Propyne in TFA

The light yellow solution of **62** in TFA-*d* gradually turned darker when propyne was bubbled through the solution. Full conversion within *ca* 5 min. One distinct product (assumed to be **123**), and many tiny resonances. ¹H NMR (500 MHz, TFA-*d*): δ 8.54 (dd, $J = 8.1, 8.1$ Hz, 1H), 8.22 (d, $J = 8.2$ Hz, 1H), 7.87 (dd, $J = 6.8, 6.8$ Hz, 1H), 7.68 (d, $J = 8.2$ Hz, 1H), 7.44 (s, 2H), 4.84 (m, 5H), 2.42 (s, 3H). The δ for Me-group from inserted propyne overlaps with excess propyne, but presumably appear at 1.83 ppm.

Au(OCOCF₃)₂(tpy) (62) + Propyne in CH₃CN

The colourless solution of **62** in CD₃CN gradually turned strongly yellow. Full conversion within 5 min. One distinct product (assumed to be **123**), and many tiny resonances. ¹H NMR (500 MHz, CD₃CN): δ 8.37 (d, $J = 5.6$ Hz, 1H), 8.19 (dd, $J = 7.9, 7.9$ Hz, 1H), 8.04 (d, $J = 8.2$ Hz, 1H), 7.83 (s, 1H), 7.64 (d, $J = 8.1$ Hz, 1H), 7.59 (dd, $J = 6.8, 6.8$ Hz, 1H), 7.25 (d, $J = 8.1$ Hz, 1H), 2.42 (s, 3H). The δ for Me-group from inserted propyne overlaps with excess propyne, but presumably appear at 2.00 ppm.

Au(OCOCF₃)₂(tpy) (62) + Acetylene in TFA-*d*

To an NMR tube for a 10 mm probe was added **62** and TFA-*d*, then acetylene was bubbled through the solution. The colourless solution turned yellow and later brown. Au-complex (assumed to be **124**): ¹H NMR (400 MHz, TFA-*d*): δ 8.64 (d, $J = 6.0$ Hz, 1H), 8.55 (dd, $J = 8.1, 8.1$ Hz, 1H), 8.23 (d, $J = 8.1$ Hz, 1H), 7.88 (dd, $J = 6.9,$

6.9 Hz, 1H), 7.69 (d, $J = 8.7$ Hz, 1H), 7.50–7.38 (m, 4H overlaps so integral might be overestimated), 6.33–6.24 (m, 1H), 5.20 (d, $J = 13.9$ Hz, 1H), 2.43 (s, 3H), 2.35–2.21 (m, 1H). The peaks at 6.3 and 5.2 ppm are integrating 1–2, slightly dependent on which spectra are investigated. Organic product (assumed to be **125**, integration with respect to Au–complex): $^1\text{H NMR}$ (400 MHz, TFA-*d*): δ 7.19 (d, $J = 13.7$ Hz, 16H), 4.90 (d, $J = 13.9$ Hz, 16H).

Acetylene in TFA-*d*

Acetylene was dissolved in TFA-*d* and $\text{CH}_2\text{ClCH}_2\text{Cl}$ added as ISTD, kept at rt and monitored for 6 d without observing any reaction.

General Setup for High Pressure NMR Reactions

The high pressure NMR reactions were performed at EPFL, Lausanne, Switzerland, see Experimental for Chapter 3 for details.

HP NMR of $\text{Au}(\text{COCF}_3)_2(\text{tpy})$ (**62**) + Ethylene

A sapphire NMR tube was loaded with **62** and TFA-*d* and pressurised with ethylene (60 bar). **94** formed over night. The tube was heated at 50 °C for 1 d in a heating jacket without any further reaction being observed.

HP NMR of $\text{Au}(\text{COCF}_3)_2(\text{tpy})$ (**62**) + Ethylene Followed by CO

A sapphire NMR tube was loaded with **62** and TFA-*d* and pressurised with ethylene (20 bar). **94** formed over night. The tube was depressurised, followed by pressurisation with CO (78 bar). No reaction after 3.5 d.

Chapter 5

Gold(III) Alkene Complexes

5.1 General Introduction

The work described in this chapter is published in Paper III¹⁷⁷ (Appendix) except for the work presented in Section 5.3 which is unpublished. The experimental work presented in Section 5.2 was performed in collaboration with Dr. Margaret L. Scheuermann (University of Washington) and a discussion of the topic is also included in her Ph.D. thesis.¹⁷⁸

As noted in Chapter 1 (Section 1.2), a key step in the catalytic cycles suggested for gold(III) catalysis, is the coordination of a C–C multiple bond to the gold centre.^{3,62,74,179,180} However, conclusive proof of any gold(III)– π complex did not exist when the work presented in this thesis was initiated.^{62,74,94,95}

As early as 1827, Zeise first reported the organometallic complex which later became known as Zeise's salt.^{181,182} Zeise's salt has the formula $\text{K}[\text{PtCl}_3(\text{C}_2\text{H}_4)]$ although it took decades before the structure, **126** (Figure 5.1), was determined. This platinum(II) complex is today the prototype of a transition-metal alkene complex.⁹⁴

With gold(III) being isoelectronic to platinum(II), the analogous gold(III) complex can be imagined, and has been by a number of chemists in the past. Several attempts have been made to react the common AuX_3 ($\text{X} = \text{halogen}$) with alkenes or alkynes.⁹⁴ Even gold(I) alkene complexes did not appear until 1964 when Chalk reported the adduct of AuCl with 1,5-cyclooctadiene, $(\text{AuCl})_2(\text{cod})$ (**128**, Fig-

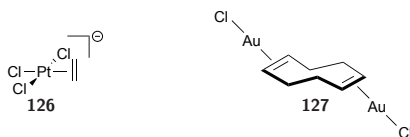
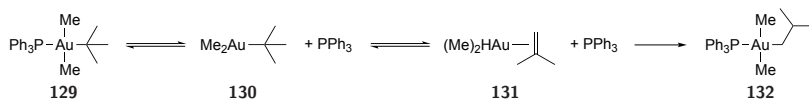


Figure 5.1: Zeise's salt^{181,182} and the first Au(I) alkene complex.⁸¹

ure 5.1).⁸¹ The work on preparing gold(I) alkene complexes was continued by Hüttel *et al.* during the 1960s and 1970s.^{183–193}

Since then, several groups have attempted to prepare alkene complexes of gold(III) chlorides and bromides, but clear identification of a gold(III) alkene complex has been elusive.^{18,94,95,194–197} Gas phase calculations of AuCl₃ and ethylene suggest the alkene binding to be exothermic.^{198,199} Alkene complexes of gold(I) have been known for some time with several examples reported^{81–90} and in part reviewed.^{3,16,74,91–93} In the 1970s, Kochi *et al.* tried to prepare gold(III) alkene complexes from dimethylgold(III) to investigate if the observed isomerisation was by a β-hydride elimination to give a π-complex of gold(III), they were however unsuccessful.⁷⁹

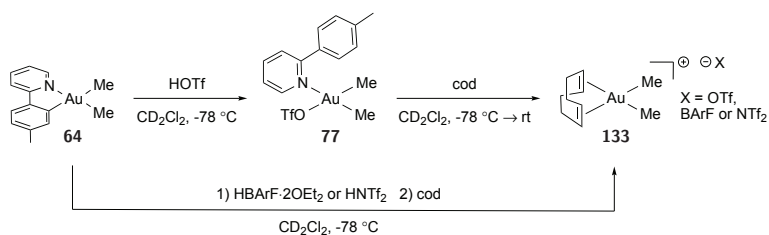


Scheme 5.1: Isomerisation observed by Kochi *et al.* believed to proceed via β-hydride elimination and formation of a Au(III) alkene, although not confirmed.⁷⁹

5.2 Generation of a Gold(III) Alkene Complex

Intrigued by the ‘open’ coordination site in AuMe₂(tpyH)X (**77–X**) discussed in Chapter 3 (Section 3.3.3), we wanted to see if an alkene would successfully bind to gold to finally yield a gold(III) alkene complex. Addition of cod (1 equiv) to a solution of AuMe₂(tpyH)OTf (**77–OTf**) at -78 °C followed by slow warming to 0 °C gradually provided the gold(III) alkene complex Au(cod)Me₂OTf (**133–OTf**, Scheme 5.2). Protonolysis with 2.2 equivalents HOTf gave **133–OTf** in 85% yield based on NMR (ISTD). The byproduct of the reaction from **64** with 2 equivalents

of HOTf is 2-(*p*-tolyl)pyridinium triflate, because the second equivalent protonates the nitrogen of tolylpyridine liberated from gold upon coordination of cod. Other acids were also successful for generating Au(cod)Me₂X (**133**-X); HNTf₂ gave a yield of 95% from **64** based on NMR (ISTD), HBARf (HBArF·2OEt₂) gave 70–75% based on NMR (ISTD) and HBF₄ (HBF₄·OMe₂) also produced the gold(III) alkene complex. In the attempts utilising HBF₄ (in Et₂O) the stoichiometry of the acid was difficult to control, the 2 equivalents needed in the case of the other three acids was not enough with HBF₄, raising the question of whether or not the stock solution of HBF₄ kept its concentration after it was prepared.



Scheme 5.2: Protonation of AuMe₂(tpy) at low temperature followed by addition of cod to generate Au(III) alkene complex **133**-X *in situ*.

In situ generation of Au(cod)Me₂X (**133**-X) was possible from AuMe₂(tpy) (**64**). Section 5.2.1 describes the generation of **133**-X starting from another gold(III) complex as the precursor, before returning to the full characterisation of **133**-X in Section 5.2.2 and Section 5.2.4.

5.2.1 Another Approach Towards Au(cod)Me₂⁺

From the protonation experiments conducted with AuMe₂(tpy) (**64**) and HOTf, it was suspected that a dimeric species of the proposed structure **134** (Figure 5.2) could form with 2 equivalents of triflic acid. The observation of this assumed gold dimer **134** by addition of triflic acid to **64** at low temperature, raised the question of what would happen if **64** was protonated with hydrochloric acid. Indeed, the gold dimer **135** was generated. A new procedure to prepare the gold dimer with a chloride bridge was thus established. The reported procedure for preparing **135** from HAuCl₄·3H₂O using SnMe₄²⁰⁰ is quite sensitive. The procedure involv-

ing SnMe_4 had been attempted by co-workers in the group on several occasions, although never by the author of this thesis. The procedure is apparently quite tricky, and is strongly dependent on temperature. If the temperature is too low (below $-55\text{ }^\circ\text{C}$) the reaction does not take place, but if the temperature is too high, decomposition to metallic gold results.²⁰¹ In addition, SnMe_4 is toxic and volatile. Based on the toxicity of the tin reagent and the sensitive procedure, it was very useful to have access to the gold dimer **135** through another simpler route. The work-up of the procedure described in Scheme 5.3 is unfortunately slightly tedious, as after removing the solvent, up to ten extractions with pentane were necessary. If dichloromethane was used for the extraction, protonated ligand (tpyH_2^+) followed into the organic phase as well.

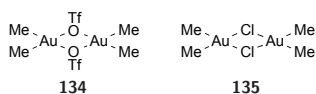
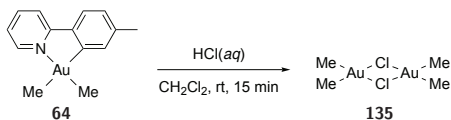


Figure 5.2: Proposed Au-dimer formed with HOTf and the analogous Cl-bridged dimer.

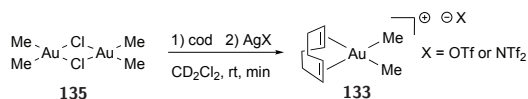


Scheme 5.3: Synthesis of Au-dimer.

From **135**, the preparation of **133-X** was possible at room temperature with a silver(I) salt to abstract the chlorine to give precipitation of silver(I) chloride and formation of **133-X**. If no silver salt was used, no reaction was observed. As AgNTf_2 is quite expensive to use on larger scale whereas the lithium salt is much less so, an attempt to treat **135** with cod and LiNTf_2 in dichloromethane- d_2 at room temperature was made, without success.

5.2.2 Characterisation of $\text{Au}(\text{cod})\text{Me}_2^+$

A single resonance was observed for the AuMe groups at 1.71 ppm (in CD_2Cl_2) in the ^1H NMR spectrum of **133-OTf** at $0\text{ }^\circ\text{C}$, the two CH_2 -groups in the backbone



Scheme 5.4: Generation of Au(cod)Me₂X from Au–dimer.

Table 5.1: NMR yields (by ISTD) with different acids or Ag(I)–salts and Au–complexes.

Starting Au–complex	HX/AgX	Yield of 133–X
AuMe ₂ (tpy) (64)	HOTf	85%
AuMe ₂ (tpy) (64)	HNTf ₂	95%
AuMe ₂ (tpy) (64)	HBArF·2OEt ₂	70–75%
AuMe ₂ (tpy) (64)	HBF ₄ ·OMe ₂	75–80%
Au ₂ Cl ₂ Me ₄ (135)	AgOTf	75%
Au ₂ Cl ₂ Me ₄ (135)	AgNTf ₂	90%

showed up as a pair of multiplets at 2.75 and 2.99 ppm. The vinylic protons showed as a broad singlet at 6.39 ppm, 0.8 ppm higher than for free cod. Upon binding to transition metals, vinylic protons usually shift upfield.^{150,202} Some examples of gold(I) alkene complexes are shown in Table 5.2 as well as appropriate rhodium and platinum complexes demonstrating large upfield shifts. There are however some examples of downfield shifts for electron deficient metals such as silver(I) or the gold(III) alkene complexes reported by Bochmann *et al.*¹⁰⁹ at the same time as complex **133** was reported. The ¹³C resonance of the *sp*²-C in **133–OTf** appears at 134 ppm, 5 ppm higher than in free cod. As can be seen from Table 5.2, the vinyl resonances in Au(cod)Me₂⁺ (**133**) are shifted to significantly higher ppm values compared to free cod, also in the ¹³C spectrum. The gold(III) alkene complexes reported by Bochmann *et al.*¹⁰⁹ all show upfield shifts in ¹³C and downfield shifts in ¹H NMR (except for the norbornene complex **138** which show upfield shifts for both ¹H and ¹³C), whereas **133–X** shows downfield shifts both in ¹H and ¹³C NMR. The binding of cod to gold was confirmed by a through-space NOE interaction (700 MHz, -40 °C) between the vinylic protons of the bound cod and the AuMe groups.

The stability of **133–OTf** in solution is somewhat limited; after 12 hours at room temperature the concentration of **133–OTf** (initially *ca* 14 mM) decreased by a approximately 50% even with an excess of cod (*ca* 40 mM).

Table 5.2: ^1H and ^{13}C NMR shifts for selected transition metal alkene complexes.

Complex	^1H δ ($\Delta\delta$)	^{13}C δ ($\Delta\delta$)
Au(cod)Me ₂ OTf (133-OTf)	6.39 (+0.84)	134 (+5)
Au(cod)Me ₂ BARf (133-BARf)	6.29 (+0.74)	–
Au(cod)Me ₂ NTf ₂ (133-NTf₂)	6.38 (+0.83)	–
Au(C–N–C)(CH ₂ CH ₂)B(C ₆ F ₅) ₃ (OCOCF ₃) (136) ^a	6.29 (+0.91)	109 (-14)
Au(C–N–C)(cyclopentene)B(C ₆ F ₅) ₃ (OCOCF ₃) (137) ^a	6.31 (+0.57)	123.2 (-8)
Au(C–N–C)(norbornene)B(C ₆ F ₅) ₃ (OCOCF ₃) (138) ^a	5.97 (-0.03)	133.3 (-3)
Au(CH ₂ CH ₂) ₃ SbF ₆ (139)	4.49 (-0.91)	92.7 (-30)
Au(bipy ^{<i>i</i>-Pr}) ₂ (μ -cod)(PF ₆) ₂ (140)	4.79 (-0.76)	80.5 (-19)
HB(3,5-(CF ₃) ₂ Tz) ₃ Ag(CH ₂ CH ₂) (142) ^b	5.70 (+0.30)	109.7 (-13)
Rh(cod)(Me-Im) ₂ PF ₆ (143)	4.54 (-1.01)	90.3 (-39)
Pt(cod)Me ₂ (141) ^b	4.78 (-0.77)	–
1,5-Cyclooctadiene	5.55	129
CH ₂ CH ₂	5.40	123.3
Cyclopentene	5.74	131.0
Norbornene	6.00	135.9

The δ listed are in ppm in CD₂Cl₂ unless otherwise noted. The structures and references for the metal complexes of this table are shown in Figure 5.3. $\Delta\delta = \delta_{\text{bound}} - \delta_{\text{free}}$.

^a At -40 °C. ^b Shifts in CDCl₃.

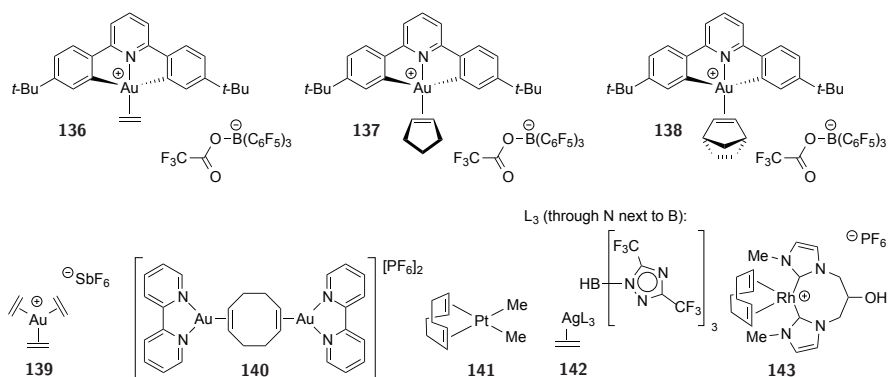


Figure 5.3: Selected transition metal alkene complexes: **136**, **137** and **138** reported by Bochmann,¹⁰⁹ Au(I) complexes **139**⁹⁰ and **140**,⁸³ Pt(II) complex **141**,²⁰³ Ag(I) complex **142**²⁰⁴ and Rh(I) complex **143**.²⁰⁵

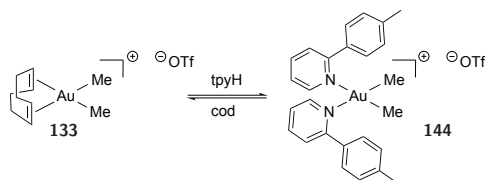
5.2.3 Attempts of Crystal Growth

Isolation of $\text{Au}(\text{cod})\text{Me}_2\text{X}$ (**133-X**) by crystallisation was attempted numerous times. Attempts of removing the tolylpyridinium salt by crystallisation proved difficult. The counter anions used were BF_4^- and $^- \text{OTf}$, both proving unsuccessful. It was seen that diethyl ether was not suitable for crystallisation purposes as it seemed to decompose the gold(III) alkene complex to metallic gold. Dichloromethane layered with pentane instead of diethyl ether did not produce crystals of **133-X**, *vide infra*, but at least decomposition was avoided with that solvent combination. Isolation of large amounts of **133-X** has been unsuccessful. When **133-OTf** was generated from the dimeric gold species **135**, it was also not possible to obtain pure **133-OTf**, although with more time at hand it should be possible.

Several attempts at growing crystals suitable for X-ray structure determination were made. All attempts at crystal growth from solutions of **133-OTf** obtained by >2 equivalents of acid ended in isolation of 2-(*p*-tolyl)pyridinium triflate. This led to the idea of suppressing the formation of the protonated ligand in solution by lowering the equivalents of added acid to 0.9 equivalents. However, even with 50 equivalents of cod this resulted in only 30% yield of **133-OTf** (by NMR, ISTD). In addition to **133-OTf**, the solution contained $\text{AuMe}_2(\text{tpyH})\text{OTf}$ (**77-OTf**, *ca* 20%) and a new species (*ca* 20%) subsequently identified to be $\text{AuMe}_2(\text{tpyH})_2\text{OTf}$ (**144**, Scheme 5.5). $\text{AuMe}_2(\text{tpyH})_2\text{OTf}$ (**144**) was independently synthesised as well as crystallographically characterised (Figure 5.4).

Addition of 2-(*p*-tolyl)pyridine (*ca* 6 equiv) to the equilibrium mixture containing only 30% of **133-OTf** changed the composition of the reaction mixture to <5% of **133-OTf**, approximately 20% of **77-OTf** and approximately 60% of **144**. These observations suggest that **77**, **133-OTf**, **144**, free cod, and free tolylpyridine are in equilibrium, that is, cod and tolylpyridine compete for coordination sites at the gold(III) moiety. Importantly, the ^1H NMR resonances of **133-OTf** remain unchanged regardless of whether the other species present in the reaction mixture are tpyH_2OTf (resulting from excess acid) or **77-OTf** and **144** (<1 equiv acid). From this observation, **133-OTf** does not appear to have an associated tolylpyridine ligand in solution. All attempts to obtain crystals from reaction mixtures without excess HOTf resulted only in crystals of **144** (Figure 5.4).

The Au–N distances in **144** are 2.162(2) and 2.171(2) Å, significantly longer than in AuMe₂(tpy) (**64**, 2.130(3) Å), AuBrMe(tpy) (**70**, 2.138(5) Å) and AuBrPh(tpy) (**72**, 2.132(3) Å). The Au–C_{Me} distances in **144** are 2.035(2) and 2.039(2) Å which are almost identical to those in AuMe₂(tpy) (**64**) where the Au–C_{Me} distance *trans* to nitrogen in the chelating C–N ligand is 2.038(4) Å. The two tpy ligands at gold show π -stacking; intramolecular π -stacking between each tolyl and each pyridine ring (distances of 3.672 and 3.709 Å).



Scheme 5.5: In CD₂Cl₂ solution at rt, an equilibrium is present between the Au(III) alkene complex and an Au-complex bearing two tpy ligands bound through N in a monodentate fashion.

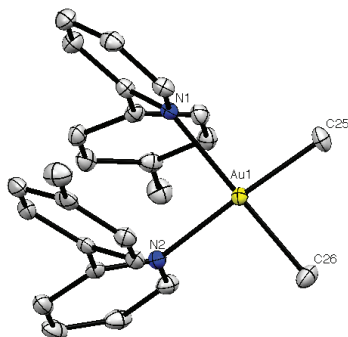


Figure 5.4: ORTEP view of AuMe₂(tpyH)₂⁺ (100(2) K) with 50% probability ellipsoids. Anion (OTf), CD₂Cl₂ and hydrogens are omitted for clarity. Selected bond lengths [Å] and angles [°]: Au(1)–C(25), 2.039(2); Au(1)–C(26), 2.035(2); Au(1)–N(1), 2.162(2); Au(1)–N(2), 2.171(2); N(1)–Au(1)–N(2), 90.89(7); N(1)–Au(1)–C(25), 92.00(8); C(25)–Au(1)–C(26), 86.33(9); C(26)–Au(1)–N(2), 90.93(8); N(1)–Au(1)–C(26), 176.80(8); N(2)–Au(1)–C(25), 175.64(8).

5.2.4 X-Ray Structure of Au(cod)Me₂BArF

As already mentioned, preparation of the gold(III) alkene complex **133-BArF** by use of HBArF (HBArF·2OEt₂) is possible in approximately 70% yield (NMR, ISTD). Approximately one equivalent of HBArF was used for the protonolysis in dichloromethane-*d*₂ followed by addition of 15 equivalents of cod. In an attempt to grow crystals of **133-BArF**, the solution was layered with pentane and left in a freezer at -35 °C. Satisfactorily, this resulted in small crystalline demispheres suitable for X-ray diffraction. According to the crystallographer,ⁱ the crystals seemed to melt at room temperature, and thus selecting a crystal from the refrigerated solution needed to happen quite rapidly. The crystals were stable in the fridge (*ca* 4 °C), but not at room temperature. The structure is shown in Figure 5.5.

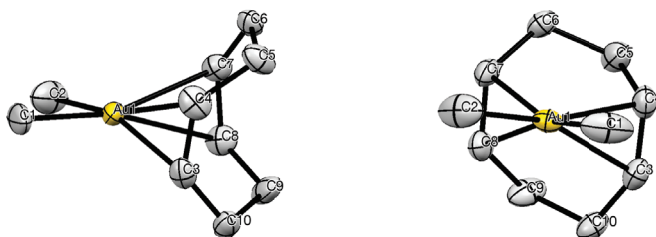


Figure 5.5: ORTEP view of the solid-state structure of Au(cod)Me₂BArF (**133-BArF**) (100 K) with 50% probability ellipsoids seen from two different angles. Anion (BArF⁻) and hydrogens are omitted for clarity. Selected bond lengths [Å] and angles [°]: Au(1)–C(1), 2.049(4); Au(1)–C(2), 2.055(4); Au(1)–C(3), 2.371(4); Au(1)–C(4), 2.415(4); Au(1)–C(7), 2.362(4); Au(1)–C(8), 2.406(4); C(3)–C(4), 1.348(5); C(7)–C(8), 1.364(5); C(3)–Au(1)–C(4), 32.71(13); C(7)–Au(1)–C(8), 33.23(12); C(7)–Au(1)–C(4), 77.86(13); C(3)–Au(1)–C(8), 77.87(13); C(1)–Au(1)–C(2), 85.0(2).

Au(cod)Me₂BArF (**133-BArF**) crystallised in the monoclinic space group *P*2₁/*c*. The gold cation is located in a pocket formed by the aryl groups of several BArF⁻ anions, see Figure 5.6 where the packing is depicted.

The Au–C_{cod} bonds of 2.389 Å (average) are rather long for a metal alkene complex (see Table 5.3 for comparison of bond lengths in selected metal alkene complexes). The gold cation is nearly C₂-symmetric (not crystallographically imposed). Each cod C=C bond is asymmetrically bonded to gold; one Au–C bond is

ⁱDr. Werner Kaminsky, University of Washington

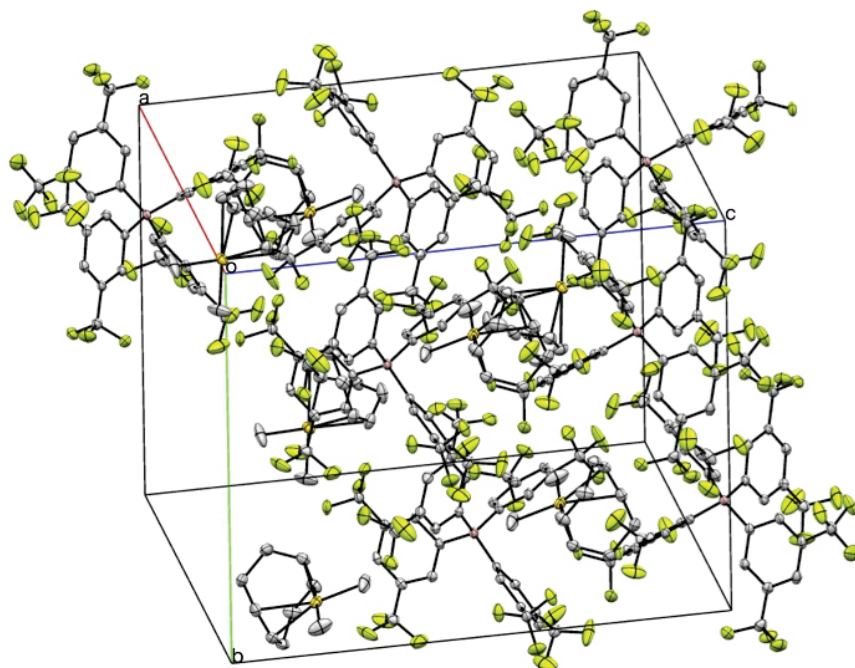


Figure 5.6: Packing in the solid-state structure of Au(cod)Me₂BArF (**133-BArF**).

Table 5.3: Comparison of average M–C and C–C bond lengths in some transition metal alkene complexes.

Complex	Av. M–C [Å]	Av. C–C [Å]
Au(cod)Me ₂ BArF (133-BArF)	2.389(4)	1.365(5)
Au(CH ₂ CH ₂) ₃ SbF ₆ (139)	2.268(5)	1.364(7)
HB(3,5-(CF ₃) ₂ Tz) ₃ Ag(CH ₂ CH ₂) (142) ^a	2.296(6) & 2.285(8)	1.336(10) & 1.326(13)
Pt(cod)Me ₂ (141)	2.232(8)	1.381(12)
CH ₂ CH ₂	–	1.313(1)

Structures and references are given in Figure 5.3. ^a Two chemically similar but crystallographically different molecules in the asymmetric cell, according to the authors.

significantly longer than the other (2.362(4) vs 2.406(4) and 2.371(4) vs 2.415(4) Å, respectively). The two long Au–C_{cod} distances in **133–BArF** are longer than the longest Au–C_{alkene} distances in several recently structurally characterised cationic gold(I) complexes.^{82–88,90} The Au–C_{alkene} bond lengths in the gold(I) complexes are in the range of 2.098(5)⁸²–2.37(1)⁸⁸ and the C=C distances are in the range of 1.319⁸⁵–1.409(4)⁸³ Å. The C=C bond distance for **133–BArF** is essentially in the middle of the range seen for the cationic gold(I) complexes, thus indicating some back-bonding from gold(III) to the C=C bonds, despite the strong *trans* influence of the two methyl groups.

The neutral platinum(II) complex Pt(cod)Me₂ (**141**) included in Table 5.3 is isoelectronic to Au(cod)Me₂⁺ (**133**) and hence it is relevant to compare **133–BArF** with **141**. The Au–C_{cod} distances in the cationic **133–BArF** are significantly longer than the Pt–C_{cod} in the neutral **141** (2.232(8) Å²⁰⁶). The C=C bonds are shorter in the gold complex **133–BArF** than in the corresponding platinum complex **141**, which might indicate reduced back-bonding from the $d_{M \rightarrow \pi^*_{cod}}$ orbitals going from isoelectronic platinum(II) to gold(III). The Au–C_{Me} bond lengths in **133–BArF** are 2.049(4) and 2.055(4) Å, quite typical for cationic Au(III)Me₂ fragments with relatively weak donor ligands *trans* to the methyl groups^{207,208} and being situated between the Au–C_{Me} in AuMe₂(tpy) (**64**) of 2.038(4) and 2.134(4) *trans* to carbon and nitrogen, respectively.

5.2.5 DFT Calculations

Dr. David Balcells (University of Oslo) and Professor Odile Eisenstein (Université Montpellier 2) performed DFT calculations on the cationic gold(III) alkene complex Au(cod)Me₂⁺ (**133**) as well as Pt(cod)Me₂ (**141**) for comparison. The structures of Au(cod)Me₂⁺ (**133**) and Pt(cod)Me₂ (**141**) were optimised at the DFT level with the hybrid PBE0 functional and quasi relativistic effective core potential (ECP) for goldⁱⁱ indispensable for representing the structures and reac-

ⁱⁱThe DFT calculations were carried out using Gaussian09.²⁰⁹ C and H were described with the all-electron triple- ζ 6-311 + G** basis set,^{210,211} whereas Au was described with the new Stuttgart–Köln basis set including a small-core quasi-relativistic pseudopotential.²¹² Geometries were fully optimised without any constraint. Vibrational frequencies were computed analytically to verify that the stationary points found were minima. PBE0²¹³ gave the lowest root-mean-square deviation from the experimental X-ray Au–C bond lengths of the functionals used. PBE0

tivity of gold complexes.^{215,216} The geometry of **133** was optimised with several functionals,ⁱⁱⁱ where PBE0 gave the best resemblance to the experimental geometry obtained by X-ray crystallography.

The structures of Au(cod)Me₂⁺ (**133**) and Pt(cod)Me₂ (**141**) are in excellent agreement with the solid-state structures (see Table 5.4 for comparison). As mentioned in the previous section, the M–C_{cod} bonds are nonequivalent and this was very well reproduced in the calculations, as was the greater difference between these distances for gold compared to platinum. The calculated distances for Au(cod)Me₂⁺ (**133**) differs by 0.052 Å compared to the solid-state structure, and only by 0.024 Å for Pt(cod)Me₂ (**141**). The platinum complex **141** is numbered in the same manner as the gold complex **133** in Figure 5.5. The olefinic carbon atoms C(3), C(4), C(7) and C(8) are, as previously indicated, not coplanar. The dihedral angles C(3)–C(4)–C(7)–C(8) are 13.48 ° (calculated 13.78) and 12.78 ° (calculated 11.68) for gold(III) and platinum(II), respectively. The geometries were fully optimised in the gas phase in absence of counteranion. The excellent agreement between the calculated and the solid-state values therefore show that the structural features of the cod ligand being slightly twisted are not due to crystal packing or due to the counteranion in the case of the gold(III) complex.

To investigate the origin of the twisted cod ligand, free cod was optimised at the same level of theory. The C(3)–C(4)–C(7)–C(8) dihedral angle in free cod is 23.68°; the C=C bonds are distinctly nonparallel a trend attributed to the preference for a staggered conformation of the –CH₂CH₂– backbone of cod. In free cod where no constraints are present, the two –CH₂CH₂– units are fully staggered. The C=C bonds become increasingly parallel upon coordination to gold(III) and platinum(II), although less so for gold(III) than for platinum(II). When the two C=C bonds are forced to be more parallel upon coordination to a metal, the –CH₂CH₂– linkers are set in a more eclipsed conformation. As apparent from the nonequivalent M–C bonds, the –CH₂CH₂– backbone does not reach a fully eclipsed conformation. The energy cost of distorting cod from its preferred staggered con-

was also selected in a recent study of gold(I) and gold(III) alkene complexes, based on reference coupled cluster calculations.¹⁹⁹ The geometry optimisation of Pt(cod)Me₂ and the NBO (5.9 version) analysis²¹⁴ were thus carried out with PBE0.

ⁱⁱⁱThe geometry of **133** was optimised using Gaussian09²⁰⁹ with several functionals, including BP86,²¹⁷ B3LYP,²¹⁸ B97D,²¹⁹ M06L,²²⁰ M06,²²¹ PBE,²²² PBE0.²¹³

Table 5.4: Selected geometrical parameters for Au(cod)Me₂⁺ (**133**), Pt(cod)Me₂ (**141**) and free cod and distortion energies for the cod ligand. See Figure 5.5 for atom labelling.

	Au(cod)Me ₂ ⁺		Pt(cod)Me ₂		cod	
	Exp. ^a	Theo. ^b	Exp. ^c	Theo. ^b	Exp. ^d	Theo. ^b
Distances [Å]						
M–C(1)	2.049(4)	2.055	2.040(11)	2.057	–	–
M–C(2)	2.055(4)	2.055	2.072(11)	2.057	–	–
M–C(3) (d ₁)	2.362(4)	2.390	2.204(11)	2.211	–	–
M–C(4) (d ₂)	2.406(4)	2.442	2.255(12)	2.235	–	–
Δ(d ₂ –d ₁)	0.044	0.052	0.051	0.024	–	–
M–C(7) (d ₃)	2.371(4)	2.390	2.224(11)	2.211	–	–
M–C(8) (d ₄)	2.415(4)	2.442	2.230(11)	2.235	–	–
Δ(d ₄ –d ₃)	0.044	0.052	0.006	0.024	–	–
Δ _{avg.}	0.044	0.052	0.029	0.024	–	–
Angles [°]						
C(3)–C(4)–C(7)–C(8)	13.4	13.7	12.7	11.6	20.2	23.6
C(4)–C(5)–C(6)–C(7)	46.5	44.4	34.5	36.7	63.8	61.2
C(8)–C(9)–C(10)–C(3)	42.6	44.4	33.1	36.7	63.8	61.2
E [kcal/mol]						
Distortion E ^e	–	4.7	–	12.7	–	0.0

^a X-Ray structure of Au(cod)Me₂BARf. ^b DFT (PBE0) calculations. ^c Data from X-ray structure.²⁰⁶ An earlier determined structure, for which the cif file is not available, gives a Δ_{avg.} of 0.024 Å.²⁰³ ^d Data from gas-phase electron diffraction structure.²²³ ^e Energy difference, E_{bound}–E_{free}, between optimised free cod and cod in the conformations calculated in **133** and **141**, respectively.

formation is 4.7 kcal/mol for gold(III) and 12.7 kcal/mol for platinum(II). The distortion energy is compensated by back donation from the metal to the two π*–orbitals. This can be seen in Figure 5.7, showing the natural bond orbital (NBO) analysis. In the NBO analysis, the four orbitals containing the 8 *d* electrons were identified amongst the natural localised molecular orbitals (NLMOs). The *d*_{z²} and *d*_{x²–y²} orbitals appear as lone pairs located on the metal centre, with no significant contribution from the ligands. The *d*_{xz} and *d*_{yz} orbitals however are involved in the *d*→π* back donation from the metal centre to the C=C bond of cod. This interaction is weaker in Au(cod)Me₂⁺ (**133**) where the contribution from the π*_{C=C} is 2.2% for the *d*_{xz} and 2.8% for the *d*_{yz}, compared to Pt(cod)Me₂ (**141**) where the corresponding numbers are 9.5% and 12%, respectively. The graphical representation of these NLMOs are shown in Figure 5.7 making the difference between gold(III)

and platinum(II) apparent. The results obtained from the solid-state structures as well as the calculations show that the metal d to $\pi^*_{\text{C}=\text{C}}$ back donation is weaker for gold(III) when compared to platinum(II) in the isoelectronic structures **133** and **141**, but is still significant in the way this type of an unprecedented gold(III) bis(alkene) complex is stabilised.

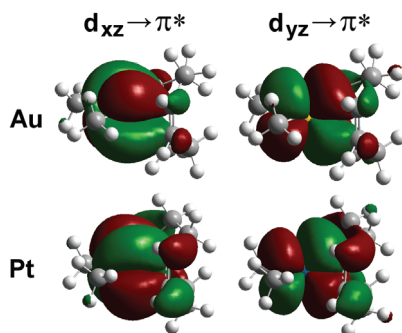


Figure 5.7: NLMOs (with orbital phases in green/red) associated with the metal $d \rightarrow \pi^*_{\text{cod}}$ back donation in complexes $\text{Au}(\text{cod})\text{Me}_2^+$ (**133**) and $\text{Pt}(\text{cod})\text{Me}_2$ (**141**).

5.2.6 Attempts at Isolation of $\text{Au}(\text{cod})\text{Me}_2^+$

Except for the few crystals suitable for single crystal X-ray structure determination, successful isolation of $\text{Au}(\text{cod})\text{Me}_2\text{X}$ (**133-X**) was not achieved while the author of this thesis was visiting the University of Washington. The reason for the absence of success in isolating the gold(III) alkene complex is likely due to the protonated ligand. As mentioned earlier, all crystallisation attempts yielded protonated ligand was obtained instead of the gold(III) alkene complex **133-X**. With only 1 equivalent of acid, the crystallised complex was $\text{AuMe}_2(\text{tpyH})_2\text{OTf}$ (**144**) due to the equilibrium presented in Scheme 5.5.

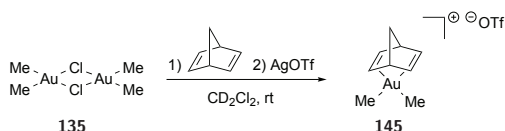
Back at the University of Oslo, once the synthesis of the gold dimer **135** was established, the isolation of **133-X** starting from **135** reacted with cod and a silver salt was attempted. Isolation was not successful likely due to the small scale on which it was attempted.

5.3 Other Gold(III) Alkene Complexes

It might seem as though the approach using cod to coordinate to gold(III) was a quite lucky event that happened out of the blue. Cod was not the first alkene that was added to $\text{AuMe}_2(\text{tpyH})\text{X}$ (**77-X**) in dichloromethane- d_2 at low temperature; ethylene was attempted first. However, it seemed that the addition of ethylene was not very successful as the gas initially did not dissolve in the solution. Cod was chosen due to the fact that it is a liquid, making for an easy addition, and it has two equivalent bonding sites. The equivalent bonding sites would supposedly make the expected ^1H NMR spectrum easy to interpret, whether cod would coordinate to gold through one or both of the C=C bonds. The symmetry of cod did indeed help with the structure elucidation as anticipated, but what was not suspected was that **133-X** was so much easier to generate than the other gold(III) alkenes that were attempted later on. This section will focus on what has been attempted with respect to preparing other gold(III) alkene complexes, although the complexes presented in this section are not fully characterised.

To investigate whether or not any other alkenes would coordinate to gold, a small screening was conducted. For any gold(III) alkene to be observed by reaction from $\text{Au}_2\text{Cl}_2\text{Me}_4$ (**135**) it was pivotal that the alkene was added before the silver salt. Even when silver salt was added after the alkene, formation of large amounts of ethane was often observed which indicate decomposition. Reaction between **135** and 2,5-norbornadiene (nbd) with AgNTf_2 in dichloromethane- d_2 gave production of large amounts of ethane, but also a complex that was tentatively assigned as the gold complex $\text{Au}(\text{nbd})\text{Me}_2\text{NTf}_2$ (**145-NTf₂**). The reaction was also performed using AgOTf . Based on the downfield shift of 0.65 ppm, as well as an NOE interaction between the protons in the AuMe and the olefinic protons in nbd, it seemed as though the gold(III) alkene complex depicted in Scheme 5.6 did indeed form. Nbd is sensitive to acid, hence starting from $\text{AuMe}_2(\text{tpy})$ (**64**) and protolytic cleavage of the Au-C(sp^2) of the tpy ligand gave some indication of a gold(III) nbd complex, but it was accompanied by reaction between the acid and nbd. This was also the case for some of the other alkenes investigated.

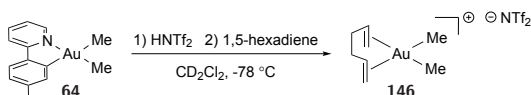
When working with silver salts,²²⁴ there is always the possibility of silver causing the observed reactivity instead of gold. To ensure that it was indeed a reaction



Scheme 5.6: *In situ* formation of a complex presumed to be $\text{Au}(\text{nbd})\text{Me}_2\text{OTf}$ (**145-OTf**).

between gold and nbd, control experiments were conducted. By ^1H NMR, neither AgNTf_2 nor AgOTf showed any sign of forming a silver alkene species in dichloromethane- d_2 between 25 °C and -90 °C.

Reaction of 1,5-hexadiene with **64** and HNTf_2 afforded a new product, presumably involving coordination of both double bonds to gold, in 57% yield based on NMR (ISTD). The symmetry observed by ^1H NMR agrees with both double bonds coordinated to gold. The proposed structure of **146** is depicted in Scheme 5.7. As the backbone of 1,5-hexadiene is rather short, i.e. low flexibility, the structure where both CH_2 -groups point in the same direction seems more likely than in opposite directions. All resonances for the gold(III) alkene complex are broad even at -20 °C, indicating an exchange or fluxional behaviour on the NMR timescale. The resonances corresponding to free 1,5-hexadiene are however sharp.



Scheme 5.7: Proposed structure of Au(III) alkene complex formed.

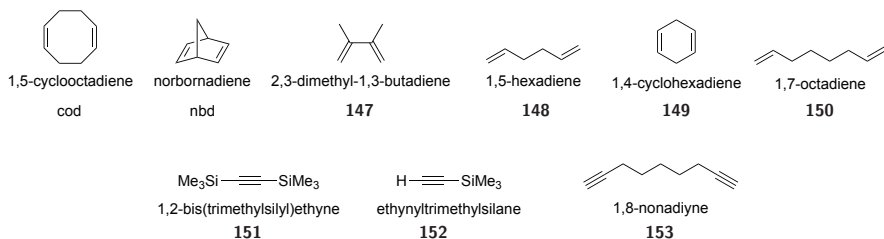


Figure 5.8: Alkenes and alkynes attempted to coordinate to Au(III).

An overview of all the alkenes and alkynes investigated are given in Figure 5.8 and Table 5.5. Table 5.5 includes comments upon whether or not a gold(III) alkene or alkyne was clearly observed, or if there were only indications of such a species.

Table 5.5: Alkenes and alkynes used in attempts to prepare Au(III) alkene complexes, starting from either AuMe₂(tpy) (**64**) or Au₂Cl₂Me₄ (**135**) in CD₂Cl₂.

[Au]	HX/AgX	Ene/yne	Yield ^d	Comments
64	HOTf	cod	85–90%	
64	HNTf ₂	cod	95%	
64	HBArF ^a	cod	70–75%	
64	HBf ₄ ^b	cod	75–80%	
135	AgOTf	cod	75%	
135	AgNTf ₂	cod	90%	
135	LiNTf ₂	cod	n.r.	
64	HOTf	nbd	n.d.	Observed
64	HNTf ₂	nbd	n.d.	Observed
64	HBArF ^a	nbd	n.d.	Observed at low T
64	HBf ₄ ^b	nbd	n.d.	Observed at low T
135	AgNTf ₂	nbd	n.d.	80% to ethane, indication at low T
135	AgOTf	nbd	n.d.	50% to ethane, indication at low T
64	HBf ₄ ^b	147	n.r.	
135	AgOTf	147	n.d.	Reaction observed
64	HOTf	148	n.d.	Observed
64	HNTf ₂	148	57%	
135	AgOTf	148	n.d.	Observed also at rt
64	HBf ₄ ^b	C ₂ H ₄	n.d.	Observed at -90 °C
64	HNTf ₂	149	n.d.	Reaction observed
135	AgOTf	149 ^c	n.d.	Reaction observed
64	HOTf	150	n.d.	Observed at low T
64	HNTf ₂	151 ^c	n.d.	Reaction observed
135	AgOTf	151	n.d.	Reaction observed
64	HBArF ^a	152	n.d.	Reaction observed
64	HNTf ₂	152	n.d.	Reaction observed
135	AgOTf	152 ^c	n.d.	Reaction observed
64	HOTf	153	n.r.	

For structures and full names of the alkenes/alkynes see Figure 5.8. Alkenes or alkynes were added at -78 °C and rt when starting from **64** and **135**, respectively. ‘Observed’: Expected Au-π complex was presumably observed. ‘Reaction observed’: Product not determined, likely a Au-π complex formed. ^a HBArF·2OEt₂, ^b HBf₄·OMe₂, ^c In toluene-*d*₈, ^d By ISTD.

5.4 Conclusions

When this project was initiated, there were no conclusive reports of gold(III) alkene complexes. The gold(III) alkene complex Au(cod)Me₂BARf (**133-BArF**) has been crystallographically characterised, demonstrating that gold(III) alkene complexes indeed exist, thus validating their inclusion in mechanistic proposals. **133-X** is bound solely to carbon atoms and is thus far the only crystallographically characterised gold(III) alkene complex reported in the literature.

Due to the preferred staggered conformation of cod, the Au-C_{cod} distances are nonequivalent and they are quite long compared to Au-C_{alkene} for gold(I) complexes. The C=C bond lengths are however within the normal range. DFT calculations on the gold(III) system showed excellent agreement with the experimentally determined solid-state structure. The stabilising ligands are methyl groups which is not so conventional. **133** showed some extent of back donation from the the gold *d*-orbitals to the π^* -orbitals in cod.

Other gold(III) alkene complexes were investigated as well, but none as thoroughly characterised as Au(cod)Me₂X (**133-X**). The reason for the observed differences between the abilities of different alkenes to coordinate to the AuMe₂⁺-moiety are likely related to entropy. Binding cod to gold has an energy cost of 4.7 kcal/mol associated with distorting cod from its preferred staggered confirmation, low enough for coordinating cod in a bidentate fashion. In the case of nbd, the flexibility of the bicyclic system is lower, not allowing as good overlap of the π -orbitals of the alkene and the *d*-orbitals at the metal but still enough to observe Au(nbd)Me₂OTf (**145-OTf**). 1,4-Cyclohexadiene and 2,3-dimethyl-1,3-butadiene lack some of the necessary flexibility to coordinate well in an η^2 -fashion to gold.

In the case of 1,5-hexadiene, an alkene complex was observed as the necessary flexibility of the ligand is present. The entropy cost associated with coordination of both double bonds to gold(III) is presumably the reason for the lower yield (based on NMR, ISTD) compared to Au(cod)Me₂X (**133-X**). The entropic cost might be too high in the case of the more flexible 1,7-octadiene, as a gold(III) alkene complex was only observed in small amounts and only at low temperatures.

Chelating ligands such as cod, nbd and 1,5-hexadiene, gave an observed gold(III) alkene complex. The entropy associated with coordinating two molecules of ethy-

lene is expected to be significant, and it was therefore reasonable that $\text{Au}(\text{CH}_2\text{CH}_2)_2\text{Me}_2\text{BF}_4$ was only observed at $-90\text{ }^\circ\text{C}$. Calculations on isodesmic reactions^{iv} (Scheme 5.8) were performed by Dr. Ainara Nova to see the differences in energies between $\text{Au}(\text{cod})\text{Me}_2^+$ (**133**) and potential other gold(III) alkene and alkyne complexes.¹⁴⁷ In agreement with what was observed experimentally, $\text{Au}(\text{nbd})\text{Me}_2^+$ (**145**) and $\text{Au}(\text{hexadiene})\text{Me}_2^+$ (**146**) were higher in energy than **133** (both ΔG and ΔE). Coordination of 2,3-dimethyl-1,3-butadiene to gold was even less favourable.



Scheme 5.8: Isodesmic reactions, calculated by Dr. Ainara Nova.¹⁴⁷

Of the alkynes investigated thus far, the selection of appropriate chelating alkynes were small, only 1,8-nonadiyne. In light of what is known now, chelating alkynes should be prioritised. 1,5-Cyclooctadiyne was one preferred candidate as the alkene version was so successful. This was of course discussed, but was left at that as there are only a few reports of how to prepare 1,5-cyclooctadiyne^{225,226} and reports of its use are very few.²²⁵ 1,5-Hexadiyne however, is commercially available and might lead to an observed gold(III) alkyne complex. The isodesmic reactions calculated¹⁴⁷ also suggested, as expected, that electron donating groups at the alkynes would be favourable over hydrogen substituents. Interesting species were observed in reactions with alkynes, as opposed to formation of only ethane, although a clear identification of a gold(III) alkyne complex were unfortunately not possible at that point in time.

5.5 Experimental

General Experimental Methods

NMR spectra were recorded on a Bruker DRX500 and a Bruker AVII400 operating at 500 MHz and 400 MHz (^1H), respectively. $\text{CH}_2\text{ClCH}_2\text{Cl}$ was used as ISTD for calculat-

^{iv}Isodesmic reactions are reactions where the chemical bonds broken in the reactants are of the same type as the bonds formed in the product.

ing NMR yields. Reagents and solvents were used as received, except for CD_2Cl_2 which was dried over molecular sieves and degassed prior to use.

Synthesis of 2-(*p*-Tolyl)pyridinium Triflate

To a solution of 2-(*p*-tolyl)pyridine (190 μL , 1.14 mmol, 1.1 equiv) in dry CD_2Cl_2 (ca 25 mL) was added HOTf (90 μL , 1.0 mmol, 1.0 equiv) and the mixture stirred at rt for 25 min. Solvent was removed *in vacuo* to yield a colourless solid that was washed with pentane (3 x ca 7 mL) and dried *in vacuo*. ^1H NMR (500 MHz, CD_2Cl_2): δ 14.42 (s, 1H), 8.83 (dd, $J = 5.2, 1.5$ Hz, 1H), 8.34 (ddd, $J = 7.9, 7.9, 1.8$ Hz, 1H), 8.11–8.03 (m, 1H), 7.89–7.81 (m, 2H), 7.76–7.69 (m, 1H), 7.42 (d, $J = 8.2$ Hz, 2H), 2.45 (s, 3H). ^{13}C NMR (126 MHz, CD_2Cl_2): δ 154.4, 145.1, 144.0, 143.8, 131.0 (2C), 129.5, 128.1 (2C), 124.7, 124.6, 21.8.

Synthesis of $\text{Au}_2\text{Cl}_2\text{Me}_4$ (**135**)

To a solution of **64** (0.102 g, 0.259 mmol, 1.0 equiv) in CH_2Cl_2 was added concentrated $\text{HCl}(aq)$ (0.40 mL) and the mixture stirred at rt for 15 min. CH_2Cl_2 was removed *in vacuo* and the residual liquid was extracted with pentane (10 x 10 mL). Solvent was removed *in vacuo* to yield **135** in 32–55% yield as a colourless solid. ^1H NMR (500 MHz, CD_2Cl_2): δ 1.30 (s, 12H). ^1H NMR (400 MHz, C_6D_6): δ 0.98 (s, 12H).

General Procedure for *In Situ* NMR Experiments

From $\text{AuMe}_2(\text{tpy})$ (**64**): A screw cap NMR tube was loaded with **64** (ca 5 mg), CD_2Cl_2 (ca 0.5 mL) and $\text{CH}_2\text{ClCH}_2\text{Cl}$ (1.0 μL , as ISTD). The sample was cooled inside the probe to at least -40 $^\circ\text{C}$, the sample was removed and placed in a dry-ice acetone bath. HX in CD_2Cl_2 (>2 equiv, 0.1 M) was added to generate $\text{AuMe}_2\text{tpyHX}$ (**77-X**). Alkene (>1 equiv) was added and the sample was monitored while it was allowed to warm to rt, or at the temperature where ethane extrusion was dominating.

From $\text{Au}_2\text{Cl}_2\text{Me}_4$ (**135**): A screw cap NMR tube was loaded with **135** (ca 3 mg), CD_2Cl_2 (ca 0.5 mL) and $\text{CH}_2\text{ClCH}_2\text{Cl}$ (1.0 μL , as ISTD). A reference spectrum was recorded at rt, and alkene (>1 equiv) was added and a spectrum was recorded. Excess AgX was then added and a spectrum was recorded. The sample was cooled down if a change was apparent at rt, and if not all the Au-complex had converted to ethane.

For experiments involving $\text{HBF}_4\cdot\text{OMe}_2$, a stock solution of 1 M $\text{HBF}_4\cdot\text{OMe}_2$ in CD_2Cl_2 was prepared at one occasion as it was necessary to add more than 1 equiv of this acid, making the added volume quite large. Such a high concentration is not

recommendable though, as the acid solution became quite violent when pulling it up with a needle from a septum covered vial.

Reference shifts for alkenes in NMR (CD_2Cl_2): 1,5-Cyclooctadiene (cod): δ_{H} 5.51 (m), δ_{C} 128.9.⁸³ 2,5-Norbornadiene (nbd): δ_{H} 6.78, δ_{C} 143.6.⁸³ 1,5-Hexadiene: δ_{H} 5.84 (dd, $J = 16.7, 10.0$ Hz, 2H), 5.13–4.84 (m, 4H).

Au(cod)Me₂NTf₂ (133–NTf₂) From 64

HNTf₂ used as acid gave a NMR yield (by ISTD) of **133–NTf₂** of 95%. ¹H NMR (500 MHz, CD_2Cl_2): δ 6.38 (s, 4H), 3.08–2.98 (m, 4H), 2.82–2.62 (m, 4H), 1.73 (s, 6H).

Au(cod)Me₂OTf (133–OTf) From 135

AgOTf used as Ag(I)–salt gave a NMR yield (by ISTD) of **133–OTf** of 75%. Very broad resonances at rt, sharp at 0 °C. ¹H NMR (500 MHz, CD_2Cl_2): δ 6.40 (br s, 4H), 3.00 (br s, 4H), 2.76 (br s, 4H), 1.73 (br s, 6H).

Au(cod)Me₂NTf₂ (133–NTf₂) From 135

AgNTf₂ used as Ag(I)–salt gave a NMR yield (by ISTD) of **133–NTf₂** of 90%. ¹H NMR (500 MHz, CD_2Cl_2): δ 6.38 (s, 4H), 3.09–2.95 (m, 4H), 2.80–2.64 (m, 4H), 2.37 (s, 6H).

Au₂Cl₂Me₄ + LiNTf₂ + 1,5-Cyclooctadiene

No reaction was observed at rt.

Au₂Cl₂Me₄ + Norbornadiene + AgOTf

Around 50% (by ISTD) of the starting material had reacted to form ethane as well as formation of **145–OTf**. ¹H NMR (500 MHz, CD_2Cl_2 , -60 °C): δ 7.43 (s, 4H), 4.42 (s, 2H), 2.25 (s, 2H), 1.52 (s, 6H). ¹³C NMR (500 MHz, CD_2Cl_2 , -60 °C): δ 134.1 (4C), 83.8 (1C), 52.7 (2C), 21.9 (2C).

AuMe₂(tpy) + HNTf₂ + 1,5-Hexadiene

HNTf₂ used as acid gave a NMR yield (by ISTD) of 57% of Au(hexadiene)Me₂NTf₂ (**146**). ¹H NMR (500 MHz, CD_2Cl_2 , -40 °C): δ 6.59 (b, 2H), 5.73–5.63 (m, 2H), 5.53 (d, $J=17.5$ Hz, 2H), 2.98 (s, 4H), 1.71 (s, 6H).

Chapter 6

Conclusions and Future Prospects

There are so many possibilities of where to go and what to do within this project that it is gratifying to see that there are students in the group that can now continue to investigate the exciting world of gold(III) chemistry, even though the work with this Ph.D. thesis has come to an end.

6.1 Synthetic Work

The microwave method developed in the group is an efficient, high yielding and clean method for preparing a variety of different cyclometalated gold(III) complexes. Synthesis of $\text{Au}(\text{OCOCF}_3)_2(\text{tpy})$ (**62**) from $\text{Au}(\text{OAc})_3$, proved to be a nice expansion of the microwave methods. The solubility in organic solvents of $\text{Au}(\text{OCOCF}_3)_2(\text{tpy})$ (**62**) bearing two trifluoroacetate ligands rather than two chlorines in $\text{AuCl}_2(\text{tpy})$ (**42**) was greatly improved. The knowledge gained from the synthesis of **62** gives potential for obtaining other gold(III) complexes bearing two trifluoroacetate ligands and a chelating ligand other than tpy. Solubility of $\text{Au}(\text{OCOCF}_3)_2(\text{tpy})$ (**62**) and the ability to undergo alkylations and arylations are beneficial. The ligands of the bipyridine type were not investigated with the microwave protocol developed for **62**. As **62** was much easier to cyclometalate than what was observed for $\text{Au}(\text{OAc})_2(\text{tpy})$ (**61**) in acetic acid, the method developed using TFA might ease cyclometalation in other systems as well. Ligand systems bearing other chelates are numerous. Instead of a C–N chelate there are

the possibilities of C–S, C–O or mixtures of the heteroatoms.

A versatile method for synthesis of different mono- and dialkylated gold(III) complexes bearing a chelating C–N ligand has been developed. Several new gold(III) alkyl and aryl complexes bearing the chelating tpy ligand were synthesised in good to excellent yields. Further investigation into the scope of this method is highly desirable. There are numerous complexes available if alkyl or aryl lithium or Grignard reagents can be utilised. The alkylations and arylations were only investigated from cyclometalated gold(III) complexes where the two ligands were trifluoroacetate or chlorine, as well as for two mixed systems (AuBrR(tpy)) where the ligand exchanged was bromine. Monoalkylation and -arylation starting from AuCl₂(tpy) (**42**) proved less straightforward but is surely a pathway that deserves more thought as it showed promise, unfortunately due to time limitations this was not investigated fully.

The mixed alkyl and aryl complexes AuMePh(tpy) **75** and **76** are undoubtedly of interest. There are many new gold complexes with different alkyl and aryl ligands available through the method described in Chapter 2. The scope should be widened and perhaps cyclometalated gold(III) complexes with two different alkyl ligands can be obtained.

A new method was developed to prepare the gold(III) dimer Au₂Cl₂Me₄ (**135**). Further expansion of this method in the form of other bridging units beyond chlorine, where triflate is one such possibility, would be valuable. The other interesting expansion would be different alkyl or silyl groups. One student has already looked into this.¹²³

6.2 Reactivity of Cyclometalated Gold(III) Complexes

The new cyclometalated gold(III) complexes showed good stability towards moisture and air. As a matter of fact, Au(OCOCF₃)₂(tpy) (**62**) is dried under a stream of air for up to an hour. With the exception of **62** which is synthesised under acidic conditions, the other cyclometalated complexes described in this thesis are somewhat sensitive to acid. In regard to the selective protonation at the

sp^2 -C of AuMe₂(tpy) (**64**) and similar cyclometalated complexes there is more work remaining. Some investigations are already taking place.¹²⁴ As protonation of AuBrPh(tpy) (**72**) show different selectivity than for the alkyl analogues, e.g. AuBrMe(tpy) (**70**) and AuMe₂(tpy) (**64**), investigating mixed aryl/aryl systems and mixed alkyl/aryl systems are of interest. Studying the reductive elimination processes at these gold(III) complexes could perhaps lead to the development of catalytic systems. And with catalysis in mind, the cyclometalated gold(III) complexes of the type AuR(tpy)X (R = alkyl, alkenyl, alkynyl, aryl) bearing labile ligands such as OTf, NTf₂, BF₄ or PF₆ are of interest. Investigations of potential catalytic application of AuR(tpy)X were only briefly touched upon, leading to the observed formal insertion of ethylene described in Chapter 4. There was simply not time to continue the search for catalytic transformations using the complexes developed and follow the path of the intriguing chemistry of the ethylene insertion. As the reader might have guessed, the choice fell upon following the alkene insertion (discussed in Chapter 4).

The reactivity of Au(OCOCF₃)₂(tpy) (**62**) with hydrogen gas could be of interest, although it is too early to know. Au(OCOCF₃)₂(tpy) (**62**) was also seen to react with carbon monoxide under high pressures which is also a matter needing more attention.

6.3 Alkene and Alkyne Insertion

Au(OCOCF₃)₂(tpy) (**62**) reacts with ethylene to give formal insertion of ethylene into the Au–O bond *trans* to nitrogen of the chelating tpy ligand. The insertion takes place rapidly in TFA or TFE, and substantially slower in dichloromethane-*d*₂ or THF-*d*₈. The resulting product was Au(CH₂CH₂OCOCF₃)(OCOCF₃)(tpy) (**94**) in TFA and dichloromethane-*d*₂, but in TFE nucleophilic attack by TFE yielded mainly Au(CH₂CH₂OCH₂CF₃)(OCOCF₃)(tpy) (**95**). In THF-*d*₈ and acetonitrile-*d*₃ the major products formed have not been determined and the identity of these products remains of interest.

Regarding the formal insertion of ethylene into the Au–OCOCF₃ bond *trans* to nitrogen in Au(OCOCF₃)₂(tpy) (**62**), there are several features to be further investigated. One interesting feature would be if the reaction could be made cat-

alytic, as functionalisation of ethylene is desirable. Solvent effects, both regarding reaction rate and determining which product is formed, are obvious candidates for investigation; which nucleophiles can be added to coordinated ethylene beyond alcohols, water and trifluoroacetate?

It might be even more interesting to follow up the reaction of acetylene with $\text{Au}(\text{OCOCF}_3)_2(\text{tpy})$ (**62**) which seems to be catalytic already at this early stage of the research. The proposed structure of the gold(III) complex formed in the presence of acetylene is (*E*)- $\text{Au}(\text{CHCHOCOCF}_3)(\text{OCOCF}_3)(\text{tpy})$ (**124**), but full characterisation of both the gold complex and the organic product formed is necessary. Also, is further functionalisation possible by addition of a second reagent, e.g. carbon monoxide or oxygen? In the reactions where alkynes are involved, possible nucleophiles have yet to be explored.

The scope of the formal insertion reactions remains to be seen. Insertion of other alkenes and alkynes into $\text{Au}-\text{OCOCF}_3$ in $\text{Au}(\text{OCOCF}_3)_2(\text{tpy})$ (**62**) should be and is currently being investigated. What the results will be here, remains to be seen but surely they will be interesting. The probable insertion observed with propyne, ethynyltrimethylsilane and 1,2-bis(trimethylsilyl)ethyne showed that substituted alkynes have potential. With the alkene insertion, 1,5-cyclooctadiene and 1,5-hexadiene showed that insertion of substituted alkenes is possible. Disubstituted double bonds are evidently not too sterically demanding, but what about trisubstituted or tetrasubstituted double bonds?

The chelating C–N ligand 2-(*p*-tolyl)pyridine was used for all the insertion chemistry investigated here. A variation of the electronics on the C–N chelate is one direction to proceed, e.g. by adding methyl groups, or using a different ligand system altogether. If the chelating ligand is changed, the sensitivity towards acids might become an issue. In the tridentate C–N–C type ligand by Bochmann *et al.*, protolytic cleavage of the $\text{Au}-\text{C}_{\text{Ar}}$ bond was observed.¹⁰⁹ When $\text{Au}(\text{OCOCF}_3)_2(\text{tpy})$ (**62**) was reacted with acetylene, a catalytic transformation was observed in the acidic TFA-*d* solution but not in dichloromethane-*d*₂, suggesting that an acidic medium might be desirable.

6.4 Gold(III) Alkene and Alkyne Complexes

In this thesis, the preparation and characterisation of the gold(III) alkene complex $\text{Au}(\text{cod})\text{Me}_2\text{X}$ (**133-X**) is described. Until the reports of **133**¹⁷⁷ and the complexes by Bochmann *et al.*¹⁰⁹ there were no proof of gold(III) alkenes existing, even though gold(III) alkenes had been proposed in numerous catalytic cycles involving gold(III). The solid-state structure of **133-BArF**, the only one for a gold(III) alkene complex reported thus far, showed unusually long $\text{Au}-\text{C}_{\text{alkene}}$ bond lengths. Isolation of the gold(III) alkene complexes described in this thesis remains to be achieved and solid-state structures of other gold(III) alkene complexes would be of great value. Are the long $\text{Au}-\text{C}_{\text{alkene}}$ bond lengths unique for **133-BArF**, or will other gold(III) alkene complexes show similar bonding? There are numerous complexes to investigate here, suggested both by experiments conducted thus far and by DFT calculations. Several gold(III) alkene complexes were observed *in situ*, amongst them $\text{Au}(\text{cod})\text{Me}_2\text{X}$ (**133-X**), $\text{Au}(\text{nbd})\text{Me}_2\text{X}$ (**145-X**) and $\text{Au}(\text{hexadiene})\text{Me}_2\text{NTf}_2$ (**146**).

The examples of gold(III) alkene complexes shown in this thesis contained methyl groups as the supporting ligands. A group member has shown that CH_2SiMe_3 can be the supporting ligands when $\text{Au}(\text{CH}_2\text{SiMe}_3)\text{Me}_2(\text{tpy})$ (**67**) is treated with acid at low temperature followed by addition of *cod*.¹²³ To increase the stability towards reductive elimination, one can envision stabilising ligands that are less prone to reductive elimination.

Unambiguous characterisation and isolation of the first gold(III) alkyne species is surely high on the list of interesting projects. If time had allowed, maybe we would have seen the very first gold(III) alkyne complex.

6.5 Coordinatively Unsaturated Gold(III) Complexes

This thesis has discussed several gold(III) complexes with loosely coordinated ligands where open coordination sites for catalysis can be envisioned. The monoalkylated complexes of the type $\text{AuR}(\text{tpy})\text{X}$ (where $\text{X} = \text{OTf}, \text{NTf}_2, \text{BF}_4, \text{PF}_6$) have

one ‘open’ coordination site at gold(III). In polar solvents, $\text{Au}(\text{OCOCF}_3)_2(\text{tpy})$ (**62**) the trifluoroacetate ligand *trans* to carbon in the chelating C–N tpy ligand can dissociate, as shown by ^{19}F NMR. The formal insertion of ethylene, however, takes place *trans* to nitrogen. The combination of these two results indicates that **62** has two sites where catalysis is conceivable; both *trans* to carbon and *trans* to nitrogen. In the gold(III) alkene complex $\text{Au}(\text{cod})\text{Me}_2\text{X}$ (**133–X**), one or two coordination sites are accessible by dissociation of the cod ligand. Complex **133–X** would have two alkyl groups as the spectator ligands if catalysis were to take place which would be rather unorthodox.

To end the story of the gold(III) complexes described herein at this point in time would be sad, it is my hope that these gold complexes that fascinate me so much will continue to prosper!

References

- (1) Lide, D. R. *CRC Handbook of Chemistry and Physics*, 84th ed.; CRC Press, 2003.
- (2) Cotton, S. A. *Chemistry of Precious Metals*, 1st ed.; Chapman & Hall, 1997.
- (3) Hashmi, A. S. K. *Chem. Rev.* **2007**, *107*, 3180–3211.
- (4) Arcadi, A. *Chem. Rev.* **2008**, *108*, 3266–3325.
- (5) Kean, W. F.; Hart, L.; Buchanan, W. W. *Rheumatology* **1997**, *36*, 560–572.
- (6) Barnard, P. J.; Berners-Price, S. J. *Coord. Chem. Rev.* **2007**, *251*, 1889–1902.
- (7) Raubenheimer, H. G.; Schmidbaur, H. *Organometallics* **2011**, *31*, 2507–2522.
- (8) Cheng, G.; Chan, K. T.; To, W.-P.; Che, C.-M. *Adv. Mater.* **2014**, 2540–2546.
- (9) To, W.-P.; Chan, K. T.; Tong, G. S. M.; Ma, C.; Kwok, W.-M.; Guan, X.; Low, K.-H.; Che, C.-M. *Angew. Chem., Int. Ed.* **2013**, *52*, 6648–6652.
- (10) Au, V. K.-M.; Wong, K. M.-C.; Zhu, N.; Yam, V. W.-W. *Chem. Eur. J.* **2011**, *17*, 130–142.
- (11) Bronner, C.; Wenger, O. S. *Dalton Trans.* **2011**, *40*, 12409–12420.
- (12) Yam, V. W.-W.; Wong, K. M.-C.; Hung, L.-L.; Zhu, N. *Angew. Chem., Int. Ed.* **2005**, *44*, 3107–3110.

- (13) Wong, K. M.-C.; Hung, L.-L.; Lam, W. H.; Zhu, N.; Yam, V. W.-W. *J. Am. Chem. Soc.* **2007**, *129*, 4350–4365.
- (14) Garg, J. A.; Blacque, O.; Venkatesan, K. *Inorg. Chem.* **2011**, *50*, 5430–5441.
- (15) Bond, G. *Gold Bull.* **2008**, *41*, 235–241.
- (16) Hashmi, A. S. K.; Hutchings, G. J. *Angew. Chem., Int. Ed.* **2006**, *45*, 7896–7936.
- (17) Hashmi, A. S. K., Toste, F. D., Eds. *Modern Gold Catalyzed Synthesis*; Wiley-VCH Verlag GmbH & Co. KGaA, 2012.
- (18) Norman, R. O. C.; Parr, W. J. E.; Thomas, C. B. *J. Chem. Soc., Perkin Trans. 1* **1976**, 1983–1987.
- (19) Bond, G. C.; Sermon, P. A.; Webb, G.; Buchanan, D. A.; Wells, P. B. *J. Chem. Soc., Chem. Commun.* **1973**, 444b–445.
- (20) Haruta, M.; Kobayashi, T.; Sano, H.; Yamada, N. *Chem. Lett.* **1987**, *16*, 405–408.
- (21) Hutchings, G. J. *J. Catal.* **1985**, *96*, 292–295.
- (22) Ito, Y.; Sawamura, M.; Hayashi, T. *J. Am. Chem. Soc.* **1986**, *108*, 6405–6406.
- (23) Hashmi, A. S. K. *Angew. Chem., Int. Ed.* **2005**, *44*, 6990–6993.
- (24) Braun, I.; Asiri, A. M.; Hashmi, A. S. K. *ACS Catal.* **2013**, *3*, 1902–1907.
- (25) Stephen, A.; Hashmi, K. *Top. Organomet. Chem.* **2013**, *44*, 143–164.
- (26) Della Pina, C.; Falletta, E.; Prati, L.; Rossi, M. *Chem. Soc. Rev.* **2008**, *37*, 2077–2095.
- (27) McMurry, J. *Organic Chemistry*, 6th ed.; Thomson, Brooks/Cole, 2004.
- (28) Hunt, L. B. *Gold Bull.* **1976**, *9*, 134–139.

- (29) Bond, G.; Sermon, P. *Gold Bull.* **1973**, *6*, 102–105.
- (30) Parish, R. *Gold Bull.* **1997**, *30*, 55–62.
- (31) Ball, L. T.; Lloyd-Jones, G. C.; Russell, C. A. *J. Am. Chem. Soc.* **2014**, *136*, 254–264.
- (32) Ball, L. T.; Lloyd-Jones, G. C.; Russell, C. A. *Science* **2012**, *337*, 1644–1648.
- (33) Jones, C. J.; Taube, D.; Ziatdinov, V. R.; Periana, R. A.; Nielsen, R. J.; Oxgaard, J.; Goddard, I., William A. *Angew. Chem., Int. Ed.* **2004**, *43*, 4626–4629.
- (34) Zhang, G.; Peng, Y.; Cui, L.; Zhang, L. *Angew. Chem., Int. Ed.* **2009**, *48*, 3112–3115.
- (35) Livendahl, M.; Espinet, P.; Echavarren, A. M. *Platinum Metals Rev.* **2011**, *55*, 212–214.
- (36) Pyykkö, P. *Angew. Chem., Int. Ed.* **2004**, *43*, 4412–4456.
- (37) Schmidbaur, H.; Schier, A. *Chem. Soc. Rev.* **2012**, *41*, 370–412.
- (38) Sculfort, S.; Braunstein, P. *Chem. Soc. Rev.* **2011**, *40*, 2741–2760.
- (39) Appleton, T. G.; Clark, H. C.; Manzer, L. E. *Coord. Chem. Rev.* **1973**, *10*, 335–422.
- (40) Hartwig, J. F. *Organotransition Metal Chemistry: From Bonding to Catalysis*; Univ. Science Books, 2010.
- (41) Harris, R. K.; Becker, E. D.; Cabral de Menezes, S. M.; Goodfellow, R.; Granger, P. *Pure Appl. Chem.* **2001**, *73*, 1795–1818.
- (42) Narath, A. *Phys. Rev.* **1967**, *163*, 232–237.
- (43) Narath, A. *Phys. Rev.* **1968**, *175*, 696–696.
- (44) Zangger, K.; Armitage, I. M. *Metal-Based Drugs* **1999**, *6*, 239–245.

- (45) Kawakami, M.; Enokiya, H.; Okamoto, T. *J. Phys. F: Met. Phys.* **1985**, *15*, 1613–1621.
- (46) Bondi, A. *J. Phys. Chem.* **1964**, *68*, 441–451.
- (47) Doerrler, L. H. *Dalton Trans.* **2010**, *39*, 3543–3553.
- (48) Doerrler, L. H. *Comments Inorg. Chem.* **2008**, *29*, 93–127.
- (49) Rudolph, M.; Hashmi, A. S. K. *Chem. Soc. Rev.* **2012**, *41*, 2448–2462.
- (50) Lansdown, A. B. G. *The Carcinogenicity of Metals: Human risk through occupational and environmental exposure*; 18; RSC Publishing, 2014; pp 216–241.
- (51) Kozin, L. F.; Hansen, S. *Mercury Handbook: Chemistry, Applications and Environmental Impact*; Royal Society of Chemistry, 2013.
- (52) Rayner-Canham, G.; Overton, T. *Descriptive Inorganic Chemistry*, 4th ed.; W. H. Freeman and Company, 2006.
- (53) Carroll, L. *Alice's Adventures in Wonderland*; Macmillan, 1865.
- (54) Risher, J. F.; Murray, H. E.; Prince, G. R. *Toxicol. Ind. Health* **2002**, *18*, 109–160.
- (55) Hutchings, G. J. *Catal. Today* **2002**, *72*, 11–17.
- (56) Brooner, R. E. M.; Widenhoefer, R. A. *Angew. Chem., Int. Ed.* **2013**, *52*, 11714–11724.
- (57) Marion, N.; Nolan, S. P. *Chem. Soc. Rev.* **2008**, *37*, 1776–1782.
- (58) Glorius, F. *Top. Organomet. Chem.* **2007**, *21*, 1–21.
- (59) Nakamura, I.; Sato, T.; Yamamoto, Y. *Angew. Chem., Int. Ed.* **2006**, *45*, 4473–4475.
- (60) Johansson, M. J.; Gorin, D. J.; Staben, S. T.; Toste, F. D. *J. Am. Chem. Soc.* **2005**, *127*, 18002–18003.

- (61) Fructos, M. R.; Belderrain, T. R.; de Frémont, P.; Scott, N. M.; Nolan, S. P.; Díaz-Requejo, M. M.; Pérez, P. J. *Angew. Chem., Int. Ed.* **2005**, *44*, 5284–5288.
- (62) Schmidbaur, H.; Schier, A. *Arab. J. Sci. Eng.* **2012**, *37*, 1187–1225.
- (63) Dankel, E. K. R. *Synthesis and properties of new gold iminocarbene complexes*; Master thesis, University of Oslo, 2014.
- (64) Langseth, E. *Unpublished results*.
- (65) Kharasch, M. S.; Isbell, H. S. *J. Am. Chem. Soc.* **1931**, *53*, 3053–3059.
- (66) Hashmi, A. S. K.; Schwarz, L.; Choi, J.-H.; Frost, T. M. *Angew. Chem., Int. Ed.* **2000**, *39*, 2285–2288.
- (67) Aksn, Ö.; Krause, N. *Adv. Synth. Catal.* **2008**, *350*, 1106–1112.
- (68) Beeler, A. B.; Su, S.; Singleton, C. A.; Porco, J. A. *J. Am. Chem. Soc.* **2007**, *129*, 1413–1419.
- (69) Hashmi, A. S. K.; Weyrauch, J. P.; Rudolph, M.; Kurpejović, E. *Angew. Chem., Int. Ed.* **2004**, *43*, 6545–6547.
- (70) Hashmi, A. S. K.; Ata, F.; Bats, J. W.; Blanco, M. C.; Frey, W.; Hamzic, M.; Rudolph, M.; Salathé, R.; Schäfer, S.; Wölfe, M. *Gold Bull.* **2007**, *40*, 31–35.
- (71) Shapiro, N. D.; Toste, F. D. *J. Am. Chem. Soc.* **2007**, *129*, 4160–4161.
- (72) Li, G.; Zhang, L. *Angew. Chem., Int. Ed.* **2007**, *46*, 5156–5159.
- (73) Aguilar, D.; Contel, M.; Navarro, R.; Urriolabeitia, E. P. *Organometallics* **2007**, *26*, 4604–4611.
- (74) Hashmi, A. S. K. *Angew. Chem., Int. Ed.* **2010**, *49*, 5232–5241.
- (75) Liu, L.-P.; Xu, B.; Mashuta, M. S.; Hammond, G. B. *J. Am. Chem. Soc.* **2008**, *130*, 17642–17643.

- (76) Weber, D.; Tarselli, M.; Gagné, M. *Angew. Chem., Int. Ed.* **2009**, *48*, 5733–5736.
- (77) Hashmi, A. *Gold Bull.* **2009**, *42*, 275–279.
- (78) Egorova, O. A.; Seo, H.; Kim, Y.; Moon, D.; Rhee, Y. M.; Ahn, K. H. *Angew. Chem., Int. Ed.* **2011**, *50*, 11446–11450.
- (79) Tamaki, A.; Magennis, S. A.; Kochi, J. K. *J. Am. Chem. Soc.* **1974**, *96*, 6140–6148.
- (80) Roşca, D.-A.; Smith, D. A.; Hughes, D. L.; Bochmann, M. *Angew. Chem., Int. Ed.* **2012**, *51*, 10643–10646.
- (81) Chalk, A. J. *J. Am. Chem. Soc.* **1964**, *86*, 4733–4734.
- (82) Cinellu, M. A.; Minghetti, G.; Stoccoro, S.; Zucca, A.; Manassero, M. *Chem. Commun.* **2004**, 1618–1619.
- (83) Cinellu, M. A.; Minghetti, G.; Cocco, F.; Stoccoro, S.; Zucca, A.; Manassero, M.; Arca, M. *Dalton Trans.* **2006**, 5703–5716.
- (84) Brown, T. J.; Dickens, M. G.; Widenhoefer, R. A. *J. Am. Chem. Soc.* **2009**, *131*, 6350–6351.
- (85) Brown, T. J.; Dickens, M. G.; Widenhoefer, R. A. *Chem. Commun.* **2009**, 6451–6453.
- (86) Hooper, T. N.; Green, M.; McGrady, J. E.; Patel, J. R.; Russell, C. A. *Chem. Commun.* **2009**, 3877–3879.
- (87) Brooner, R. E. M.; Widenhoefer, R. A. *Organometallics* **2011**, *30*, 3182–3193.
- (88) Brooner, R. E. M.; Widenhoefer, R. A. *Organometallics* **2012**, *31*, 768–771.
- (89) Dias, H. V. R.; Wu, J. *Angew. Chem., Int. Ed.* **2007**, *46*, 7814–7816.
- (90) Dias, H. V. R.; Fianchini, M.; Cundari, T. R.; Campana, C. F. *Angew. Chem., Int. Ed.* **2008**, *47*, 556–559.

- (91) Dias, H. V. R.; Lovely, C. J. *Chem. Rev.* **2008**, *108*, 3223–3238.
- (92) Dias, H. V. R.; Wu, J. *Eur. J. Inorg. Chem.* **2008**, *2008*, 509–522.
- (93) Cinellu, M. A. *Modern Gold Catalyzed Synthesis*; Wiley-VCH Verlag GmbH & Co. KGaA, 2012; pp 175–199.
- (94) Schmidbaur, H.; Schier, A. *Organometallics* **2010**, *29*, 2–23.
- (95) Norman, R. O. C.; Parr, W. J. E.; Thomas, C. B. *J. Chem. Soc., Perkin Trans. 1* **1976**, 811–817.
- (96) Henderson, W. *Adv. Organomet. Chem.* **2006**, *54*, 207–265.
- (97) Shaw, A. P.; Tilset, M.; Heyn, R. H.; Jakobsen, S. *J. Coord. Chem.* **2011**, *64*, 38–47.
- (98) Constable, E. C.; Leese, T. A. *J. Organomet. Chem.* **1989**, *363*, 419–24.
- (99) Mansour, M. A.; Lachicotte, R. J.; Gysling, H. J.; Eisenberg, R. *Inorg. Chem.* **1998**, *37*, 4625–4632.
- (100) Shaw, A. P. *Unpublished results*.
- (101) Hayes, B. L. *Microwave Synthesis: Chemistry at the Speed of Light*; CEM Publishing, 2002.
- (102) Shaw, A. P.; Ghosh, M. K.; Törnroos, K. W.; Wragg, D. S.; Tilset, M.; Swang, O.; Heyn, R. H.; Jakobsen, S. *Organometallics* **2012**, *31*, 7093–7100.
- (103) Rezsnyak, C. E.; Autschbach, J.; Atwood, J. D.; Moncho, S. *J. Coord. Chem.* **2013**, *66*, 1153–1165.
- (104) Venugopal, A.; Shaw, A. P.; Törnroos, K. W.; Heyn, R. H.; Tilset, M. *Organometallics* **2011**, *30*, 3250–3253.
- (105) Pope, W. J.; Gibson, C. S. *J. Chem. Soc., Trans.* **1907**, *91*, 2061–2066.
- (106) Langseth, E.; Görbitz, C. H.; Heyn, R. H.; Tilset, M. *Organometallics* **2012**, *31*, 6567–6571.

- (107) Langseth, E.; Nova, A.; Tråseth, E. A.; Rise, F.; Øien, S.; Heyn, R. H.; Tilset, M. *J. Am. Chem. Soc.* **2014**, *136*, 10104–10115.
- (108) Rpsca, D.-A.; Wright, J. A.; Hughes, D. L.; Bochmann, M. *Nat. Commun.* **2013**, *4*, 3167/1–3167/7.
- (109) Savjani, N.; Roşca, D.-A.; Schormann, M.; Bochmann, M. *Angew. Chem., Int. Ed.* **2013**, *52*, 874–877.
- (110) Cocco, F.; Cinellu, M. A.; Minghetti, G.; Zucca, A.; Stoccoro, S.; Maiore, L.; Manassero, M. *Organometallics* **2010**, *29*, 1064–1066.
- (111) Tråseth, E. A. *Syntese og karakterisering av nye syklometallerte gull(III)komplekser*; Master thesis, University of Oslo, 2014.
- (112) Escrivá, L. P. *Synthesis, Characterization and Catalytic Application of Rh(I) Complex bearing a Chelating N-Heterocyclic Iminocarbene Ligand and Preparation of Cyclometalated Au(III) Complexes*; Project work, University of Oslo, 2013.
- (113) Mahon, M. F.; Whittlesey, M. K.; Wood, P. T. *Organometallics* **1999**, *18*, 4068–4074.
- (114) Chaudhari, S. R.; Mogurampelly, S.; Suryaprakash, N. *J. Phys. Chem. B* **2013**, *117*, 1123–1129.
- (115) Li, H.; Frieden, C. *Biochemistry* **2006**, *45*, 6272–6278.
- (116) Buchanan, G. W.; Munteanu, E.; Dawson, B. A.; Hodgson, D. *Magn. Reson. Chem.* **2005**, *43*, 528–534.
- (117) Battiste, J. L.; Jing, N.; Newmark, R. A. *J. Fluorine Chem.* **2004**, *125*, 1331–1337.
- (118) Plaumann, M.; Bommerich, U.; Trantzsche, T.; Lego, D.; Dillenberger, S.; Sauer, G.; Bargon, J.; Buntkowsky, G.; Bernarding, J. *Chem. Eur. J.* **2013**, *19*, 6334–6339.

- (119) Battiste, J.; Newmark, R. A. *Prog. Nucl. Magn. Reson. Spectrosc.* **2006**, *48*, 1–23.
- (120) Fan, D.; Melendez, E.; Ranford, J. D.; Lee, P. F.; Vittal, J. J. *J. Organomet. Chem.* **2004**, *689*, 2969–2974.
- (121) Fan, D.; Yang, C.-T.; Ranford, J. D.; Lee, P. F.; Vittal, J. J. *Dalton Trans.* **2003**, 2680–2685.
- (122) Garg, J. A.; Blacque, O.; Fox, T.; Venkatesan, K. *Inorg. Chem.* **2010**, *49*, 11463–11472.
- (123) Sundsdal, A. *Syntese og karakterisering av organogull(III)komplekser fra organolitiumreagenser*; Master thesis, University of Oslo, 2014.
- (124) Heen, E. A. *Unpublished results*.
- (125) Spingler, B.; Schnidrig, S.; Todorova, T.; Wild, F. *CrystEngComm* **2012**, *14*, 751–757.
- (126) Rigamonti, L.; Manassero, C.; Rusconi, M.; Manassero, M.; Pasini, A. *Dalton Trans.* **2009**, 1206–1213.
- (127) Rigamonti, L.; Forni, A.; Manassero, M.; Manassero, C.; Pasini, A. *Inorg. Chem.* **2010**, *49*, 123–135.
- (128) Sheldrick, G. M. *Acta Crystallogr. A* **2008**, *64*, 112–122.
- (129) Allen, F. H.; Johnson, O.; Shields, G. P.; Smith, B. R.; Towler, M. *J. Appl. Cryst.* **2004**, *37*, 335–338.
- (130) Claridge, T. D. W. *High-Resolution NMR Techniques in Organic Chemistry*, 2nd ed.; Elsevier, 2009; Vol. 27.
- (131) Kharasch, M. S.; Isbell, H. S. *J. Am. Chem. Soc.* **1930**, *52*, 2919–2927.
- (132) Roe, C. D. *J. Magn. Reson.* **1985**, *63*, 388–391.
- (133) Cusanelli, A.; Frey, U.; Richens, D. T.; Merbach, A. *J. Am. Chem. Soc.* **1996**, *118*, 5265–5271.

- (134) Laurency, G.; Dyson, P. J. *Z. Naturforsch. B* **2008**, *63b*, 681–684.
- (135) Johansson, L.; Tilset, M.; Labinger, J. A.; Bercaw, J. E. *J. Am. Chem. Soc.* **2000**, *122*, 10846–10855.
- (136) Haghighi, M. G.; Nabavizadeh, S. M.; Rashidi, M.; Kubicki, M. *Dalton Trans.* **2013**, *42*, 13369–13380.
- (137) Wolf, W. J.; Winston, M. S.; Toste, F. D. *Nat. Chem.* **2014**, *6*, 159–164.
- (138) Komiya, S.; Shibue, A. *Organometallics* **1985**, *4*, 684–687.
- (139) Komiya, S.; Albright, T. A.; Hoffmann, R.; Kochi, J. K. *J. Am. Chem. Soc.* **1976**, *98*, 7255–7265.
- (140) Komiya, S.; Shibue, A.; Ozaki, S. *J. Organomet. Chem.* **1987**, *319*, C31–C34.
- (141) Fulmer, G. R.; Miller, A. J. M.; Sherden, N. H.; Gottlieb, H. E.; Nudelman, A.; Stoltz, B. M.; Bercaw, J. E.; Goldberg, K. I. *Organometallics* **2010**, *29*, 2176–2179.
- (142) Komiya, S.; Kochi, J. K. *J. Am. Chem. Soc.* **1976**, *98*, 7599–7607.
- (143) Wang, D.; Cai, R.; Sharma, S.; Jirak, J.; Thummanapelli, S. K.; Akhmedov, N. G.; Zhang, H.; Liu, X.; Petersen, J. L.; Shi, X. *J. Am. Chem. Soc.* **2012**, *134*, 9012–9019.
- (144) Patrick, S. R.; Boogaerts, I. I. F.; Gaillard, S.; Slawin, A. M. Z.; Nolan, S. P. *Beilstein J. Org. Chem.* **2011**, *7*, 892–896, No. 102.
- (145) AIST, Spectral Database for Organic Compounds SDBS. www.sdb.sdb.aist.go.jp.
- (146) Urbano, J.; Hormigo, A. J.; de Frémont, P.; Nolan, S. P.; Díaz-Requejo, M. M.; Pérez, P. J. *Chem. Commun.* **2008**, 759–761.
- (147) Nova, A. *Unpublished results*.

- (148) Shilov, A. E.; Shul'pin, G. B. *Chem. Rev.* **1997**, *97*, 2879–2932.
- (149) Parshall, G. W.; Ittel, S. D. *Homogeneous Catalysis. The Applications and Chemistry of Catalysis by Soluble Transition Metal Complexes.*, 2nd ed.; Wiley-Interscience, 1992.
- (150) Atwood, J. D. *Inorganic and Organometallic Reaction Mechanisms*, 2nd ed.; VCH, 1996.
- (151) Lv, H.; Zhan, J.-H.; Cai, Y.-B.; Yu, Y.; Wang, B.; Zhang, J.-L. *J. Am. Chem. Soc.* **2012**, *134*, 16216–16227.
- (152) Basak, A.; Chakrabarty, K.; Ghosh, A.; Das, G. K. *J. Org. Chem.* **2013**, *78*, 9715–9724.
- (153) Soriano, E.; Marco-Contelles, J. *Top. Curr. Chem.* **2011**, *302*, 1–29.
- (154) Tkatchouk, E.; Mankad, N. P.; Benitez, D.; Goddard, W. A.; Toste, F. D. *J. Am. Chem. Soc.* **2011**, *133*, 14293–14300.
- (155) Comas-Vives, A.; Ujaque, G. *J. Am. Chem. Soc.* **2012**, *135*, 1295–1305.
- (156) Wang, Y.; McGonigal, P. R.; Herlé, B.; Besora, M.; Echavarren, A. M. *J. Am. Chem. Soc.* **2013**, *136*, 801–809.
- (157) Hashmi, A. S. K. *Angew. Chem., Int. Ed.* **2012**, *51*, 12935–12936.
- (158) Guenther, J.; Mallet-Ladeira, S.; Estevez, L.; Miqueu, K.; Amgoune, A.; Bourissou, D. *J. Am. Chem. Soc.* **2014**, *136*, 1778–1781.
- (159) Joost, M.; Gualco, P.; Coppel, Y.; Miqueu, K.; Kefalidis, C. E.; Maron, L.; Amgoune, A.; Bourissou, D. *Angew. Chem., Int. Ed.* **2014**, *53*, 747–751.
- (160) Mankad, N. P.; Toste, F. D. *Chem. Sci.* **2012**, *3*, 72–76.
- (161) Ghidui, M. J.; Pistner, A. J.; Yap, G. P. A.; Lutterman, D. A.; Rosenthal, J. *Organometallics* **2013**, *32*, 5026–5029.
- (162) Dupuy, S.; Slawin, A. M. Z.; Nolan, S. P. *Chem. Eur. J.* **2012**, *18*, 14923–14928.

- (163) Chen, Y.; Chen, M.; Liu, Y. *Angew. Chem., Int. Ed.* **2012**, *51*, 6181–6186.
- (164) delPozo, J.; Carrasco, D.; Pérez-Temprano, M. H.; García-Melchor, M.; Álvarez, R.; Casares, J. A.; Espinet, P. *Angew. Chem., Int. Ed.* **2013**, *52*, 2189–2193.
- (165) Liu, L.-P.; Hammond, G. B. *Chem. Soc. Rev.* **2012**, *41*, 3129–3139.
- (166) Chiarucci, M.; Bandini, M. *Beilstein J. Org. Chem.* **2013**, *9*, 2586–2614.
- (167) Hashmi, A. S. K.; Weyrauch, J. P.; Frey, W.; Bats, J. W. *Org. Lett.* **2004**, *6*, 4391–4394.
- (168) Zhu, J.; Germain, A. R.; Porco, J. A. *Angew. Chem., Int. Ed.* **2004**, *43*, 1239–1243.
- (169) Johnson, M. W.; Shevick, S. L.; Toste, F. D.; Bergman, R. G. *Chem. Sci.* **2013**, *4*, 1023–1027.
- (170) Krauter, C. M.; Hashmi, A. S. K.; Pernpointner, M. *ChemCatChem* **2010**, *2*, 1226–1230.
- (171) Kovács, G.; Lledós, A.; Ujaque, G. *Angew. Chem., Int. Ed.* **2011**, *50*, 11147–11151.
- (172) LaLonde, R. L.; Brenzovich, Jr., W. E.; Benitez, D.; Tkatchouk, E.; Kelley, K.; Goddard, III, W. A.; Toste, F. D. *Chem. Sci.* **2010**, *1*, 226–233.
- (173) Luinstra, G.; Wang, L.; Stahl, S.; Labinger, J.; Bercaw, J. *J. Organomet. Chem.* **1995**, *504*, 75–91.
- (174) Bäckvall, J. E.; Åkermark, B.; Ljunggren, S. O. *J. Am. Chem. Soc.* **1979**, *101*, 2411–2416.
- (175) Lide, D. R., Ed. *CRC Handbook of Chemistry and Physics*, 86th ed.; CRC Press, 2004.
- (176) Ihlefeldt, F. *Unpublished results*.

- (177) Langseth, E.; Scheuermann, M. L.; Balcells, D.; Kaminsky, W.; Goldberg, K. I.; Eisenstein, O.; Heyn, R. H.; Tilset, M. *Angew. Chem., Int. Ed.* **2013**, *52*, 1660–1663.
- (178) Scheuermann, M. L. *Investigations of the reactivity of palladium and platinum complexes with molecular oxygen and characterisation of a gold(III)-alkene complex*; Ph.D. thesis, University of Washington, 2013.
- (179) Xiao, Y.-P.; Liu, X.-Y.; Che, C.-M. *J. Organomet. Chem.* **2009**, *694*, 494–501.
- (180) Nguyen, R.-V.; Yao, X.; Li, C.-J. *Org. Lett.* **2006**, *8*, 2397–2399.
- (181) Zeise, W. C. *Poggendorf's Ann. Phys.* **1827**, *9*, 632.
- (182) Zeise, W. C. *Ann. Phys. Chem.* **1831**, *21*, 497–541.
- (183) Hüttel, R.; Dietl, H. *Angew. Chem., Int. Ed. Engl.* **1965**, *4*, 438.
- (184) Hüttel, R.; Reinheimer, H.; Dietl, H. *Chem. Ber.* **1966**, *99*, 462–468.
- (185) Hüttel, R.; Reinheimer, H. *Chem. Ber.* **1966**, *99*, 2778–2781.
- (186) Hüttel, R.; Reinheimer, H.; Nowak, K.; Dietl, H. *Tetrahedron Lett.* **1967**, 1019–1022.
- (187) Hüttel, R.; Reinheimer, H.; Nowak, K. *Chem. Ber.* **1968**, *101*, 3761–3776.
- (188) Hüttel, R.; Tauchner, P.; Forkl, H. *Chem. Ber.* **1972**, *105*, 1–7.
- (189) Hüttel, R.; Forkl, H. *Chem. Ber.* **1972**, *105*, 1664–1673.
- (190) Hüttel, R.; Forkl, H. *Chem. Ber.* **1972**, *105*, 2913–2921.
- (191) Tauchner, P.; Hüttel, R. *Tetrahedron Lett.* **1972**, *46*, 4733–4736.
- (192) Tauchner, P.; Hüttel, R. *Chem. Ber.* **1974**, *107*, 3761–3770.
- (193) Coutelle, H.; Hüttel, R. *J. Organomet. Chem.* **1978**, *153*, 359–368.

- (194) Brain, F. H.; Gibson, C. S.; Jarvis, J. A. J.; Phillips, R. F.; Powell, H. M.; Tyabji, A. *J. Chem. Soc.* **1952**, 3686–3694.
- (195) Monaghan, P. K.; Puddephatt, R. J. *Inorg. Chim. Acta* **1975**, *15*, 231–234.
- (196) Armer, B.; Schmidbaur, H. *Angew. Chem., Int. Ed. Engl.* **1970**, *9*, 101–113.
- (197) Schmidbaur, H. *Angew. Chem., Int. Ed. Engl.* **1976**, *15*, 728–740.
- (198) García-Mota, M.; Cabello, N.; Maseras, F.; Echavarren, A. M.; Pérez-Ramírez, J.; Lopez, N. *ChemPhysChem* **2008**, *9*, 1624–1629.
- (199) Kang, R.; Chen, H.; Shaik, S.; Yao, J. *J. Chem. Theory Comput.* **2011**, *7*, 4002–4011.
- (200) Paul, M. *Z. Naturforsch. B* **1994**, *49*, 647–650.
- (201) Scheuermann, M. L.; Heyn, R. H. *Unpublished results*.
- (202) Crabtree, R. H. *The Organometallic Chemistry of the Transition Metals*, 4th ed.; John Wiley & Sons, Inc., 2005.
- (203) Klein, A.; Klinkhammer, K.-W.; Scheiring, T. *J. Organomet. Chem.* **1999**, *592*, 128–135.
- (204) Kou, X.; Dias, H. V. R. *Dalton Trans.* **2009**, 7529–7536.
- (205) Straubinger, C. S.; Jokić, N. B.; Högerl, M. P.; Herdtweck, E.; Herrmann, W. A.; Kühn, F. E. *J. Organomet. Chem.* **2011**, *696*, 687–692.
- (206) Hughes, R. P.; Overby, J. S.; Lam, K.-C.; Incarvito, C. D.; Rheingold, A. L. *Polyhedron* **2002**, *21*, 2357–2360.
- (207) Venugopal, A.; Ghosh, M. K.; Jürgens, H.; Törnroos, K. W.; Swang, O.; Tilstet, M.; Heyn, R. H. *Organometallics* **2010**, *29*, 2248–2253.
- (208) Brookhart, M.; Grant, B.; Volpe, A. F. *Organometallics* **1992**, *11*, 3920–3922.

- (209) Frisch, M. J.; Trucks, G. W.; Schlegel, H. B.; Scuseria, G. E.; Robb, M. A.; Cheeseman, J. R.; Scalmani, G.; Barone, V.; Mennucci, B.; Petersson, G. A.; Nakatsuji, H.; Caricato, M.; Li, X.; Hratchian, H. P.; Izmaylov, A. F.; Bloino, J.; Zheng, G.; Sonnenberg, J. L.; Hada, M.; Ehara, M.; Toyota, K.; Fukuda, R.; Hasegawa, J.; Ishida, M.; Nakajima, T.; Honda, Y.; Kitao, O.; Nakai, H.; Vreven, T.; Montgomery, J., J. A.; Peralta, J. E.; Ogliaro, F.; Bearpark, M.; Heyd, J. J.; Brothers, E.; Kudin, K. N.; Staroverov, V. N.; Kobayashi, R.; Normand, J.; Raghavachari, K.; Rendell, A.; Burant, J. C.; Iyengar, S. S.; Tomasi, J.; Cossi, M.; Rega, N.; Millam, N. J.; Klene, M.; Knox, J. E.; Cross, J. B.; Bakken, V.; Adamo, C.; Jaramillo, J.; Gomperts, R.; Stratmann, R. E.; Yazyev, O.; Austin, A. J.; Cammi, R.; Pomelli, C.; Ochterski, J. W.; Martin, R. L.; Morokuma, K.; Zakrzewski, V. G.; Voth, G. A.; Salvador, P.; Dannenberg, J. J.; Dapprich, S.; Daniels, A. D.; Farkas, Ö.; Foresman, J. B.; Ortiz, J. V.; Cioslowski, J.; Fox, D. J. *Gaussian 09, Rev. B.01, Gaussian Inc., Wallingford, CT* **2009**,
- (210) McLean, A. D.; Chandler, G. S. *J. Chem. Phys.* **1980**, *72*, 5639–5648.
- (211) Krishnan, R.; Binkley, J. S.; Seeger, R.; Pople, J. A. *J. Chem. Phys.* **1980**, *72*, 650–654.
- (212) Figgen, D.; Rauhut, G.; Dolg, M.; Stoll, H. *Chem. Phys.* **2005**, *311*, 227–244.
- (213) Adamo, C.; Barone, V. *J. Chem. Phys.* **1999**, *110*, 6158–6170.
- (214) Reed, A. E.; Curtiss, L. A.; Weinhold, F. *Chem. Rev.* **1988**, *88*, 899–926.
- (215) Pernpointner, M.; Hashmi, A. S. K. *J. Chem. Theory Comput.* **2009**, *5*, 2717–2725.
- (216) Lein, M.; Rudolph, M.; Hashmi, S. K.; Schwerdtfeger, P. *Organometallics* **2010**, *29*, 2206–2210.
- (217) Perdew, J. P. *Phys. Rev. B* **1986**, *33*, 8822–8824.
- (218) Becke, A. D. *J. Chem. Phys.* **1993**, *98*, 5648–5652.
- (219) Grimme, S. *J. Comput. Chem.* **2006**, *27*, 1787–1799.

- (220) Zhao, Y.; Truhlar, D. G. *J. Chem. Phys.* **2006**, *125*, 194101/1–194101/18.
- (221) Zhao, Y.; Truhlar, D. G. *Theor. Chem. Acc.* **2008**, *120*, 215–241.
- (222) Perdew, J. P.; Burke, K.; Ernzerhof, M. *Phys. Rev. Lett.* **1996**, *77*, 3865–3868.
- (223) Hagen, K.; Hedberg, L.; Hedberg, K. *J. Phys. Chem.* **1982**, *86*, 117–121.
- (224) Wang, D.; Cai, R.; Sharma, S.; Jirak, J.; Thummanapelli, S. K.; Akhmedov, N. G.; Zhang, H.; Liu, X.; Petersen, J. L.; Shi, X. *J. Am. Chem. Soc.* **2012**, *134*, 9012–9019.
- (225) Nishinaga, T. *Sci. Synth.* **2009**, *45a*, 383–406.
- (226) Detert, H.; Rose, B.; Mayer, W.; Meier, H. *Chem. Ber.* **1994**, *127*, 1529–1532.

Appendices

Paper I

Versatile Methods for Preparation of New Cyclometalated Gold(III) Complexes

Langseth, E.; Görbitz, C. H.; Heyn, R. H.; Tilset, M.

Organometallics **2012**, *31*, 6567–6571.

Paper II

A Gold Exchange: A Mechanistic Study of a Reversible,
Formal Ethylene Insertion Into a Gold(III)–Oxygen Bond

Langseth, E.; Nova, A.; Tråseth, E. Aa.; Rise, F.; Øien, S.; Heyn, R. H.; Tilset, M.

J. Am. Chem. Soc. **2014**, *136*, 10104–10115.

Paper III

Generation and Structural Characterization of a Gold(III) Alkene Complex

Langseth, E.; Scheuermann, M. L.; Balcells, D.; Kaminsky, W.; Goldberg, K. I.;
Eisenstein, O.; Heyn, R. H.; Tilset, M.

Angew. Chem., Int. Ed. **2013**, *52*, 1660–1663.

